

The Eversion and Bifurcation of Elastic Cylinders

by

Anthony Orr

A thesis submitted to
the Faculty of Science
at the University of Glasgow
for the degree of
Doctor of Philosophy.

©Anthony Orr, 1995

August 1995

ProQuest Number: 11007924

All rights reserved

INFORMATION TO ALL USERS

The quality of this reproduction is dependent upon the quality of the copy submitted.

In the unlikely event that the author did not send a complete manuscript and there are missing pages, these will be noted. Also, if material had to be removed, a note will indicate the deletion.



ProQuest 11007924

Published by ProQuest LLC (2018). Copyright of the Dissertation is held by the Author.

All rights reserved.

This work is protected against unauthorized copying under Title 17, United States Code
Microform Edition © ProQuest LLC.

ProQuest LLC.
789 East Eisenhower Parkway
P.O. Box 1346
Ann Arbor, MI 48106 – 1346

Thesis
10474
Copy 1



Contents

Preface	iii
Summary	iv
1 Introduction	1
2 Basic Equations	11
2.1 Kinematics	11
2.2 Strain-energy and Stress-Strain Relations	14
2.3 Compressible Elasticity	16
2.4 Incompressible Elasticity	18
3 Eversion of Incompressible Cylinders	19
3.1 Basic Eversion Equations	19
3.2 Material Forms	22
3.3 Existence and Uniqueness	24
3.4 Numerical results	33
4 Eversion of Compressible Cylinders	38
4.1 Equilibrium Equations	38
4.2 Exact solution	41
4.3 Existence and Uniqueness	45
4.4 Varga Materials	47
4.5 Numerical results	50
4.6 Blatz-Ko Materials	66

5	The Incremental Equations	68
5.1	Basic Incremental Theory	68
5.2	Incompressible Incremental Equations	70
5.3	Compressible Incremental Equations	71
6	Bifurcation Analysis	72
6.1	Incremental Deformation Gradient	72
6.2	Incompressible Materials	74
6.3	Compressible Materials	79
6.3.1	Varga Materials	82
6.3.2	Blatz-Ko	82
6.3.3	Exact Solution	83
7	Incompressible Bifurcation Results	84
7.1	Numerical Results	84
7.2	Comparison of Numerical Methods	91
7.3	Analysis of Limiting Cases	95
7.4	Conclusions	100
8	Compressible Bifurcation Results	101
8.1	Varga materials	102
8.2	Blatz-Ko materials	109
8.3	Exact Solution	113
8.4	Conclusions	118
9	Numerical Methods	121
	References	129

Preface

This thesis was submitted to the University of Glasgow in accordance with the requirements for the degree of Doctor of Philosophy.

I would like to thank Dr. D. M. Haughton for his guidance, assistance and encouragement throughout the period of my research.

My sincere thanks also go to Professor R. W. Ogden for the help and advice he has given me during my time in the Department of Mathematics.

I also thank Dr K. A. Lindsay for various suggestions, help and advice concerning the numerical aspects of this thesis.

I also thank the Science and Engineering Research Council of Great Britain for financing this research through a three year earmarked award.

Summary

In this thesis we consider the eversion and bifurcation of both incompressible and compressible isotropic elastic cylinders.

To begin we give a brief account of the basic equations of non-linear elasticity. We then study the basic eversion of hollow cylinders composed of both incompressible and compressible material for a variety of strain-energy functions and offer some analysis for the existence and uniqueness of the cylindrical everted state achieved.

Next we study the effect of applying an incremental deformation to the basic everted state and formulate the bifurcation problem with the undeformed thickness ratio as a parameter. We study the bifurcation problem in detail for a variety of strain-energy functions and consider the effects of compressibility, initial tube thickness and mode numbers on the bifurcation produced. The bifurcation problems are solved numerically and we use the present problem to study two different numerical methods. We find that the standard determinantal method, extensively used in the past for elastic bifurcation problems, is not adequate for the problems considered in this thesis and thus adopt the Compound Matrix method. We compare both methods and give a derivation of the Compound Matrix method.

Chapter 1

Introduction

This thesis is concerned with the study of eversion and bifurcation for both compressible and incompressible isotropic hyperelastic right circular cylinders. This work is motivated by a paper of Truesdell (1977) in which he describes experimental work on everting elastic cylinders. By the eversion of an elastic cylinder we refer to turning the shell inside out so that the deformed shape is a perfectly right circular cylinder with the surfaces traction free. We include in Figure 1.1 a photograph of a cylindrical shell before such a deformation and in Figure 1.2 a photograph of the same shell after the deformation is applied. This tube is composed of foam rubber and will therefore be highly compressible. From Figure 1.2 it can be seen that the tube turned inside out has flared ends. From experimental work by other authors this would seem to be a typical case. Flaring suggests that we will not be able to make the ends of our theoretical solution pointwise stress-free since we shall assume that the everted shape is a right circular cylinder. We shall require loads to correct the end deformation. Since it is apparent that this distortion is confined to a small area at the ends we should expect the theoretical solution to provide a good approximation to the actual solution away from the ends. Truesdell (1977) concluded that the part of the tube greater than one fifth of the diameter away from the ends was very nearly a right-circular cylinder. The tube considered by Truesdell was originally a piece of a garden hosepipe composed of solid rubber and thus was nearly incompressible.

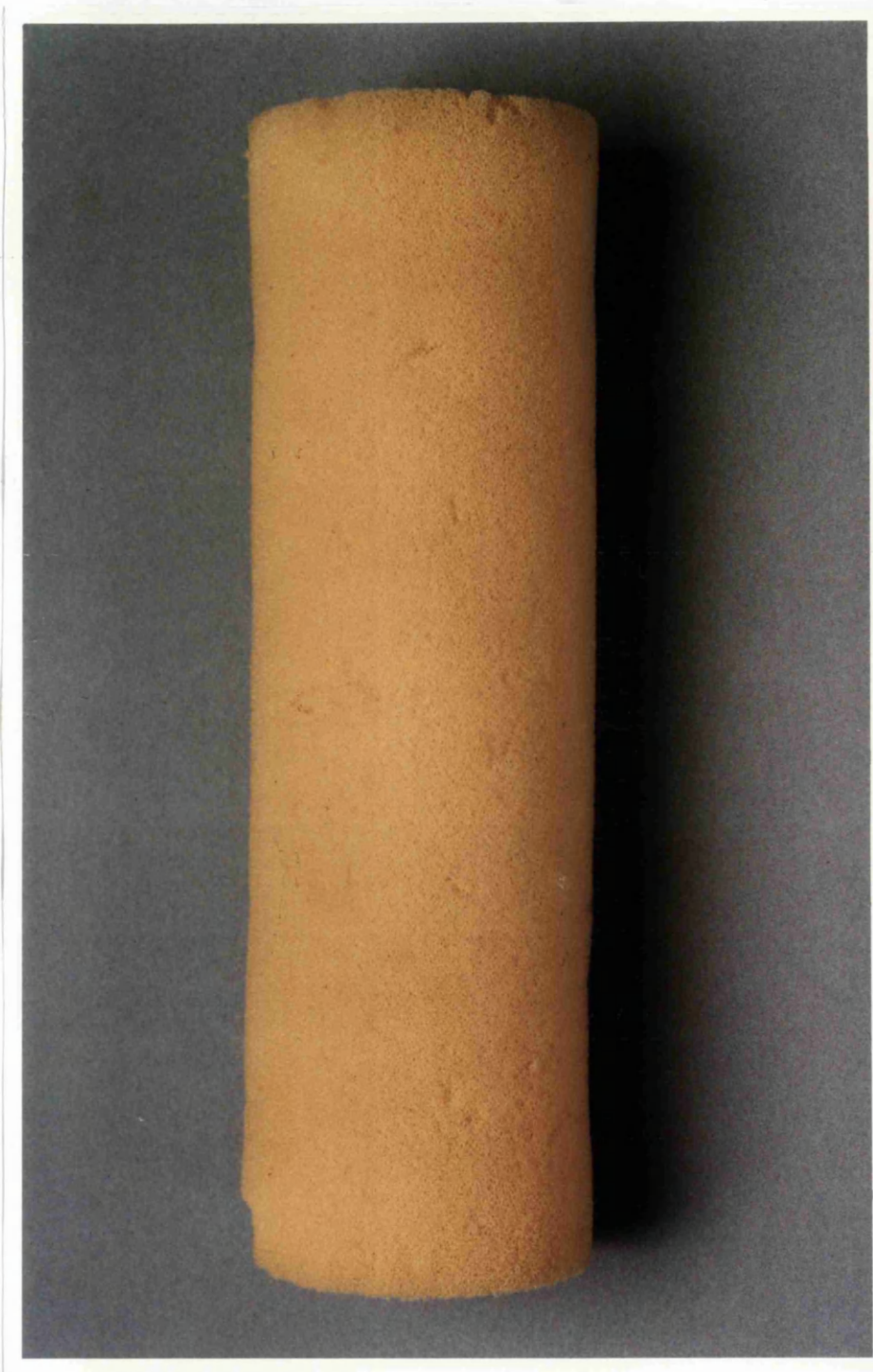


Figure 1.1 Photograph of a foam rubber tube before eversion.

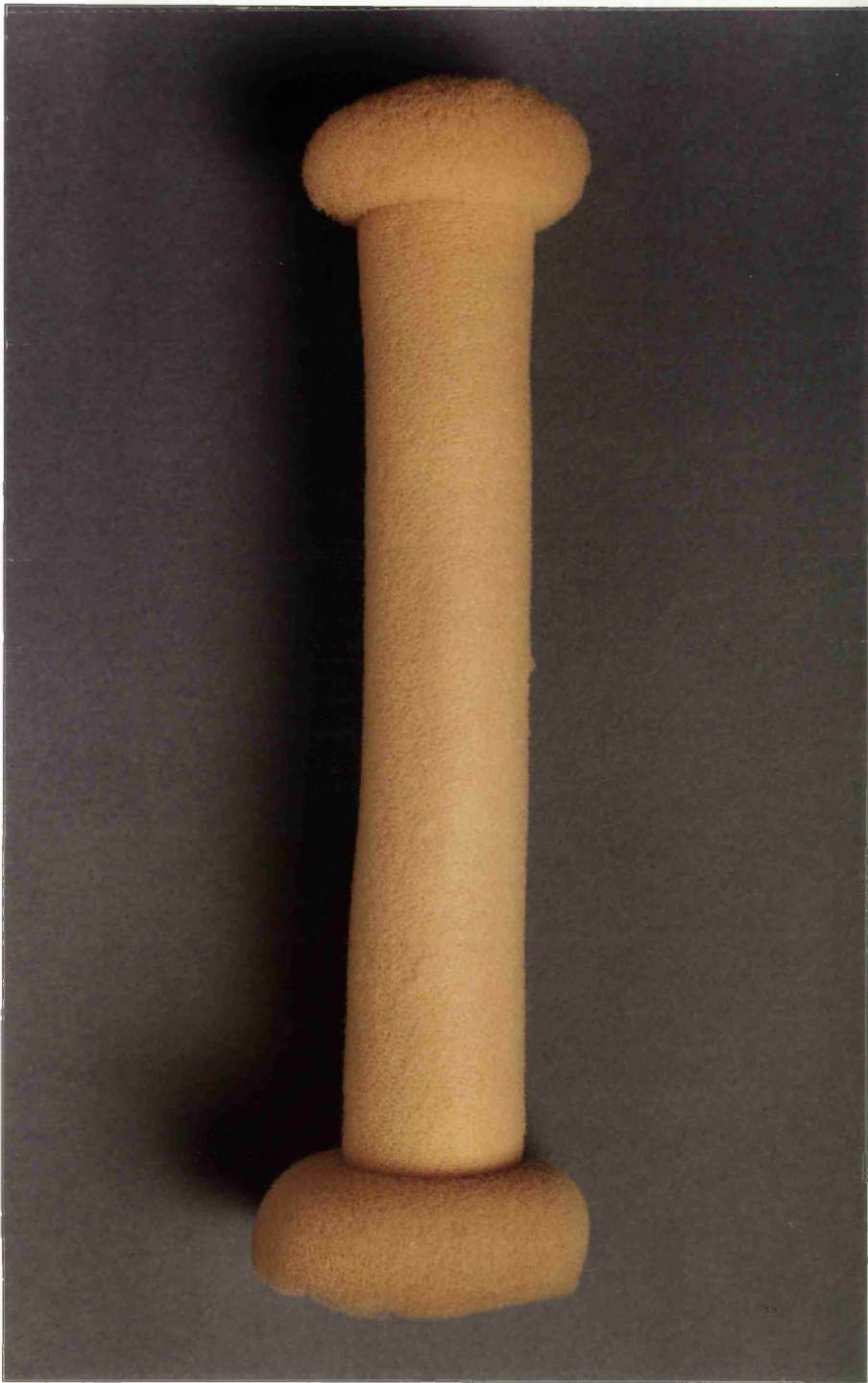


Figure 1.2 Photograph of a foam rubber tube after the eversion is applied.

From the photograph in Truesdell (1977) it is clear that the everted tube is slightly longer in length and hence we should expect, since the material is almost incompressible, a specimen made longer to shrink in diameter.

In Figure 1.2 we can readily see that the ends of the deformed tube are flared and thus the deformed shape is not in fact a perfect right circular cylinder.

A similar experiment conducted by Truesdell (1977) on a foam rubber cylinder two feet long, one foot in diameter and with a one inch thick wall produced surprisingly different results. These dimensions were chosen so that the radial proportions of the tube matched that of the hosepipe, although the foam rubber shell was proportionately shorter. Truesdell (1977) found that upon eversion the foam rubber tube collapsed. The ends of the cylinder remained roughly circular but the mantle was depressed into several large lobes. He also observed that everting the tube again resulted in a perfect right-circular cylinder of the original form. The collapsed form was forced into a cylindrical shape by applying struts across its cavity. However, once the external traction was removed the everted tube collapsed again. Indeed it was found that all tests on the foam rubber cylinder resulted in a stable lobed shape being formed. It is our main aim in this work to investigate this phenomena.

The eversion of incompressible cylinders was also considered experimentally by Varga (1966) where results for various cylinders of different geometries are given. In all cases he was able to show that the everted cylinder was nearly cylindrical with minor distortions at the ends. Unfortunately all the considered samples are quite short since Varga chose the shortest lengths that could be everted without tearing, thus the effects of differing length to radius ratios' are not apparent. The fact that none of the tubes considered in Varga (1966) collapsed (although such cases may have been deliberately excluded) provides us with the motivation for studying the existence of possible bifurcation modes of everted states of incompressible and compressible materials. We also investigate the possible effects of varying the initial length to diameter ratio of the uneverted cylinder.

The basic problem of everting incompressible cylinders has been considered by various authors as a theoretical problem. Rivlin (1949) first considered the

problem for Mooney–Rivlin materials. Ideally we would like the surface of the everted tube to be traction free. Unfortunately, this proves to be very difficult and hence approximate solutions are looked for. We assume that the everted cylinder is perfectly cylindrical with the curved surfaces traction free. On the cylinder ends we need tractions to remove the flaring that would otherwise exist but we impose the constraint of zero resultant load. Rivlin (1949) was able to solve this approximate problem and provide numerical solutions for the everted shape of the cylinder for Mooney–Rivlin materials. Chadwick and Haddon (1972) considered the problem for a class of strain–energy functions W introduced by Ogden (1972a), namely,

$$W(\lambda_1, \lambda_2, \lambda_3) = \sum_{i=1}^N \mu_i (\lambda_1^{\alpha_i} + \lambda_2^{\alpha_i} + \lambda_3^{\alpha_i} - 3) / \alpha_i, \quad \alpha_i \neq 0 \quad (1.1)$$

where $\lambda_1, \lambda_2, \lambda_3$ are the principal stretches of the deformation and $\alpha_1, \dots, \alpha_N, \mu_1, \dots, \mu_N, N$ are all parameters to be chosen. Here the attention was focused on the existence and uniqueness of the cylindrical everted solution within the class of perfect right circular cylinders (non–cylindrical shapes were not considered). In particular it was shown that solutions exist for all Ogden materials (1.1) provided that the restriction (3.2.6), which is normally used, was placed on the strain–energy form. However, little could be said about the uniqueness of the solution. Chadwick (1972) proved existence and uniqueness of the everted perfectly cylindrical shape for all Mooney–Rivlin materials. Here uniqueness refers to the non–existence of other perfectly cylindrical everted solutions satisfying the same equilibrium equations and boundary conditions, non–cylindrical shapes were not considered. Chadwick’s existence and uniqueness results have been strengthened by Adeleke (1983) where it was shown that the cylindrical everted shape exists for all materials satisfying the E–inequalities, as defined in Truesdell and Noll (1965) and given in (3.2.6).

We begin this work by considering the eversion of such cylinders. We also study the existence and uniqueness of such everted states. We then proceed to apply an incremental deformation to the everted cylinder to investigate the existence of

any possible bifurcation modes which will take the everted cylinder away from the cylindrical shape.

In chapter 2 we give the basic equations of elasticity which will provide us with the tools to study the problems considered in the resulting work. In chapter 3 we find everted states for several materials which all belong to the class of Ogden materials proposed by Ogden (1972a). Namely we find the everted states for a three-term Ogden material, the Neo-Hookean material and the Varga material. The strain-energy forms of these materials are given in (3.2.5), (3.2.4) and (3.2.3) respectively. We then proceed to obtain criteria for the existence of all incompressible materials that satisfy the weakened E- inequalities (3.3.4). This is basically an extension of the work done by Adeleke (1983) and follows a very similar path to a more general result. In particular this extension allows us to attain existence results for the Varga material and other strain-energy forms not governed by the work of Adeleke (1983).

In chapter 4 we study the eversion of compressible cylinders for a variety of strain-energy forms. In section 4.2 we introduce a new strain-energy form that admits an exact solution to the true eversion problem where the ends are pointwise traction free. This strain-energy form has no physical motivation. The ratio of bulk modulus to shear modulus is $2/3$ and so it is likely to be applicable to highly compressible foam rubbers. This could be possibly used as an alternative to the Blatz-Ko (1962) strain-energy. We look at the problems involved in attaining results on existence and uniqueness of everted compressible materials and, at the moment, the problem seems to be intractable. We solve the approximate problem for a range of compressible Varga materials ranging from highly compressible to almost incompressible and, for comparison, the Blatz-Ko (1962) material. One useful feature of the compressible Varga strain-energy is that the incompressible version is attained as a limiting case. These forms are given in (4.4.1) and (4.5.1) respectively. We note that this form is a member of a general class of materials proposed in Ogden (1972b).

After finding everted states for several materials we now apply an incremental deformation to the everted cylinder. This is done to examine possible bifurcation

modes of the everted shell and follows the ideas of Haughton and Ogden (1979b) where they examined bifurcation problems for the inflation of a cylinder. In chapter 5 we describe the equations governing the incremental deformation and derive the incremental equations of motion. The bifurcation problem here is different from the standard bifurcation problems encountered in elasticity. In most, if not all previous bifurcation problems considered, it is a measure of some loading or deformation that is the basic parameter. For example, in Ogden (1984, Section 6.3.4) the bifurcation of an incompressible spherical shell is considered. He examines the possibility of bifurcation by the application of a pressure P to the inner surface of the deformed sphere. Again in Haughton and Ogden (1979b) an incompressible cylinder is stretched and then subjected to an internal pressure to investigate bifurcation modes. Other geometries, such as a rectangular block or cube, have been subjected to dead loads. A plate with traction-free lateral surfaces was considered by Sawyers and Rivlin (1974). Here the authors were able to obtain necessary conditions for the existence of bifurcation points when the block was compressed along its length.

For the bifurcation of an everted cylinder we have the unusual situation where no extra loading is imposed on the surface of the body. We then have a different type of bifurcation criteria where the bifurcation will be regarded as a function of the initial thickness of the undeformed cylinder. Essentially we will evert the cylinder and once the incremental displacement is applied we will investigate if the tube undergoes a spontaneous bifurcation. The initial thickness of the tube is then adjusted until we find that bifurcation is possible.

In chapter 6 we describe the incremental displacement and use it to derive the incremental equations of motion in component form. Three different modes of bifurcation will be considered. These differ only on the degrees of freedom permitted in the incremental displacements. In cylindrical co-ordinates we discuss Asymmetric modes (with r, θ and z dependence), Prismatic modes (no z dependence) and Axisymmetric modes (no θ dependence).

Taking into account the nature of the material we provide separate treatments for incompressible and compressible materials. We will see that the incompress-

ibility condition permits some simplifications of the system. For both types of materials we solve the equations by using a separation of variables method. In doing so we introduce two parameters m and α which are mode numbers in the θ and z directions respectively. We are able to use these numbers to characterise the type of bifurcation mode that will occur. In the special case choosing $m = 0$ we remove the θ dependence and have an Axisymmetric mode produced. From the permissible range of values of α we will be able to choose α to add physical meaning to this parameter. We find that α is inversely proportional to the length of the tube so that we will be able to examine the widest possible range of tube lengths.

In each case we solve the problem numerically using two different numerical methods. We use the straightforward determinantal method used previously by other authors examining bifurcation problems in elasticity, see Haughton and Ogden (1979b) for example. However we find that the determinantal method is not adequate to cope with the demands of the present system. We then turn our attention to the compound matrix method which has been used before by Lakin, Nq and Reid (1978) and by Ng and Reid (1979) for problems in fluid mechanics. Lindsay (1992) also gives a very readable description of the method. A variety of authors have used the compound matrix method for similar homogeneous eigenvalue problems in fluid mechanics but it does not appear to have been used in elasticity since Gilbert and Backus (1966) used this approach for some linear elastic wave problems. We compare the results given by the two numerical methods and clearly show that the Compound Matrix method is superior. In our view this should become the method of choice for all bifurcation problems in elasticity. In section 6.2 we derive the incremental equations for the compressible case and repeat the analysis above. Here we consider the problem for the compressible Varga, the Blatz–Ko and the exact solution materials.

We present results on the bifurcation of incompressible everted cylinders in chapter 7. Considering incompressible bifurcations we begin with the relationship between the bifurcation modes and the length of the initial tube since, as stated above, only short examples have been considered experimentally. We then

examine the different results for various mode numbers and highlight those which deserve special attention. We then compare the basic eversion curve to the bifurcation curves for various mode numbers to help establish critical radii beyond which the tube will collapse. In this way we are using the non-dimensionalised undeformed inner radius as our bifurcation variable. For each material we provide results on the the two different numerical methods adopted and explain the differences. For the mode $m = 1$ we find that multiple solutions exist and concentrate on the limit of an infinitely long cylinder where we find that the bifurcation curve appears to intersect the eversion curve. We can then supply an analytical treatment of this special case in order to discover the bifurcation criteria. Finally we consider $m = 0$, which is an Axisymmetric bifurcation, which will provide a simplified set of equations.

In chapter 8 we present results on the bifurcation of compressible everted cylinders. Here we study the bifurcation modes in an analogous way to the incompressible case. We begin by examining the effects of the length to radius ratio of the tube. We may expect different results for cylinders of varying compressibility as we show in chapter 4 that the everted tube behaves very differently for highly compressible materials. As in the incompressible case we attempt an analytical treatment of the limiting cases $m \rightarrow \infty, \alpha \rightarrow 0$, i.e. the infinite mode and infinitely long cylinder cases. We then proceed to vary the mode number m to see how it effects the bifurcation points produced. For all three materials considered here, the compressible Varga, the Blatz–Ko and the Exact material, we adopt the same strategy. Here we differ from the incompressible case because we do not have $r = r(R)$ analytically. We again use the undeformed thickness as our independent variable. We do this so that we are able to establish critical values of the cylinder thickness beyond which we may expect the tube to collapse. With the compressible Varga material we have an additional variable to consider, the compressibility parameter. This should enable us to complete the picture on the effect the compressibility of the material has on the critical thickness ratios attained. We then compare the graphical results for all compressible materials to look for any recurring themes.

In chapter 9 we discuss the solution procedure to the bifurcation problem. We essentially show that the problem is reduced to a homogeneous set of ordinary differential equations. We give a description of the compound matrix and show in some detail how it is applied to the problems considered here. The importance of this method is stressed as it enables us to solve the numerical problem efficiently and with accuracy.

The work presented on the eversion and bifurcation of incompressible elastic cylinders has been published in Haughton and Orr (1995). In this paper we also include a brief demonstration of the differences between the two numerical methods. However, the paper doesn't include the proof for the extension of the existence and uniqueness criteria to cover all strain-energy functions. This result is merely stated. I plan to produce a paper on the results obtained for the compressible materials. This paper should follow the same ideas presented in the incompressible paper.

One aspect of the problem that hasn't been treated here is the stability of the bifurcated cylinders. There is also the problem of attaining existence and uniqueness conditions for the compressible case where we found, by our methods, that the inability to express $r = r(R)$ halted any progress towards an analytical solution. Although there may be some compressible materials for which we can express the deformation as $r = r(R)$, such as the exact material considered in this work, we find that in general this will not be the case.

Chapter 2

Basic Equations

In this section we introduce the basic equations of elasticity, following the approach of Truesdell and Noll (1965), Wang and Truesdell (1973) and Ogden (1984). We also introduce the notation adopted in this thesis.

2.1 Kinematics

We consider a body which in an unstressed state occupies the region B_o in three-dimensional Euclidean space. We refer to this region as the reference or undeformed configuration. On choosing an arbitrary origin we assign the position vector \mathbf{X} to material points of B_o . Deformation of the body into a new configuration B , which we call the current or deformed configuration, maps the material point \mathbf{X} to \mathbf{x} where the deformation is described by

$$\mathbf{x} = \chi(\mathbf{X}) , \tag{2.1.1}$$

where $\chi : B_o \rightarrow B$ is a bijection. The mapping χ is called a deformation of the body from B_o to B . We assume the body in question is *isotropic*. That is, the material properties of the material at a point \mathbf{X} are the same in all directions. The deformation gradient tensor \mathbf{F} is defined as

$$\mathbf{F} = \text{Grad } \mathbf{x} , \tag{2.1.2}$$

where Grad is the gradient operator in the reference configuration. The deformation (2.1.1) is *homogeneous* if the deformation gradient \mathbf{F} does not depend on \mathbf{X} .

We define

$$J = \det\left(\frac{\partial x_i}{\partial X_j}\right) = \det \mathbf{F} . \quad (2.1.3)$$

Physically we interpret J as the relative change in volume when a body occupying infinitesimal volume dV is deformed into a body occupying a volume dv . Since J must then be positive we conclude that \mathbf{F} is non-singular. In view of this we apply the Polar Decomposition theorem on \mathbf{F} which permits the unique decompositions

$$\mathbf{F} = \mathbf{R}\mathbf{U}, \mathbf{F} = \mathbf{V}\mathbf{R} , \quad (2.1.4)$$

where \mathbf{U} and \mathbf{V} are positive-definite symmetric tensors and \mathbf{R} is proper orthogonal. We expand this by defining the right and left Cauchy-Green strain tensors as

$$\mathbf{C} = \mathbf{F}^T \mathbf{F} , \mathbf{B} = \mathbf{F} \mathbf{F}^T \quad (2.1.5)$$

respectively. Considering (2.1.4) it can be seen that \mathbf{B} and \mathbf{C} are symmetric with

$$\mathbf{C} = \mathbf{U}^2 , \mathbf{B} = \mathbf{V}^2 . \quad (2.1.6)$$

The characteristic equation for \mathbf{B} is

$$\det(B_{kl} - \lambda^2 \delta_{kl}) = 0 ,$$

where λ^2 is an eigenvalue of \mathbf{B} with λ the corresponding eigenvalue for \mathbf{V} . The characteristic equation of \mathbf{B} can then be expressed as the polynomial

$$\lambda^6 - I_1 \lambda^4 + I_2 \lambda^2 - I_3 = 0 , \quad (2.1.7)$$

where

$$\begin{aligned} I_1 &= \text{tr} \mathbf{B}, \\ I_2 &= \frac{1}{2} \{ (\text{tr} \mathbf{B})^2 - \text{tr} \mathbf{B}^2 \} , \\ I_3 &= \det \mathbf{B} , \end{aligned} \quad (2.1.8)$$

and tr denotes the trace. The quantities I_1 , I_2 and I_3 are defined as the principal invariants of \mathbf{B} . It should be noted that on considering $\mathbf{C} = \mathbf{U}^2$, the right Cauchy-Green strain tensor, for the above treatment, we would obtain identical invariants but the principal axes do not coincide in general. We also observe a useful physical interpretation of I_3 . Considering (2.1.3), (2.1.4) we write

$$I_3 = \det \mathbf{C} = (\det \mathbf{F})^2 = J^2 . \quad (2.1.9)$$

For an incompressible material we may also write

$$I_3 = 1 , \tag{2.1.10}$$

and hence we also have the incompressibility constraint

$$J = 1 . \tag{2.1.11}$$

Thus for an incompressible material with solutions $\lambda_1^2, \lambda_2^2, \lambda_3^2$ to the characteristic equation (2.1.7) we can express (2.1.8) in terms of the eigenvalues as

$$\begin{aligned} I_1 &= \lambda_1^2 + \lambda_2^2 + \lambda_3^2 , \\ I_2 &= \lambda_1^{-2} + \lambda_2^{-2} + \lambda_3^{-2} , \\ I_3 &= 1 , \end{aligned} \tag{2.1.12}$$

where the eigenvalues are known as the principal stretches, each of which is taken to be positive. Here we have used $I_3 = 1$ to express I_2 as above. For a compressible material we lose the constraint $I_3 = 1$ and subsequently write the invariants as

$$\begin{aligned} I_1 &= \lambda_1^2 + \lambda_2^2 + \lambda_3^2 , \\ I_2 &= \lambda_1^2 \lambda_2^2 + \lambda_2^2 \lambda_3^2 + \lambda_1^2 \lambda_3^2 , \\ I_3 &= J^2 = \lambda_1^2 \lambda_2^2 \lambda_3^2 . \end{aligned} \tag{2.1.13}$$

2.2 Strain-energy and Stress-Strain Relations

For the deformations that follow, the strain-energy function W , which characterises an isotropic hyperelastic solid, is a symmetric function

$$W = W(\mathbf{F}) . \quad (2.2.1)$$

In terms of the principal stretches $\lambda_1, \lambda_2, \lambda_3$ (2.2.1) is given by

$$W = W(\lambda_1, \lambda_2, \lambda_3) = \tilde{W}(I_1, I_2, I_3) , \quad (2.2.2)$$

where the invariants are given above. We can see that the strain-energy can be simplified for a constrained material, which has invariants (2.1.12), to

$$W = \hat{W}(\lambda_1, \lambda_2) = \overline{W}(I_1, I_2) . \quad (2.2.3)$$

We now consider the surface traction vector \mathbf{t} which is defined as the load per unit area in \mathbf{B} .

$$\mathbf{t} = \boldsymbol{\sigma} \mathbf{n} , \quad (2.2.4)$$

where $\boldsymbol{\sigma}$ is the *Cauchy stress tensor* and \mathbf{n} is a unit normal in \mathbf{B} . For a body which is self-equilibrated with no body forces the equation of motion is

$$\operatorname{div} \boldsymbol{\sigma} = \mathbf{0} . \quad (2.2.5)$$

For the problems considered in this thesis, the equation of motion (2.2.5) will not always be suitable as it employs \mathbf{x} as the independent variable. In particular the basic eversion problems considered later, for both compressible and incompressible materials, will use different formulations. To combat this problem we define the *nominal stress tensor* \mathbf{S} . This stress, whose transpose \mathbf{S}^T is referred to as the Piola-Kirchhoff stress, is evaluated in terms of the reference variable \mathbf{X} . This will be utilised when we consider the eversion of compressible materials. In this case we lose the constraint (2.1.11) and are therefore unable to calculate \mathbf{x} explicitly. We therefore introduce

$$\mathbf{S} = J \mathbf{F}^{-1} \boldsymbol{\sigma} , \quad (2.2.6)$$

where J , \mathbf{F} are as before. We should note that although $\boldsymbol{\sigma}$ is symmetric, i.e. $\boldsymbol{\sigma}^T = \boldsymbol{\sigma}$, in general \mathbf{S} is not symmetric. The corresponding equation to (2.2.5) is then

$$\text{Div } \mathbf{S} = \mathbf{0} , \quad (2.2.7)$$

where Div is the divergence operator in the reference configuration. The corresponding surface traction vector \mathbf{T} is

$$\mathbf{T} = \mathbf{S}^T \mathbf{N} , \quad (2.2.8)$$

where \mathbf{N} is a unit normal in B_o .

2.3 Compressible Elasticity

A convenient starting point for the theory of compressible elasticity is to postulate a set of *constitutive equations* in which the stress is a single-valued function of the deformation gradient tensor. For an isotropic elastic solid the *Cauchy stress* $\boldsymbol{\sigma}$ is

$$\boldsymbol{\sigma} = \mathbf{G}(\mathbf{F}) = \mathbf{G}(\mathbf{VR}) , \quad (2.3.1)$$

where \mathbf{G} is the response function of the material relative to a reference configuration. Since \mathbf{G} is an isotropic function of \mathbf{B} we are able to write

$$\boldsymbol{\sigma} = \psi_0 \mathbf{1} + \psi_1 \mathbf{B} + \psi_2 \mathbf{B}^{-1} , \quad (2.3.2)$$

where ψ_0, ψ_1, ψ_2 , given in Truesdell and Noll (1965, p148), are functions of the invariants of the left stretch tensor \mathbf{B} defined in (2.1.13) and

$$\psi_0 = \frac{2}{I_3^{1/2}} \left(I_2 \frac{\partial W}{\partial I_2} + I_3 \frac{\partial W}{\partial I_3} \right) , \quad \psi_1 = \frac{2}{I_3^{1/2}} \frac{\partial W}{\partial I_1} , \quad \psi_2 = -2I_3^{1/2} \frac{\partial W}{\partial I_2} . \quad (2.3.3)$$

Consider a surface element $d\mathbf{a}$ at a point P of B with position vector \mathbf{x} and let \mathbf{n} be a current unit normal to one side of $d\mathbf{a}$. The force per unit area acting on that side of $d\mathbf{a}$ is

$$\mathbf{t} = \mathbf{t}(\mathbf{x}, \mathbf{n}) . \quad (2.3.4)$$

This vector will be in the direction \mathbf{n} only for those directions \mathbf{n} which satisfy

$$\mathbf{t}(\mathbf{x}, \mathbf{n}) = \rho \mathbf{n} , \quad (2.3.5)$$

for some scalar ρ . Using (2.2.4) we can write (2.3.5) in component form as

$$(\sigma_{ij} - \rho \delta_{ij}) n_j = 0 , \quad (2.3.6)$$

where the summation convention is not implied. Henceforth unless explicitly stated the summation convention is not implied throughout this thesis. The directions of \mathbf{n} for which this is possible lie along the principal axes of $\boldsymbol{\sigma}$ which are called the *principal axes of stress*. The associated values of ρ are the principal values of $\boldsymbol{\sigma}$ and are known as the *principal stresses*. These are the real roots obtainable from the characteristic equation

$$\det(\sigma_{ij} - \rho \delta_{ij}) = 0 . \quad (2.3.7)$$

The principal stresses can then be related to the principal stretches λ_i by

$$\sigma_{ii} = \psi_o + \psi_1 \lambda_i^2 + \psi_2 \lambda_i^{-2}, i = (1, 2, 3), \quad (2.3.8)$$

where we may regard ψ_o, ψ_1, ψ_2 as symmetric functions of $\lambda_1, \lambda_2, \lambda_3$. In terms of the strain-energy W and the deformation gradient \mathbf{F} we can propose a *constitutive equation*

$$J\boldsymbol{\sigma} = \mathbf{F} \frac{\partial W}{\partial \mathbf{F}^T}, \quad (2.3.9)$$

which, on using (2.2.6), can be recast as

$$\mathbf{S} = \frac{\partial W}{\partial \mathbf{F}^T}. \quad (2.3.10)$$

We are able to express the principal stresses in a similar way:

$$J\sigma_{ii} = \lambda_i \frac{\partial W}{\partial \lambda_i}. \quad (2.3.11)$$

2.4 Incompressible Elasticity

In the theory of incompressible elasticity we have the constraint $\det \mathbf{F} = 1$. This has the effect of stipulating that incompressible materials can only sustain deformations where there is no change in volume i.e. *isochoric deformations*. We therefore have to re-examine our constitutive assumptions. We retain

$$W = W(\mathbf{F}) . \quad (2.4.1)$$

However, in place of the constitutive assumption (2.3.1) for compressible materials, we suppose the constitutive equation has the form

$$\boldsymbol{\sigma} = -p\mathbf{1} + \mathbf{f}(\mathbf{F}) . \quad (2.4.2)$$

where p is an undetermined scalar and \mathbf{f} is a symmetric function known as the response function. The quantity p is a Lagrange multiplier which arises due to the incompressibility constraint and can be interpreted in a physical manner as given below. By repeating the above analysis we produce

$$\boldsymbol{\sigma} = \phi_o\mathbf{1} + \phi_1\mathbf{B} + \phi_2\mathbf{B}^{-1} , \quad (2.4.3)$$

where ϕ_o, ϕ_1, ϕ_2 are functions of the invariants of the left stretch tensor \mathbf{B} and

$$\phi_o = -p , \quad \phi_1 = 2\frac{\partial W}{\partial I_1} , \quad \phi_2 = -2\frac{\partial W}{\partial I_2} , \quad (2.4.4)$$

with p an arbitrary scalar. In component form the principal stresses are connected to the principal stretches by

$$\sigma_{ii} = \phi_o + \phi_1\lambda_i^2 + \phi_2\lambda_i^{-2} . \quad (2.4.5)$$

The corresponding constitutive equation is then

$$\boldsymbol{\sigma} = \mathbf{F}\frac{\partial W}{\partial \mathbf{F}^T} - p\mathbf{1} , \quad (2.4.6)$$

and, in component form, the principal stresses are written

$$\sigma_{ii} = \lambda_i \frac{\partial W}{\partial \lambda_i} - p . \quad (2.4.7)$$

The scalar p can be regarded as acting as a *hydrostatic pressure* and is obtainable from the equilibrium equation (2.2.5) with appropriate boundary conditions.

Chapter 3

Eversion of Incompressible Cylinders

3.1 Basic Eversion Equations

Suppose that the undeformed incompressible isotropic homogeneous elastic tube occupies the region

$$A \leq R \leq B, \quad 0 \leq \Theta \leq 2\pi, \quad 0 \leq Z \leq L, \quad (3.1.1)$$

where (R, Θ, Z) are cylindrical polar coordinates. The cylinder is now everted into another right circular cylinder occupying the region

$$a \leq r \leq b, \quad 0 \leq \theta \leq 2\pi, \quad -\ell \leq z \leq 0, \quad (3.1.2)$$

where (r, θ, z) are also cylindrical polar coordinates. Note in particular that the surface $R = A$ is mapped to the surface $r = b$ and $R = B$ is mapped to $r = a$. We assume that the deformation can be described by

$$r = r(R), \quad \theta = \Theta, \quad z = -\lambda Z, \quad (3.1.3)$$

where $\lambda > 0$ is a constant such that $\ell = \lambda L$. The components of the deformation gradient \mathbf{F} referred to cylindrical coordinates are then

$$\mathbf{F} = \begin{bmatrix} \frac{dr}{dR} & 0 & 0 \\ 0 & \frac{r}{R} & 0 \\ 0 & 0 & -\lambda \end{bmatrix}. \quad (3.1.4)$$

The principal stretches of the deformation can be written

$$\lambda_r = -\frac{dr}{dR}, \quad \lambda_\theta = \frac{r}{R}, \quad \lambda_z = \lambda, \quad (3.1.5)$$

where the subscripts denote the appropriate directions. Since the material is incompressible we must have $\det(\mathbf{F}) = 1$ and so

$$r\lambda \frac{dr}{dR} = -R, \quad (3.1.6)$$

hence

$$r^2 = a^2 + (B^2 - R^2)/\lambda. \quad (3.1.7)$$

This also gives the connexion

$$b^2 = a^2 + (B^2 - A^2)/\lambda. \quad (3.1.8)$$

The equilibrium equations for the deformation above reduce to the single equation

$$r \frac{d\sigma_{rr}}{dr} + (\sigma_{rr} - \sigma_{\theta\theta}) = 0, \quad (3.1.9)$$

where the principal Cauchy stresses σ_{rr} , $\sigma_{\theta\theta}$ and σ_{zz} can be written in terms of the strain-energy function $W = W(\lambda_r, \lambda_\theta, \lambda_z)$ of the material as

$$\sigma_{ii} = \sigma_i - p = \lambda_i \frac{\partial W}{\partial \lambda_i} - p, \quad (3.1.10)$$

where the subscript i should be regarded as one of (r, θ, z) and $p = p(r)$ is the hydrostatic pressure that arises due to the incompressibility constraint.

Ideally we would like to satisfy the point-wise boundary conditions of zero traction on the surface of the cylinder,

$$\sigma_{rr}(a) = \sigma_{rr}(b) = 0, \quad 0 \leq \theta \leq 2\pi, \quad -\lambda L \leq z \leq 0, \quad (3.1.11)$$

and

$$\sigma_{zz}(0) = \sigma_{zz}(-\lambda L) = 0, \quad 0 \leq \theta \leq 2\pi, \quad a \leq r \leq b. \quad (3.1.12)$$

Unfortunately the point-wise end conditions (3.1.12) are not consistent with the assumption $r = r(R)$, except in exceptional cases. [In general $\sigma_{zz} = \sigma_{zz}(\lambda_r, \lambda_\theta, \lambda_z)$ and will not depend explicitly on z , thus (3.1.12) is equivalent to insisting that

$\sigma_{zz} \equiv 0$. Using (3.1.10), (3.1.9), (3.1.5) and (3.1.7) we see that, in general, $\sigma_{zz} = \sigma_{zz}(R)$ which will not be identically zero]. Following Rivlin (1949) and all subsequent authors who have considered this problem, we look instead for approximate solutions that satisfy (3.1.11) and give a zero resultant load N on the ends, i.e., we replace the end conditions (3.1.12) with the approximate, averaged, end conditions

$$N = 2\pi \int_a^b r \sigma_{zz} dr = 0, \quad z = -\lambda L, 0. \quad (3.1.13)$$

The eversion problem is now fully defined, (3.1.9) with one of (3.1.11) gives the hydrostatic pressure $p(r)$ and the remaining equations (3.1.11)₂ and (3.1.13) give the axial stretch λ and the deformed inner radius a . Using (3.1.8) completes the definition of the deformed geometry. Rather than using equations (3.1.9), (3.1.11) and (3.1.13) as they now appear we can simplify them by eliminating the hydrostatic pressure $p(r)$ as follows. Integrating (3.1.9) and using (3.1.10) and (3.1.11)₁ we have

$$p(r) = \sigma_r + \int_a^r \left(\frac{\sigma_r - \sigma_\theta}{r} \right) dr. \quad (3.1.14)$$

The condition of a traction-free curved surface can now be written

$$\int_a^b \left(\frac{\sigma_r - \sigma_\theta}{r} \right) dr = 0. \quad (3.1.15)$$

having used (3.1.11)₂. Substituting (3.1.10) with (3.1.14) into (3.1.13) produces

$$\int_a^b r(\sigma_z - \sigma_r) dr + \int_a^b r \left[\int_a^r \left(\frac{\sigma_\theta(s) - \sigma_r(s)}{s} \right) ds \right] dr = 0. \quad (3.1.16)$$

Integrating the second term by parts and using (3.1.15) we rewrite the end conditions as

$$\int_a^b r(2\sigma_z - \sigma_r - \sigma_\theta) dr = 0. \quad (3.1.17)$$

Equations (3.1.15) and (3.1.17) with (3.1.5), (3.1.7), (3.1.8) and (3.1.10) are then two simultaneous equations for λ and a . These equations can then be solved numerically for specific forms of strain–energy functions.

3.2 Material Forms

In this chapter we shall consider three explicit material models, all three are members of a general class of strain–energy functions proposed by Ogden (1972a);

$$W(\lambda_1, \lambda_2, \lambda_3) = \sum_{i=1}^N \mu_i (\lambda_1^{\alpha_i} + \lambda_2^{\alpha_i} + \lambda_3^{\alpha_i} - 3) / \alpha_i, \quad (3.2.1)$$

where $N, \mu_1, \dots, \mu_N, \alpha_1, \dots, \alpha_N$ are parameters to be chosen. The constraint

$$\mu_i \alpha_i > 0 \quad \text{for each } i, \quad (3.2.2)$$

is usually adopted as it is sufficient (but not necessary) to ensure that the ground state shear modulus of the material $\mu = \frac{1}{2} \sum_{i=1}^N \mu_i \alpha_i$ is positive. Firstly, the Varga material, which has a single term strain–energy function $N = 1, \alpha_1 = 1$ and $\mu_1 = 2\mu$, i.e.,

$$W = 2\mu(\lambda_1 + \lambda_2 + \lambda_3 - 3). \quad (3.2.3)$$

This material is introduced in Varga (1966). The Neo–Hookean material ($N = 1, \alpha_1 = 2, \mu_1 = \mu$) has strain–energy function

$$W = \frac{\mu}{2}(\lambda_1^2 + \lambda_2^2 + \lambda_3^2 - 3), \quad (3.2.4)$$

and a three–term material

$$\begin{aligned} \alpha_1 &= 1.3, & \alpha_2 &= 5.0, & \alpha_3 &= -2.0, \\ \mu_1 &= 1.491\mu, & \mu_2 &= 0.003\mu, & \mu_3 &= -0.0237\mu, \end{aligned} \quad (3.2.5)$$

which was found by Ogden (1972a) to give good agreement with a variety of experimental data (taking $\mu = 4.225 \text{ kg cm}^{-2}$).

The existence and uniqueness of solutions for (λ, a) has received some formal attention. Chadwick (1972) has established both existence and uniqueness for Mooney–Rivlin materials and hence for the Neo–Hookean material (3.2.4). Chadwick and Haddon (1972) have shown that at least one solution exists for Ogden materials (3.2.1) with (3.2.5). Adeleke (1983) has shown that values of (λ, a) exist and are unique provided that the strain–energy function of the material satisfies the E–inequalities given by

$$\frac{\partial W}{\partial I_1}(I_1, I_2) > 0, \quad \frac{\partial W}{\partial I_2}(I_1, I_2) \geq 0, \quad (3.2.6)$$

where I_1, I_2 are the principal invariants of $\mathbf{B} = \mathbf{F}\mathbf{F}^T$, namely $I_1 = \text{tr}\mathbf{B}$, $I_2 = \text{tr}\mathbf{B}^{-1}$, and $W = W(I_1, I_2)$ since the incompressibility condition gives $I_3 = \det \mathbf{B} = 1$.

Before proceeding with any numerical calculations we shall discuss the existence and uniqueness of an everted state for all materials whose strain-energy satisfies the appropriate constraints given below.

3.3 Existence and Uniqueness

Here we seek to generalise the results of Adeleke (1983) where he proved the existence of an everted shell for any incompressible material whose strain-energy satisfies (3.2.6). Although this provides conditions on the eversion of many materials it has the draw-back that you must be able to express the strain-energy W in terms of I_1, I_2 , as given in (2.1.12) for an incompressible material. However, with materials such as the Varga (3.2.3) this is often not practical. We therefore propose to solve the problem for a more general set of invariants with conditions (3.2.6) suitably modified.

Consider an incompressible isotropic elastic material, then we can write

$$\boldsymbol{\sigma} = -p\mathbf{1} + \psi_\alpha(I_{\alpha 1}, I_{\alpha 2})\mathbf{B} + \psi_{-\alpha}(I_{\alpha 1}, I_{\alpha 2})\mathbf{B}^{-1}, \quad (3.3.1)$$

where $\boldsymbol{\sigma}$ is the Cauchy stress, $\mathbf{B} = \mathbf{F}\mathbf{F}^T$ the left Cauchy-Green tensor, p the hydrostatic pressure as defined in (2.4.7) and $\psi_\alpha, \psi_{-\alpha}$ are arbitrary functions of the principal invariants defined as

$$\begin{aligned} I_{\alpha 1} &= \lambda_1^\alpha + \lambda_2^\alpha + \lambda_3^\alpha, \\ I_{\alpha 2} &= \lambda_1^{-\alpha} + \lambda_2^{-\alpha} + \lambda_3^{-\alpha}, \end{aligned} \quad (3.3.2)$$

where $\alpha > 0$ is a parameter. Since the material is incompressible, $W(I_{\alpha 1}, I_{\alpha 2})$ is the strain-energy of the material. We then write the principal components of (3.3.1) in component form as

$$\sigma_{ii} = -p + \alpha[W_{\alpha 1}\lambda_i^\alpha - W_{\alpha 2}\lambda_i^{-\alpha}], \quad (3.3.3)$$

where

$$W_{\alpha i} = \frac{\partial W}{\partial I_{\alpha i}}.$$

Before proceeding further, we make use of the E-inequalities to provide conditions on the derivatives $W_{\alpha i}$. These inequalities, although having no theoretical motivation, are supported by the available experimental data. As detailed in Truesdell and Noll (1965) any material which satisfies the E-inequalities will satisfy the Baker-Ericksen inequalities. Physically the Baker-Ericksen inequalities say that

the greatest principal stress always occurs in the direction of the greatest principal stretch. We assume the extended E-inequalities

$$\frac{\partial W}{\partial I_{\alpha 1}}(I_{\alpha 1}, I_{\alpha 2}) > 0, \quad \frac{\partial W}{\partial I_{\alpha 2}}(I_{\alpha 1}, I_{\alpha 2}) \geq 0, \quad \text{for some } \alpha > 0. \quad (3.3.4)$$

We find that for any $\alpha > 0$ (3.3.4) implies the Baker–Ericksen inequalities. For $\alpha = 2$ (3.3.4) is equivalent to the E-inequalities. Hence we will prove the more general result for any incompressible material whose strain–energy satisfies (3.3.4).

For the deformation described in (3.1.3) we have

$$r^2 = a^2 + (B^2 - R^2)/\lambda_z. \quad (3.3.5)$$

As detailed above the problem is reduced to finding solutions of (3.1.15) and (3.1.16).

Using the incompressibility condition and (3.1.5) we write

$$\lambda_1 = \frac{1}{\lambda_2 \lambda_3}, \quad \lambda_2 = \frac{r}{R}, \quad \lambda_3 = \lambda_z. \quad (3.3.6)$$

Thus, substituting (3.3.3) into (3.1.15) we find the problem for traction free curved surfaces reduces to

$$H = \alpha \int_a^b \frac{1}{r} (\lambda_1^\alpha - \lambda_2^\alpha) [W_{\alpha 1} + \lambda_z^\alpha W_{\alpha 2}] dr = 0. \quad (3.3.7)$$

A similar substitution for the axial load N reduces to

$$N = \alpha \int_a^b r \left\{ W_{\alpha 1} (\lambda_1^\alpha + \lambda_2^\alpha - \frac{2}{\lambda_1^\alpha \lambda_2^\alpha}) - W_{\alpha 2} \lambda_z^\alpha (\lambda_1^\alpha + \lambda_2^\alpha - 2\lambda_1^{2\alpha} \lambda_2^{2\alpha}) \right\} dr = 0. \quad (3.3.8)$$

As has been shown before the problem of finding an everted cylindrical shell can be regarded as choosing a, λ_z such that (3.3.7), (3.3.8) have a solution. For the eversion problem we have $r(A) = b$, which in (3.3.5) produces

$$b = \sqrt{a^2 + (B^2 - A^2)/\lambda_z}. \quad (3.3.9)$$

Taking each function H and N in turn we will show a solution exists provided only that the inequalities (3.3.4) are satisfied for some $\alpha > 0$. This will be achieved by

application of the Intermediate Value Theorem and closely following the methods adopted by Adeleke (1983).

Now considering (3.3.7) we express the integral for H in terms of R , the undeformed radial variable, to achieve

$$H(a) = \frac{\alpha}{\lambda_z} \int_A^B \frac{(\lambda_2^\alpha - \lambda_1^\alpha)}{r^2} (W_{\alpha 1} + \lambda_z^\alpha W_{\alpha 2}) R dR, \quad (3.3.10)$$

where we have made use of the incompressibility condition (3.1.6). From (3.3.5) we write

$$r^2 = DR^2 + E,$$

where $D = -1/\lambda_z$, $E = a^2 + B^2/\lambda_z$ and we also define

$$C = \frac{E}{D} = -(\lambda_z a^2 + B^2). \quad (3.3.11)$$

We now assume that $C \in [-2B^2, -(A^2 + B^2)]$ so that the extremities of the interval correspond to

$$a^2 = \frac{B^2}{\lambda_z}, \quad a^2 = \frac{A^2}{\lambda_z}. \quad (3.3.12)$$

We will investigate the sign of (3.3.10) at each endpoint (3.3.12) in order to isolate a root of H for $\lambda_z > 0$, $a \in (A/\lambda_z^{1/2}, B/\lambda_z^{1/2})$. From (3.3.5), (3.3.6) we may write

$$\lambda_1^\alpha = \frac{R^\alpha}{\lambda_z^\alpha (a^2 + (B^2 - R^2)/\lambda_z)^{\alpha/2}}, \quad \lambda_2^\alpha = \frac{(a^2 + (B^2 - R^2)/\lambda_z)^{\alpha/2}}{R^\alpha}. \quad (3.3.13)$$

It is clear that in (3.3.10) the difference of the two eigenvalue terms is of importance in determining the sign of the integrand since all remaining terms are positive. We shall consider each endpoint separately.

Case(i)

$C = -2B^2$ corresponds to $a^2 = B^2/\lambda_z$, hence substitution into (3.3.13) produces

$$\lambda_2^\alpha - \lambda_1^\alpha = -\frac{R^{2\alpha} - (2B^2 - R^2)^\alpha}{R^\alpha (2B^2 - R^2)^{\alpha/2} \lambda_z^{\alpha/2}}.$$

Since $B > R$,

$$(2B^2 - R^2) \geq R^2,$$

so

$$(2B^2 - R^2)^\alpha \geq R^{2\alpha}, \quad \alpha > 0.$$

Hence $\lambda_2^\alpha - \lambda_1^\alpha \geq 0$ and from (3.3.10) we conclude $H(B/\lambda_z^{1/2}) \geq 0$.

Case(ii)

Firstly, we observe from (3.3.12) that $C = -A^2 - B^2$ corresponds to $a^2 = A^2/\lambda_z$. On application of the method in case(i) we find the sign of $\lambda_2^\alpha - \lambda_1^\alpha$ is indeterminate and thus we adopt the following. Consider the change of variable

$$x = \frac{R^2}{A^2 + B^2} - \frac{1}{2}, \quad (3.3.14)$$

then evaluation at $R = A, B$ gives

$$x_A = \frac{A^2 - B^2}{2(A^2 + B^2)}, \quad x_B = \frac{B^2 - A^2}{2(A^2 + B^2)} = -x_A, \quad (3.3.15)$$

where we can see $x_B < \frac{1}{2}$. From (3.3.13) and using (3.3.14) we obtain

$$\lambda_1 = \left(\frac{1+2x}{1-2x}\right)^{1/2} \lambda_z^{-1/2}, \quad \lambda_2 = \left(\frac{1-2x}{1+2x}\right)^{1/2} \lambda_z^{-1/2}.$$

Thus $I_{\alpha 1}$ and $I_{\alpha 2}$ are clearly even functions of x and hence so are the $W_{\alpha i}$.

Substitution of (3.3.14) and (3.3.15) into (3.3.10) allows us to write

$$H = \frac{\alpha}{2\lambda_z^{\alpha/2}} \int_{-x_B}^{x_B} \left[\frac{(\frac{1}{2} - x)^\alpha - (x + \frac{1}{2})^\alpha}{(x + \frac{1}{2})^{\frac{\alpha}{2}} (\frac{1}{2} - x)^{\frac{\alpha}{2} + 1}} \right] (W_{\alpha 1} + \lambda_z^\alpha W_{\alpha 2}) dx. \quad (3.3.16)$$

As in case(i) we use (3.3.4) to see that $(W_{\alpha 1} + \lambda_z^\alpha W_{\alpha 2})$ is again positive. Thus far we have essentially mimicked the proof of Adeleke (1983) where he proved the existence of an everted shell for $\alpha = 2$. Here we are not able to follow the method that Adeleke proposed since, as will become clear in due course, losing $\alpha = 2$ restricts our ability to use the properties of even and odd functions to manipulate (3.3.10). At this point Adeleke (1983) was able to decompose (3.3.16) into an odd part and an even negative part to establish $H(A^2/\lambda_z) < 0$. However, as can be found from (3.3.16) we can only apply this for $\alpha = 2$. For a general α we first note from (3.3.16) that

$$\frac{(\frac{1}{2} - x)^\alpha - (x + \frac{1}{2})^\alpha}{(x + \frac{1}{2})^{\frac{\alpha}{2}} (\frac{1}{2} - x)^{\frac{\alpha}{2} + 1}} = \left[\frac{(\frac{1}{2} - x)^\alpha - (x + \frac{1}{2})^\alpha}{(x + \frac{1}{2})^{\frac{\alpha}{2}} (\frac{1}{2} - x)^{\frac{\alpha}{2}}} \right] \left[1 + \frac{(\frac{1}{2} + x)}{(\frac{1}{2} - x)} \right].$$

Considering the above it is clear that the first term is an odd function of x and hence, since the integration is over $[-x_B, x_B]$, the integral of this term is trivially zero. We can then write

$$H = \frac{\alpha}{2\lambda_z^{\alpha/2}} \int_{-x_B}^{x_B} F(x) dx. \quad (3.3.17)$$

where

$$F(x) = \left[\frac{(\frac{1}{2} - x)^\alpha - (x + \frac{1}{2})^\alpha}{(x + \frac{1}{2})^{\frac{\alpha}{2}} (\frac{1}{2} - x)^{\frac{\alpha}{2}}} \right] \left[\frac{(\frac{1}{2} + x)}{(\frac{1}{2} - x)} \right] (W_{\alpha 1} + \lambda_z^\alpha W_{\alpha z}), \quad -\frac{1}{2} < x < \frac{1}{2}. \quad (3.3.18)$$

We are now able to turn our attention to the behaviour of $F(x)$. Firstly, we observe $F(0) = 0$.

If $0 < x < \frac{1}{2}$ then

$$0 < \frac{1}{2} - x < \frac{1}{2} + x$$

Thus from (3.3.18),

$$F(x) < 0 \text{ provided } \alpha > 0.$$

Considering $0 < x < \frac{1}{2}$ we can write

$$F(-x) = -\left(\frac{\frac{1}{2} - x}{\frac{1}{2} + x}\right)^2 F(x) < |F(x)|,$$

We can now categorise the integrand as follows:

- (i) $F(x) < 0$ for $x > 0$,
- (ii) $F(x) > 0$ for $x < 0$,
- (iii) $F(0) = 0$,
- (iv) $|F(x)| > |F(-x)|$ for $0 < x \leq x_B$.

To prove $H(A^2/\lambda) < 0$ we define

$$G(x) = \begin{cases} F(x), & x > 0, \\ 0, & x = 0, \\ -\left(\frac{\frac{1}{2} - x}{\frac{1}{2} + x}\right)^2 F(x), & x < 0. \end{cases} \quad (3.3.19)$$

Thus use of (3.3.19) in (3.3.17) produces

$$H = \frac{\alpha}{2\lambda_z^{\alpha/2}} \left\{ \int_{-x_B}^0 G(x) dx + \int_0^{x_B} G(x) dx \right\}. \quad (3.3.20)$$

We now consider the lower Riemann Sum of $H(A^2/\lambda_z)$. Let

$$P_n : -x_B = -1/2 = -1/2 + 0/n < -1/2 + 1/n < \dots < -1/2 + n/n = 1/2 = x_B$$

be a dissection of the closed interval $[-x_B, x_B]$. Then $|P_n| = 1/n \rightarrow 0$ as $n \rightarrow \infty$.

The Lower Riemann Sum S_n for $H(A^2/\lambda_z)$ can then be expressed

$$S_n = \sum_{i=0}^n G\left(\frac{i}{n}\right) \frac{1}{n} + \sum_{i=0}^n G\left(-\frac{i}{n}\right) \frac{1}{n} \quad \text{where } 0 < x < 1/2, \quad (3.3.21)$$

substitution of (3.3.19) yields

$$S_n = \sum_{i=0}^n F\left(\frac{i}{n}\right) \frac{1}{n} - \sum_{i=0}^n \frac{n-2i}{n+2i} F\left(\frac{i}{n}\right) \frac{1}{n} \quad \text{where } 0 < x < 1/2. \quad (3.3.22)$$

Thus in the limit as $n \rightarrow \infty$, we can say

$$H(A^2/\lambda_z) = S_n, \quad \text{as } n \rightarrow \infty. \quad (3.3.23)$$

Rearranging (3.3.22) and using the properties of $F(x)$ we have

$$\sum_{i=0}^n F\left(\frac{i}{n}\right) \frac{4i}{n(n+2i)} < 0,$$

since $F(x) < 0$ for $0 < x < 1/2$. Which finally allows us to say

$$H\left(\frac{A^2}{\lambda_z}\right) = S_\infty < 0.$$

Since H is a continuous function with a sign change over $[A/\sqrt{\lambda_z}, B/\sqrt{\lambda_z}]$ we conclude that $H = 0$ has a solution for a given $\lambda_z > 0$ with $a \in (A/\sqrt{\lambda_z}, B/\sqrt{\lambda_z})$.

Also from (3.3.18)-(3.3.22) and the continuity of $W_{\alpha_1}, W_{\alpha_2}$ it is clear that the integrand in $H(C,D)$ is continuous in (C,D,x) and therefore we conclude $H(C,D)$ is continuous in (C,D) upon integration. Let $C(D)$ be the unique C such that (3.3.25) holds, if $C(D)$ is not continuous at D_o , say, then $\exists \varepsilon > 0$ and a sequence $\{D_n\}$ such that $D_n \rightarrow D_o$ as $n \rightarrow \infty$ while

$$|C(D_n) - C(D_o)| > \varepsilon, \quad \forall n > 0. \quad (3.3.24)$$

However, $C(D) \in [-2B^2, -A^2 - B^2]$ which, since every closed bounded interval of \mathbb{R} is a compact set, has a subsequence $\{D_{n_k}\}$ of $\{D_n\}$ such that

$$C(D_{n_k}) \rightarrow C' \quad \text{as } k \rightarrow \infty, \quad C \in [-2B^2, -A^2 - B^2],$$

since H is continuous $H(C', D_o) = 0$ which by the uniqueness of $C(D)$ implies $C' = C(D_o)$ contradicting (3.3.24). We therefore conclude that $C=C(D)$ is continuous, or equivalently $a = a(\lambda)$ is continuous.

If from (3.3.11) we consider H as a function of C, D , the solution can be written

$$H(C, D) = 0 . \quad (3.3.25)$$

Now that existence of a continuous solution of $H = 0$ has been established we will proceed to prove partial uniqueness of such a state . By partial uniqueness we mean that given any $\lambda_z > 0$ there is exactly one value of $a > 0$ such that (3.3.25) has a solution. Choosing a real $\lambda_z > 0$, then for $C \in [-2B^2, -A^2 - B^2]$, from (3.3.15), $x_A < 0$ and $x_B > 0$. If we rewrite (3.3.10) as

$$H = \frac{\alpha}{2\lambda_z^{\alpha/2}} \int_{-x_B}^{x_B} f(x)W(x)dx. \quad (3.3.26)$$

where

$$F(x) = f(x)W(x) ,$$

is defined in (3.3.18). We also define

$$f(x) = \left[\frac{(\frac{1}{2} - x)^\alpha - (x + \frac{1}{2})^\alpha}{(x + \frac{1}{2})^{\frac{\alpha}{2}}(\frac{1}{2} - x)^{\frac{\alpha}{2}}} \right] \left[\frac{(\frac{1}{2} + x)}{(\frac{1}{2} - x)} \right] , \quad -\frac{1}{2} < x < \frac{1}{2} ,$$

and

$$W(x) = (W_{\alpha 1} + \lambda_z^\alpha W_{\alpha z}) , .$$

We can then see

$$\frac{\partial H}{\partial C} = \frac{\partial x_B}{\partial C} f(x_B)W(x_B) - \frac{\partial(-x_B)}{\partial C} f(-x_B)W(-x_B) . \quad (3.3.27)$$

Using (3.3.14), the definition of $f(x)$ and the evenness of W in x we yield

$$\frac{\partial H}{\partial C} = W(x_B) \frac{\partial x_B}{\partial C} [F(x_B) + F(-x_B)] , \quad (3.3.28)$$

from (3.3.11) and (3.3.15) we find

$$\frac{\partial x_B}{\partial C} = \frac{\partial x_B}{\partial B} \frac{\partial B}{\partial C} = \frac{-A^2}{(A^2 + B^2)^2} < 0 ,$$

From the conditions on $F(x)$ we can see
 $F(x) < 0$ for $x > 0$ and $F(x) > 0$ for $x < 0$.

Now since

$|F(x_B)| > |F(-x_B)|$ we can write

$$F(x_B) + F(-x_B) < 0 .$$

Using the fact that $W(x) \geq 0$ for all x , we conclude

$$\frac{\partial H}{\partial C} < 0 . \quad (3.3.29)$$

We have therefore shown that given $\lambda_z > 0$ there exists a unique $a > 0$ such that $H = 0$ has a solution.

Considering (3.3.8), the axial load N , we investigate the coefficients of $W_{\alpha 1}, W_{\alpha 2}$ in the integrand to locate an interval on which the integral has a possible root.

Defining

$$\left. \begin{aligned} c_1 &= \lambda_1^\alpha + \lambda_2^\alpha - 2\lambda_z^\alpha , \\ c_2 &= \lambda_z^\alpha (\lambda_1^\alpha + \lambda_2^\alpha - 2\lambda_1^{2\alpha} \lambda_2^{2\alpha}) , \end{aligned} \right\} \quad (3.3.30)$$

we transform (3.3.8) to

$$N = \int_a^b \alpha r \{W_{\alpha 1} c_1 - W_{\alpha 2} c_2\} dr = 0 . \quad (3.3.31)$$

Recalling (3.3.9) we choose $a > 0$ and consider λ_z both large and small. Thus

$$\lambda_z \rightarrow \infty \Rightarrow b \rightarrow a$$

$$\lambda_z \rightarrow 0^+ \Rightarrow b \rightarrow \sqrt{\frac{B^2 - A^2}{\lambda_z}} \rightarrow \infty .$$

where we have used the fact that a is fixed. Hence the principal stretches using (3.3.6), (3.3.9) and the above have limiting values

$$\lambda_2 = \frac{(a^2 + (B^2 - R^2)/\lambda_z)^{\frac{1}{2}}}{R} \rightarrow \begin{cases} \frac{a}{R} \text{ as } \lambda_z \rightarrow \infty , \\ \frac{(B^2 - R^2)^{\frac{1}{2}}}{R\lambda_z^{\frac{1}{2}}} \text{ as } \lambda_z \rightarrow 0^+ , \end{cases} \quad (3.3.32)$$

and

$$\lambda_1 = 1/\lambda_2\lambda_z = \frac{R}{\sqrt{\lambda_z^2 a^2 + \lambda_z(B^2 - R^2)}} \rightarrow \begin{cases} \frac{R}{a\lambda_z} & \text{as } \lambda_z \rightarrow \infty, \\ \frac{R}{\sqrt{\lambda_z(B^2 - R^2)}} & \text{as } \lambda_z \rightarrow 0^+. \end{cases} \quad (3.3.33)$$

Substitution of (3.3.32), (3.3.33) into (3.3.30) yields

$$c_1 \rightarrow \begin{cases} \left(\frac{R}{\lambda_z a}\right)^\alpha + \left(\frac{a}{R}\right)^\alpha - 2\lambda_z^2 \rightarrow -2\lambda_z^2 & \text{as } \lambda_z \rightarrow \infty, \\ \left[\frac{R^\alpha}{(B^2 - R^2)^{\alpha/2}} + \frac{(B^2 - R^2)^{\alpha/2}}{R^\alpha}\right] \frac{1}{\lambda_z^{\alpha/2}} = k > 0 & \text{as } \lambda_z \rightarrow 0^+, \end{cases} \quad (3.3.34)$$

and

$$c_2 \rightarrow \begin{cases} \left(\frac{R}{\lambda_z a}\right)^\alpha + \left(\frac{a}{R}\right)^\alpha - \frac{2}{\lambda_z^\alpha} \rightarrow \left(\frac{a}{R}\right)^\alpha & \text{as } \lambda_z \rightarrow \infty, \\ \left[\frac{R^\alpha}{(B^2 - R^2)^{\alpha/2}} + \frac{(B^2 - R^2)^{\alpha/2}}{R^\alpha} - \frac{2}{\lambda_z^{\alpha/2}}\right] \lambda_z^{\alpha/2} \rightarrow -2, & \text{as } \lambda_z \rightarrow 0^+. \end{cases} \quad (3.3.35)$$

Thus N has the limiting forms

$$N \rightarrow \begin{cases} \alpha \int_a^b r [W_{\alpha 1} (-2\lambda_z)^\alpha - W_{\alpha 2} \left(\frac{a}{R}\right)^\alpha] dr < 0, & \lambda_z \rightarrow \infty, \\ \alpha \int_a^b r [W_{\alpha 1} k + 2W_{\alpha 2}] dr > 0, & \lambda_z \rightarrow 0^+, \end{cases} \quad (3.3.36)$$

since the material satisfies the inequalities (3.3.4) and the integrands in (3.3.36) are continuous. Hence given any $a > 0$, $\exists \lambda_z > 0$ such that N has at least one zero.

Unfortunately it is not possible to provide any monotonicity conditions on the derivative $\frac{\partial N}{\partial C}$ as we did for the traction free curved surface function H . Therefore there remains the possibility that there exist more than one value of $\lambda_z > 0$ which satisfies (3.3.30) for a given value of a . However, we have no evidence to suggest that the cylindrical everted solution is not unique and we believe that it is.

We have therefore proved existence of an everted shape for all materials with principal invariants (3.3.2) which satisfy (3.3.4).

3.4 Numerical results

We now give some numerical results for the straightforward eversion of cylindrical shells. In Figure 3.1 we plot values of λ_z and the non-dimensionalised deformed outer radius b/B obtained from (3.1.15) and (3.1.16) for tubes of different initial thickness A/B . Results for each of the materials (3.2.3), (3.2.4), and (3.2.5) are shown. Chadwick and Haddon (1972) give a table of results corresponding to Figure 3.1 for the three-term material (3.2.5) and a particular Mooney–Rivlin material over a limited range of values of A/B . In particular we note that the values of λ_z increase with the undeformed thickness of the shell and, in every case, $\lambda_z > 1$. In connexion with these results we recall that $\lambda_z > 1$ is not a universal result since Chadwick and Haddon (1972) has proved that shortening may accompany eversion for some Mooney–Rivlin materials. Conversely the deformed outer radius of the shell may increase or decrease depending on the material model and initial geometry.

Also of interest is the stress distribution throughout the cylinder. Chadwick and Haddon (1972) have given results for all three principal stretches for the Mooney–Rivlin material and three-term Ogden material (3.2.5). Due to the approximate nature of the end conditions adopted, the actual distribution of the axial stress σ_{zz} is of particular interest and so, in Figure 3.2 we give results for the three materials (3.2.3)–(3.2.5) for a cylinder of initial thickness $A/B = 0.5$. Results for other undeformed geometries are qualitatively similar. The deformed inner portion of the cylinder is subjected to an axial compression (the magnitude of which increases with increasing undeformed thickness A/B) and the outer portion is subjected to an axial tension (the magnitude of which also increases with shell thickness). These results are consistent with the experimental results detailed by Varga (1966, pp 150–151), see also Chadwick and Haddon (1972, Fig.8) where σ_{zz}/μ has been plotted against the deformed radius.

Chadwick and Haddon (1972) have plotted values of non-dimensionalised principal stresses against deformed radius for the material (3.2.5) and a Mooney–Rivlin material in (1972, Figs. 6, 7 and 8). For completeness, we plot in Figure 3.3 non-

dimensionalised values for the three principal stresses against the undeformed radius of the tube. We have chosen the three-term material (3.2.5) and a tube with thickness ratio $A/B = 0.75$. The eversion produces a large hoop stress, $\sigma_{\theta\theta}$, and a small radially compressive stress, σ_{rr} , along with the axial loading required to eliminate the end effects and produce a perfectly cylindrical everted tube. Since it is well known that non-everted rubberlike cylinders will bifurcate into a non-cylindrical shape when subjected to only a very modest radial compression, the compressive stress induced by the eversion process may be significant.

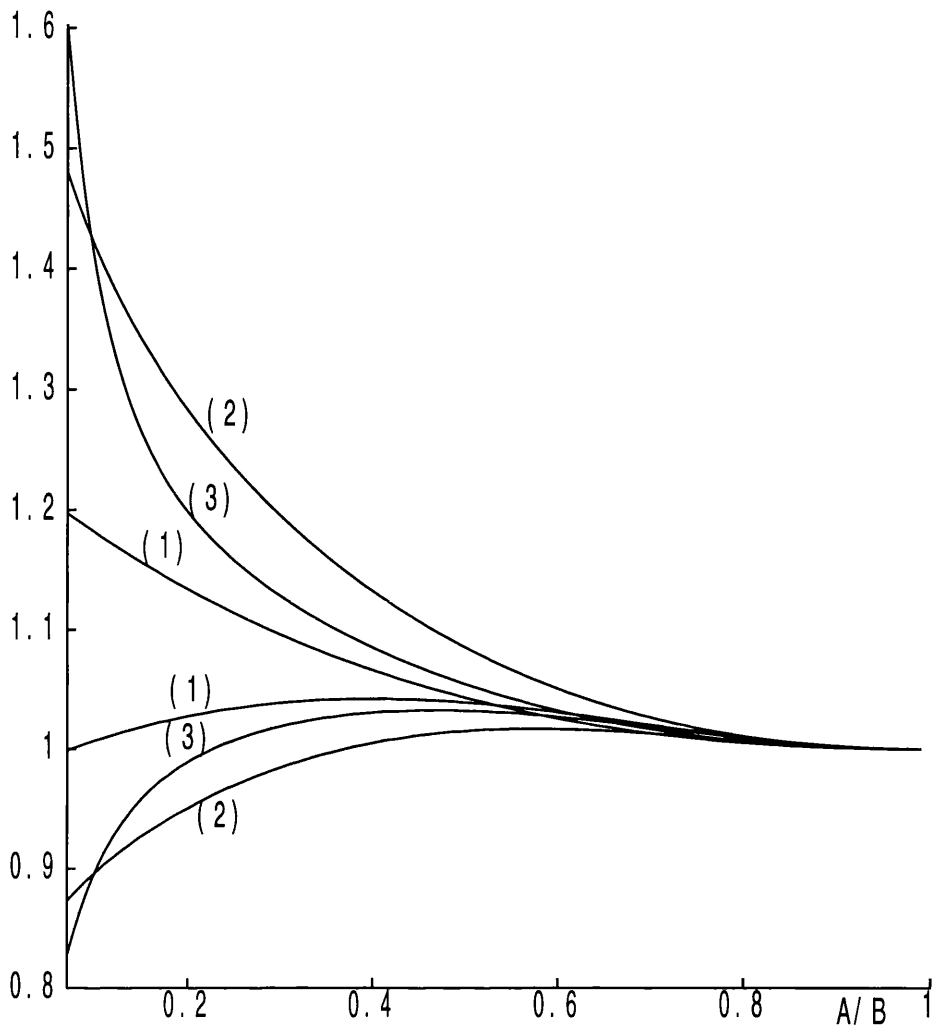


Figure 3.1 Plot of λ_z (upper three curves) and b/B (lower three curves) against A/B for the three materials, (1)-Varga, (2)-Neo-Hookean, (3)-three-term.

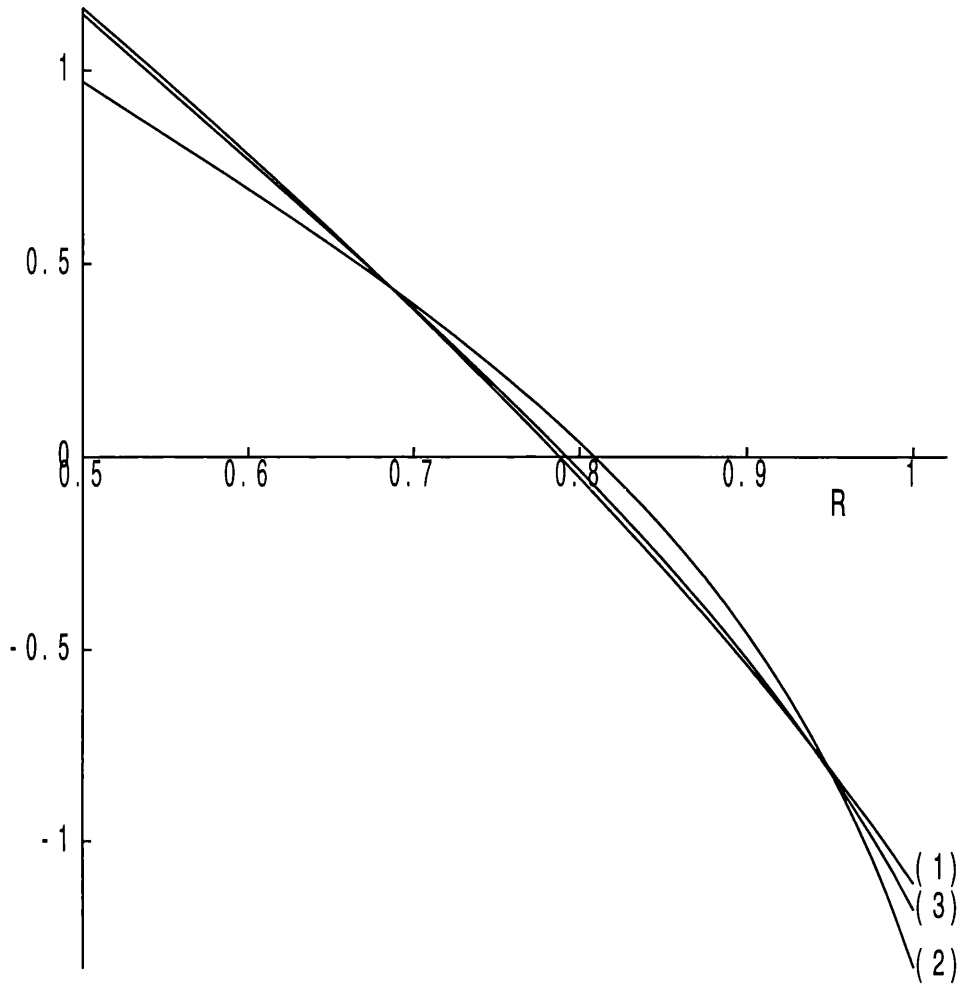


Figure 3.2 Plot of the non-dimensionalised axial load σ_{zz}/μ vs. undeformed radius R for a tube with $A/B = 0.5$ in respect of the three materials, (1)-Varga, (2)-Neo-Hookean, (3)-three-term.

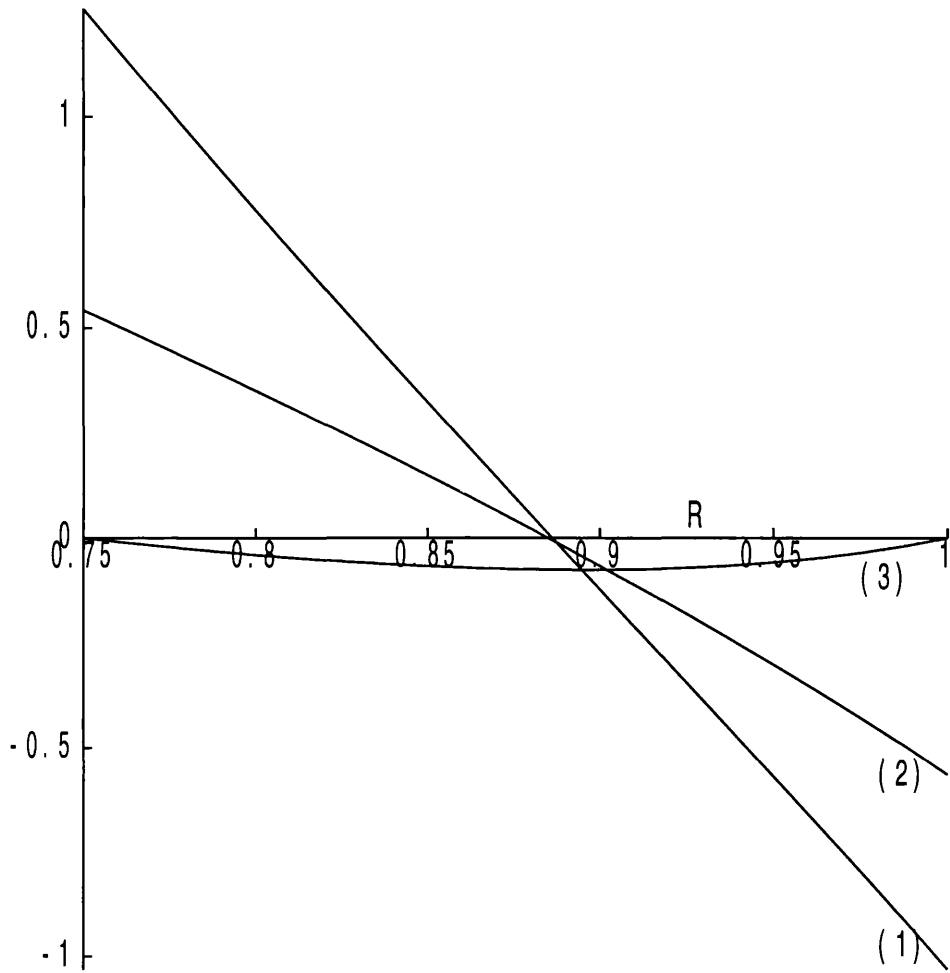


Figure 3.3 Plot of the non-dimensionalised stresses (1)- $\sigma_{\theta\theta}/\mu$, (3)- σ_{zz}/μ , (3)- σ_{rr}/μ , vs. undeformed radius R for a tube with $A/B = 0.75$ in respect of the three-term material (3.2.5).

Chapter 4

Eversion of Compressible Cylinders

4.1 Equilibrium Equations

Suppose that the undeformed compressible isotropic homogeneous elastic tube occupies the region

$$0 < A \leq R \leq B, \quad 0 \leq \Theta \leq 2\pi, \quad 0 \leq Z \leq L, \quad (4.1.1)$$

where (R, Θ, Z) are cylindrical polar coordinates. The cylinder is now everted into another right circular cylinder occupying the region

$$0 \leq a \leq r \leq b, \quad 0 \leq \theta \leq 2\pi, \quad -\ell \leq z \leq 0, \quad (4.1.2)$$

where (r, θ, z) are also cylindrical polar coordinates and $\ell > 0$ is a constant. The deformation is given by (3.1.3) i.e.

$$r = r(R), \quad \theta = \Theta, \quad z = -\lambda Z, \quad (4.1.3)$$

where $\lambda > 0$ is a constant such that $\ell = \lambda L$. The components of the deformation gradient \mathbf{F} referred to cylindrical coordinates are given in (3.1.4) and the principal stretches of the deformation are given in (3.1.5).

For a compressible material the dilatation J must be positive and so we can write

$$J = \det(\mathbf{F}) = -\lambda \frac{r}{R} \frac{dr}{dR} > 0 . \quad (4.1.4)$$

As for the incompressible case the equilibrium equations for the deformation above reduce to the single equation

$$r \frac{d\sigma_{rr}}{dr} + \sigma_{rr} - \sigma_{\theta\theta} = 0 , \quad (4.1.5)$$

where the principal Cauchy stresses σ_{rr} , $\sigma_{\theta\theta}$ and σ_{zz} can be written in terms of the strain-energy function $W = W(\lambda_r, \lambda_\theta, \lambda_z)$ of the material as

$$J\sigma_{ii} = \lambda_i \frac{\partial W}{\partial \lambda_i} , \text{ no sum,} \quad (4.1.6)$$

where we recall $J = \lambda_r \lambda_z \lambda_\theta$. Here the subscript i should be regarded as one of (r, θ, z) . Following chapter 3 where we considered this problem for incompressible materials, we look for approximate solutions that satisfy the boundary conditions (3.1.11) and give a zero resultant load N on the ends, i.e.,

$$N = 2\pi \int_a^b r \sigma_{zz} dr = 0 , \quad z = -\lambda L , 0 . \quad (4.1.7)$$

Firstly integration of the equilibrium equation (4.1.5) and use of (3.1.11) allows us to express the zero traction conditions $\sigma_{rr}(A) = \sigma_{rr}(B) = 0$, $0 \geq z \geq -\lambda L$, on the curved surface as

$$\int_a^b \frac{\sigma_{\theta\theta} - \sigma_{rr}}{r} dr = 0 . \quad (4.1.8)$$

Since we have insisted $r = r(R)$, we can write

$$\frac{d}{dr}(\cdot) = \frac{d}{dR}(\cdot) \frac{dR}{dr} = \frac{1}{r'} \frac{d}{dR}(\cdot)$$

where we have written $r' = \frac{dr}{dR}$. Using this in (4.1.5), we yield

$$\frac{d\sigma_{rr}}{dR} + \frac{r'}{r}(\sigma_{rr} - \sigma_{\theta\theta}) = 0 . \quad (4.1.9)$$

Changing to the reference configuration the axial load N (4.1.7) becomes

$$N = 2\pi \int_A^B \lambda_\theta \lambda_r \sigma_{zz} R dR = 0 , \quad z = -\lambda L , 0 . \quad (4.1.10)$$

Hence (4.1.8) and (4.1.10) with (3.1.5) and (4.1.6) are two simultaneous equations for λ_z and a . These will be solved numerically for specific forms of strain-energy functions.

4.2 Exact solution

All previous investigations of possible everted states have considered only incompressible materials and offered only numerical solutions. As stated in Chapter 3 Chadwick and Haddon (1972) considered Mooney–Rivlin materials and a three term Ogden material. The latter was solved numerically for only a limited range of possible A/B . Here we are able to solve the eversion problem exactly for a highly compressible material. This has the additional benefit of being a useful check of any numerical techniques employed. Considering the strain-energy function

$$W(\lambda_1, \lambda_2, \lambda_3) = \gamma\{(\lambda_1 - \alpha)^n + (\lambda_2 - \alpha)^n + (\lambda_3 - \alpha)^n - 3(1 - \alpha)^n\}. \quad (4.2.1)$$

where $\alpha, \gamma \neq 0$ are parameters and $n \neq 0$. Using (4.2.1) in (4.1.6) we have

$$\sigma_{ii} = \frac{\lambda_i}{J} \gamma n (\lambda_i - \alpha)^{n-1}. \quad (4.2.2)$$

Since we require zero energy and zero stress in the undeformed configuration (4.2.2) gives

$$\sigma_{ii}(1, 1, 1) = 0 \Rightarrow \alpha = 1, \quad n \neq 1,$$

where all principal stretches take the value unity. Appealing to the ground state shear modulus, which is introduced with physical restrictions in Truesdell and Noll (1965, p182), we have

$$\mu = \lim_{\lambda \rightarrow 1} \frac{1}{2} \{ \gamma n (n-1) (\lambda - 1)^{n-2} \},$$

which gives $\mu = \gamma > 0$ and $n = 2$. The most general physically reasonable form of the strain-energy function (4.2.1) is then written

$$W(\lambda_1, \lambda_2, \lambda_3) = \mu\{(\lambda_1 - 1)^2 + (\lambda_2 - 1)^2 + (\lambda_3 - 1)^2\}. \quad (4.2.3)$$

Considering the bulk modulus κ which can be written

$$\kappa = \frac{1}{3} \{ W_{11} + 2W_{12} \}_{\mathbf{F}=\mathbf{I}}, \quad (4.2.4)$$

(see Truesdell and Noll (1965)) we see that

$$\kappa = \frac{2}{3} \mu > 0.$$

Here we have used the notation

$$W_{ij} = \frac{\partial W_i}{\partial \lambda_j} .$$

Since $\kappa/\mu = 2/3$ we have a highly compressible material. We note that $\kappa/\mu = 5/3$ for the Blatz–Ko (1962) material and so (4.2.1) with $\alpha = 1, n = 2$ can be thought of as a homogeneous model for a very soft foam rubber. On substituting (4.2.3) into the equilibrium equation (4.1.5) we obtain

$$r'' + \frac{r'}{R} - \frac{r}{R^2} + \frac{2}{R} = 0 . \quad (4.2.5)$$

Integrating twice produces,

$$r(R) = R \frac{c_1}{2} + \frac{c_2}{R} - R \ln R + \frac{R}{2} , \quad (4.2.6)$$

where

$$c_1 = \frac{2B^2 \ln B - 2A^2 \ln A}{B^2 - A^2} - 1 , \quad c_2 = \frac{A^2 B^2 \ln(B/A)}{B^2 - A^2} , \quad (4.2.7)$$

are obtainable from the boundary conditions (3.1.11). Using (4.2.7) and $r(A) = b$, $r(B) = a$ we find

$$a = \frac{2A^2 B \ln(B/A)}{B^2 - A^2} , \quad b = \frac{2AB^2 \ln(B/A)}{B^2 - A^2} , \quad (4.2.8)$$

where a, b are the inner and outer deformed radii respectively.

We now turn our attention to the axial stretch λ_z to discover the final geometry. For this particular material it is possible to satisfy the original eversion problem where we insist that the azimuthal stress is identically zero at each point on the ends of the cylinder. For this point-wise condition (3.1.12) we can use (4.2.3) to yield

$$\sigma_{zz}(-\lambda L) = 0, \quad A \leq R \leq B \Rightarrow \lambda_z = 1 .$$

In passing it should be noted that this is the only solution obtainable from the approximate end conditions. Using (4.2.8) we are able to show a/B and b/B are monotonic increasing functions of A/B .

In Figure 4.1 we plot the deformed inner radius a and the deformed outer radius b for a variety of initial thicknesses. Here we have non-dimensionalised the problem by setting $B = 1$. As stated we can see that both a/B and b/B are monotonic increasing functions of A/B . We can also see that as $A \rightarrow B$ then $a \rightarrow B$ and the cylinder becomes a membrane turned inside out with the same geometry as before. Also it is interesting to note that $a > 0$ for all non-trivial undeformed cylinders. This is in contrast to the particular example shown in the photograph Figure 1.1 where the inner cavity closes on eversion.

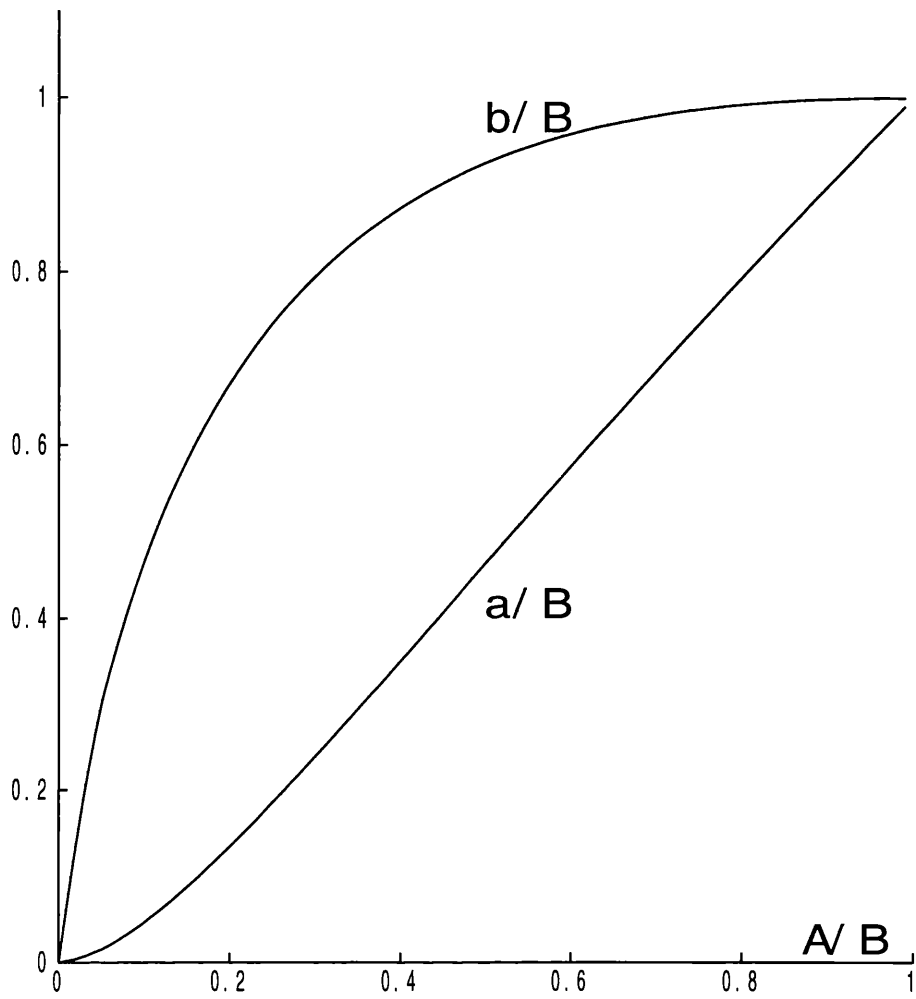


Figure 4.1 Plot of deformed radii for a variety of initial thicknesses A/B .

4.3 Existence and Uniqueness

Using the notation and method of the incompressible case we first recall (2.3.2) in component form, i.e.,

$$\sigma_{ii} = \psi_0 + \psi_\alpha \lambda_i^\alpha + \psi_{-\alpha} \lambda_i^{2\alpha} , \quad (4.3.1)$$

where

$$\left. \begin{aligned} \psi_\alpha &= \frac{\alpha}{J} (W_{\alpha 1} + W_{\alpha 2}) , \\ \psi_0 &= \alpha W_{\alpha 3} , \\ \psi_{-\alpha} &= -\frac{\alpha}{J} W_{\alpha 2} . \end{aligned} \right\} \quad (4.3.2)$$

Here $I_{\alpha 1}$, $I_{\alpha 2}$ and $I_{\alpha 3}$ are invariants given by

$$\begin{aligned} I_{\alpha 1} &= \lambda_1^\alpha + \lambda_2^\alpha + \lambda_3^\alpha , \\ I_{\alpha 2} &= \lambda_1^\alpha \lambda_2^\alpha + \lambda_1^\alpha \lambda_3^\alpha + \lambda_2^\alpha \lambda_3^\alpha , \\ I_{\alpha 3} &= J^\alpha . \end{aligned} \quad (4.3.3)$$

We have also written $W_{\alpha i} = \frac{\partial W}{\partial I_{\alpha i}}$. If we define

$$\begin{aligned} c_1 &= W_{\alpha 1} + \lambda_3^\alpha W_{\alpha 2} , \\ c_2 &= W_{\alpha 1} + \lambda_2^\alpha W_{\alpha 2} , \end{aligned} \quad (4.3.4)$$

then it is clear that both c_1, c_2 are non-negative. Substitution of (4.3.1) with (4.3.4) into (4.1.8) produces

$$H = \alpha \int_a^b \frac{1}{rJ} c_1 [\lambda_2^\alpha - \lambda_1^\alpha] dr = 0 , \quad (4.3.5)$$

for the zero traction condition. As for the incompressible case a knowledge of the sign of $\lambda_2^\alpha - \lambda_1^\alpha$ is essential to make any progress. From (3.1.5) we write

$$\lambda_2^\alpha - \lambda_1^\alpha = \left(\frac{r}{R} \right)^\alpha - (-r')^\alpha . \quad (4.3.6)$$

Without the incompressibility constraint $J = 1$ we are unable to obtain $r = r(R)$ explicitly, for a general compressible material, or express λ_1 in terms of λ_2, λ_3 . We are then unable to produce any analytical treatment on (4.3.5) and hence no results are available on the existence of solutions for H .

Similarly if we substitute (4.3.1) with (4.3.4) into (4.1.10) we construct the condition on the axial load N ,

$$\frac{\alpha}{\lambda_3} \int_A^B \left\{ c_2(\lambda_3^\alpha - \lambda_1^\alpha) - \frac{c_1}{2}(\lambda_2^\alpha - \lambda_1^\alpha) \right\} R dR = 0. \quad (4.3.7)$$

Again without any explicit knowledge of $r = r(R)$ we cannot manipulate the integrand in (4.3.7).

4.4 Varga Materials

We define a compressible form of the Varga material as

$$W(\lambda_1, \lambda_2, \lambda_3) = 2\mu(\lambda_1 + \lambda_2 + \lambda_3 - g(J)), \quad (4.4.1)$$

where $\mu > 0$ is the ground state shear modulus of the material and g is an arbitrary function of the dilation J , as defined above.

This strain-energy form is obtained from a general form for compressible materials introduced by Ogden (1972b) which is a modified form of the material (3.2.1) where the compressibility is accounted for by the addition of a function g of the dilation J . The explicit form (4.4.1) was introduced by Haughton (1987) and independently by Carroll (1988).

The only constraints on the function $g(J)$ are

$$g(1) = 3, \quad g'(1) = 1, \quad g''(1) < -\frac{2}{3}. \quad (4.4.2)$$

These conditions ensure zero energy and zero stress in the undeformed configuration and a positive bulk modulus respectively.

For explicit calculations we define

$$g(J) = -\frac{J^{-\beta} - 1}{\beta} + 3, \quad \beta \neq 0, \quad (4.4.3)$$

which satisfies conditions (4.4.2) provided $\beta > -\frac{1}{3}$, $\beta \neq 0$. In terms of (4.4.1) we can write the bulk modulus as

$$\kappa = 2\mu\left(\beta + \frac{1}{3}\right). \quad (4.4.4)$$

The parameter β then allows us to consider materials with the widest possible range of compressibilities. One attraction of this material is that an incompressible material can be attained as a limit. This is not the case for most compressible Strain–Energy forms. The incompressible Varga material corresponds to the limit as $\kappa \rightarrow \infty$ where we also see $\beta \rightarrow \infty$. Using material (4.4.1) with (4.4.3) in (4.1.6)

we yield

$$\begin{aligned}\sigma_{rr} &= \frac{2\mu R}{r\lambda} \left(1 + \frac{J^{-\beta}}{r'}\right), \\ \sigma_{\theta\theta} &= -\frac{2\mu}{r'\lambda} \left(1 - \frac{RJ^{-\beta}}{r}\right), \\ \sigma_{zz} &= -\frac{2\mu R}{r'r} \left(1 - \frac{J^{-\beta}}{\lambda}\right).\end{aligned}\tag{4.4.5}$$

which permits the expression of the axial load N (4.1.10) as

$$N = 4\pi\mu \int_A^B \left(1 - \frac{J^{-\beta}}{\lambda}\right) R dR = 0, \quad z = -\lambda L, 0.\tag{4.4.6}$$

As can be seen from (4.4.5) and (4.4.6) the role of β will be of importance in determining the final geometry and stress relations of the everted tube. From (4.4.5) we observe that the restriction $\beta \neq 0$ is removed from the stress components and we shall hence consider this limiting case later.

The task of solving the system (4.1.8) and (4.1.10) with (3.1.5) and (4.1.9) analytically proves to be highly non-trivial for even the simplest strain-energy function. In general for a compressible material the dilation J will become an integral part of the problem and hence increase the complexity of the resulting equation of motion. To solve numerically we adopt the following strategy. We first guess a value of λ_z to try to solve our simultaneous equations (4.1.8), (4.1.10). We then choose a value for $r'(B)$ and iterate over the deformed inner radius a to make $\sigma_{rr}(a) = 0$. Once we achieve this we calculate $\sigma_{rr}(b)$ and iterate over $r'(A)$ until $\sigma_{rr}(b) = 0$. In doing so we have satisfied the boundary conditions on the curved surfaces and determined a, b . We then proceed by calculating the axial load N and should it be non-zero we choose a different starting value for λ_z and iterate until the axial load N is zero. We will now have solved the problem fully and attained values for the axial stretch λ_z , the deformed inner radius a and the deformed outer radius b . The actual values obtained will be dependent on the initial thickness A/B of the cylinder. This set of equations can then be solved for a wide range of values of β for different cylindrical geometries. To add physical meaning to the resultant data we consider plots of κ/μ as opposed to β , where

κ is given in (4.4.4). It can be seen from (4.4.4) that large values of κ/μ will correspond to incompressible materials.

4.5 Numerical results

In Fig 4.2 we investigate the behaviour of the axial stretch λ_z as we vary κ/μ . As stated above varying κ/μ has the effect of choosing the compressibility of the elastic tube. We can see that λ_z tends to 1 as β tends to zero for a wide range of initial radii ratio A/B , where we have non-dimensionalised the problem by setting $B=1$. For this value of β we have $\kappa/\mu = 2/3$ which corresponds to a highly compressible cylinder. It is perhaps a coincidence that the exact material (4.2.3) has a value $\kappa/\mu = 2/3$ and also gives the solution $\lambda_z = 1$. We also observe that $\lambda_z \equiv 1$ for $A/B \rightarrow 1$. This limit coincides with the membrane limit. For the extensive range of initial radii ratio plotted we see that provided κ/μ is not close to zero all deformed tubes qualitatively mimic the behaviour of incompressible cylinders. This is the effect anticipated by Truesdell (1977). We therefore consider Fig 4.3 where we concentrate our attention on κ/μ close to zero. Here it is evident that $\lambda_z > 1$ for $\beta > 0$ and $\lambda_z < 1$ for $\beta < 0$ for all A/B values plotted.

In Fig 4.4 we show how λ_z behaves against the undeformed thickness A/B about $\beta = 0$. From (4.4.4) we see that when $\beta = 0$, $\kappa/\mu = 2/3$. As we expect from Fig 4.3 if $\beta < 0$ then λ_z increases with decreasing thickness whereas the reverse holds for $\beta > 0$. In Fig 4.5 we plot the deformed inner radius against κ/μ . In this figure we note that the deformed inner radius $a > A$ unless $\kappa/\mu \ll 1$. Physically we interpret this as the inner hole of the cylinder expanding for all but very compressible materials. In Fig 4.6 we see a increases as the initial radii ratio increases for both $\beta > 0$ and $\beta < 0$. In Fig 4.7 we turn our attention to the behaviour of the deformed outer radius b as we vary κ/μ . Here we observe an almost horizontal curve with $b/B \approx 1$ which corresponds to a very thin shell with $A/B = 0.95$.

If we fix the value of κ/μ the outer radius has a local maximum when regarded as a function of the undeformed thickness A/B as is illustrated in Fig 4.8. It is also demonstrated that the local maximum of b/B depends on the compressibility of the material. As the material becomes more compressive the local maximum disappears.

We now plot the non-dimensionalised stress against the undeformed radius. In Figures 4.9, 4.10 and 4.11 we plot the three stresses for $\kappa/\mu = 7/6$ ($\beta = 0.25$) for a variety of initial thicknesses. Qualitatively we see that the three cylinders produce similar stresses with the primary difference being that thicker tubes experience a greater radial stress upon deformation. However, for all tubes we observe that $\sigma_{rr} \leq 0$ throughout the tube and is zero on the ends of the cylinder. We also note similarities with the hoop stress $\sigma_{\theta\theta}$ where each tube will have the inner surface stretched and the outer surface will undergo compression. The axial loading produced by the eversion process will help to maintain a perfectly cylindrical tube after deformation.

From Figure 4.3 we can see that as β moves through zero the nature of the deformation is changed. We therefore consider the stress deformation for the same initial thicknesses $A/B = 0.25$, $A/B = 0.5$ and $A/B = 0.75$ we plot Figures 4.12, 4.13 and 4.14 for $\kappa/\mu = 1/6$ ($\beta = -0.25$). As can be seen from the graphs the main difference in the stresses is in the flipping of the azimuthal stress σ_{zz} . This change in the behaviour of the stress is consistent with the axial stretch changing from $\lambda_z > 1$ to $\lambda_z < 1$ as β moves through zero. From the graphs it is clear that as β moves through zero the everted tube goes through a dramatic change as all tubes, regardless of initial geometry, appear to converge at this point.

We therefore study the case $\beta \rightarrow 0$ analytically. In (4.4.5) as we let $\beta \rightarrow 0$ we find

$$\begin{aligned}\sigma_{rr} &\rightarrow \frac{2\mu R}{\lambda r} \left(1 + \frac{1}{r'}\right) \text{ as } \beta \rightarrow 0, \\ \sigma_{zz} &\rightarrow -\frac{2\mu R}{r r'} \left(1 - \frac{1}{\lambda}\right) \text{ as } \beta \rightarrow 0, \\ \sigma_{\theta\theta} &\rightarrow \frac{-2\mu}{r' \lambda} \left(1 - \frac{R}{r}\right) \text{ as } \beta \rightarrow 0.\end{aligned}\tag{4.5.1}$$

Substitution of (4.5.1) into the equilibrium equations yields the differential equation,

$$r'' - \frac{r'}{R} + (r')^2 \left(\frac{1}{r} - \frac{2}{R}\right) = 0.\tag{4.5.2}$$

Unfortunately we have not been able to solve this analytically due to its' non-linear nature. Symbolic computer programs Maple and Mathematica have had a

similar lack of success. If instead we use (4.5.1) in the radial boundary conditions (3.1.11) we obtain

$$\frac{2\mu B}{\lambda a} \left(1 + \frac{1}{r'(a)}\right) = 0, \Rightarrow r'(a) \rightarrow -1$$

similarly we write $r'(b) \rightarrow -1$, and substituting (4.5.1) into (4.1.10) and changing the integration variable to R , we have

$$-\frac{2\mu}{\lambda} (1 - 1/\lambda) \int_A^B r dR = 0,$$

thus, since $r(R) > 0$, we conclude $\lambda = 1$ and from (4.4.5) $\sigma_{zz} \equiv 0$. We are therefore able to solve the pointwise boundary conditions for the material (4.4.1) in the limit as β tends to zero.

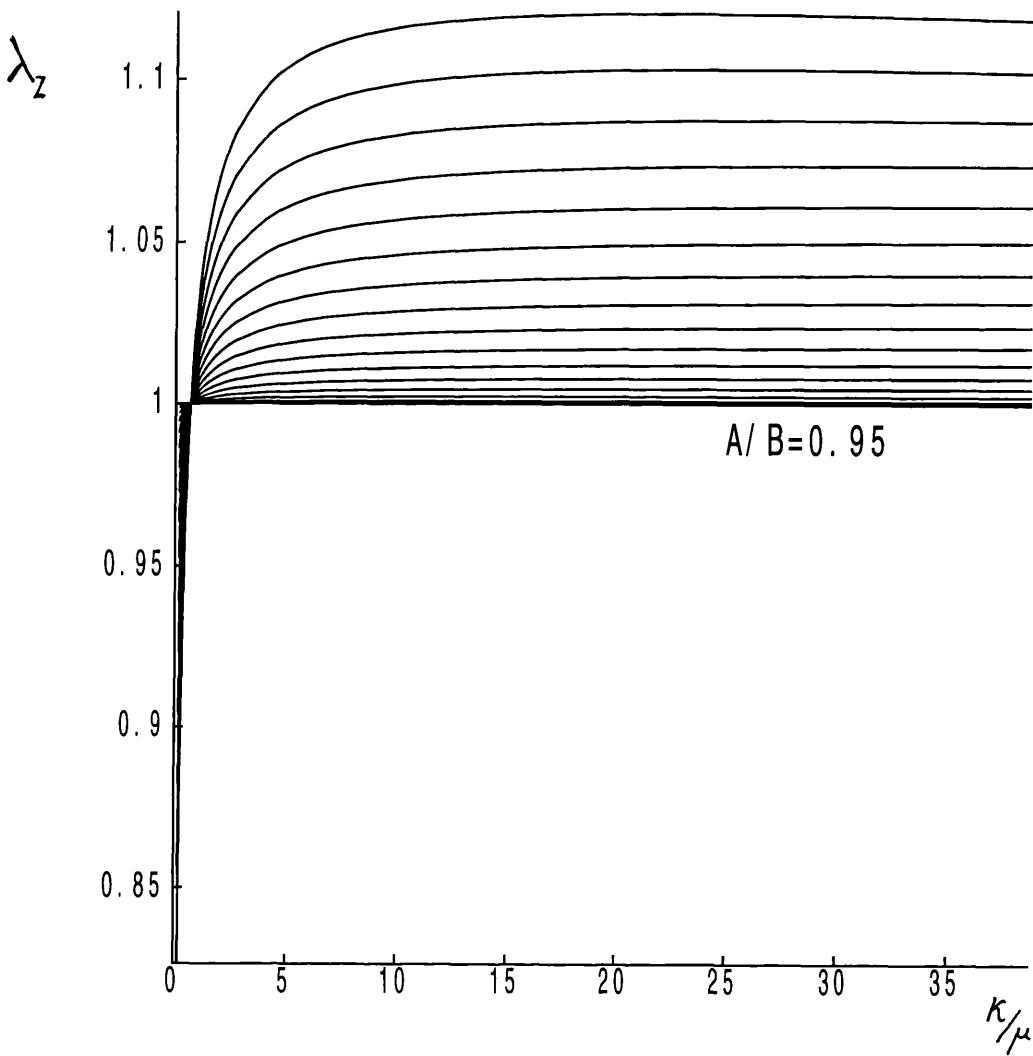


Figure 4.2 Plot of axial stretch λ_z against κ/μ for a variety of initial thicknesses $A/B = 0.2 (0.05) 0.95$.

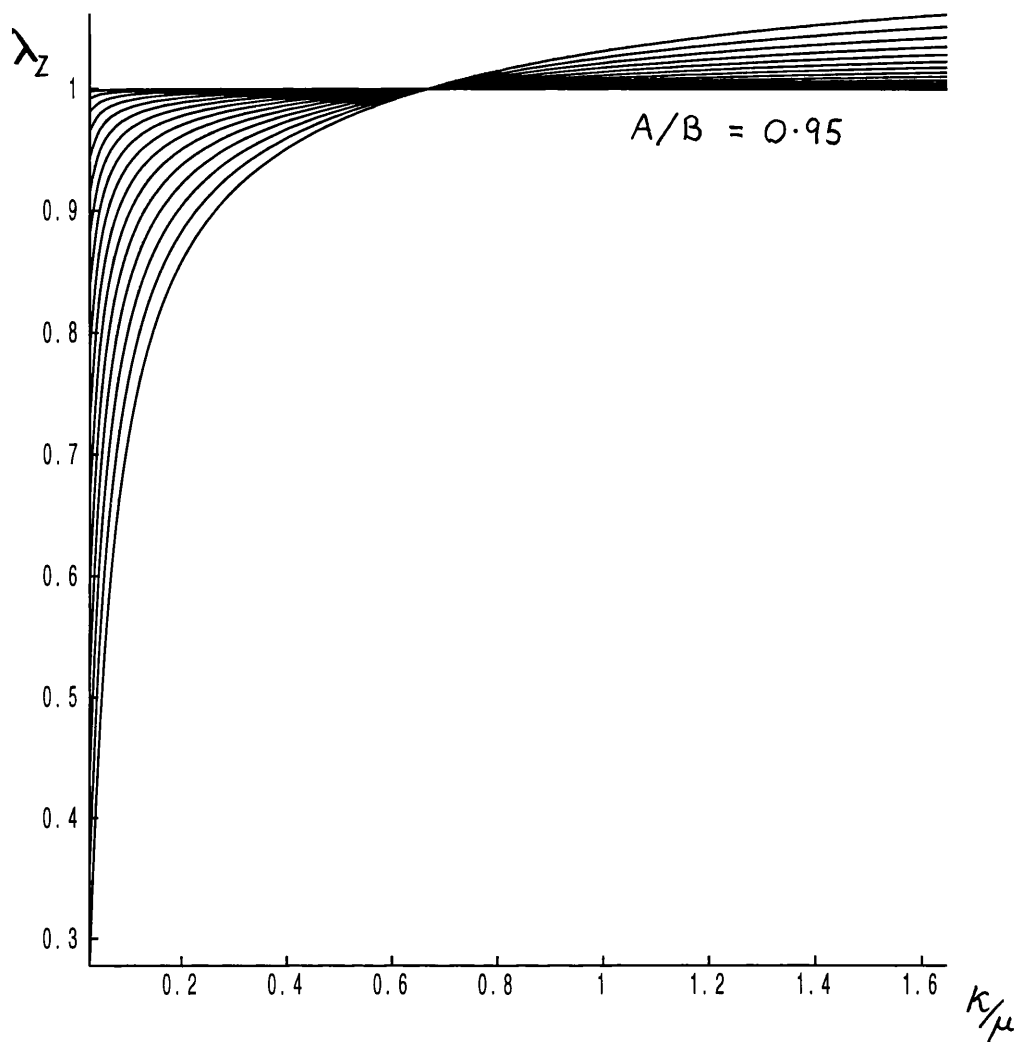


Figure 4.3 Plot of λ_z against κ/μ for highly compressible materials. Initial thicknesses $A/B = 0.2$ (0.05) 0.95.

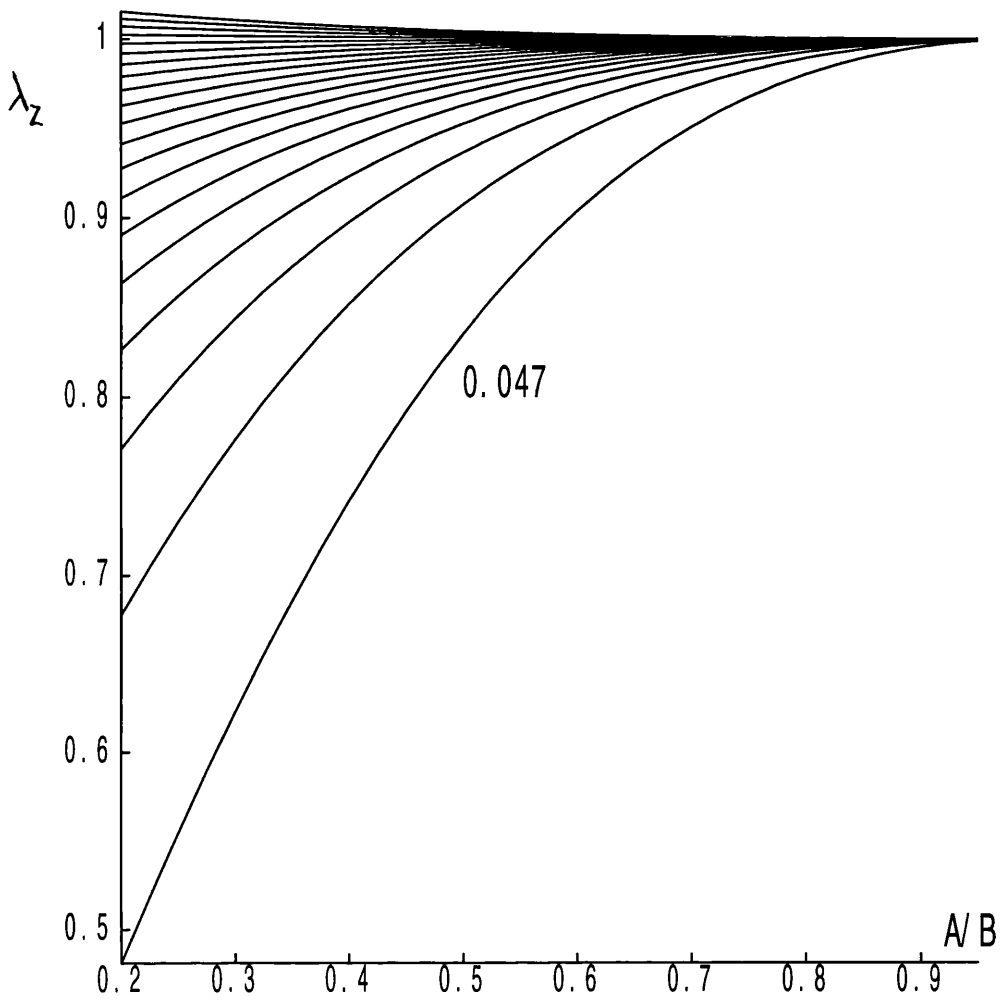


Figure 4.4 Plot of λ_z against the undeformed thickness A/B $\kappa/\mu = 0.047, \dots, 0.81$.

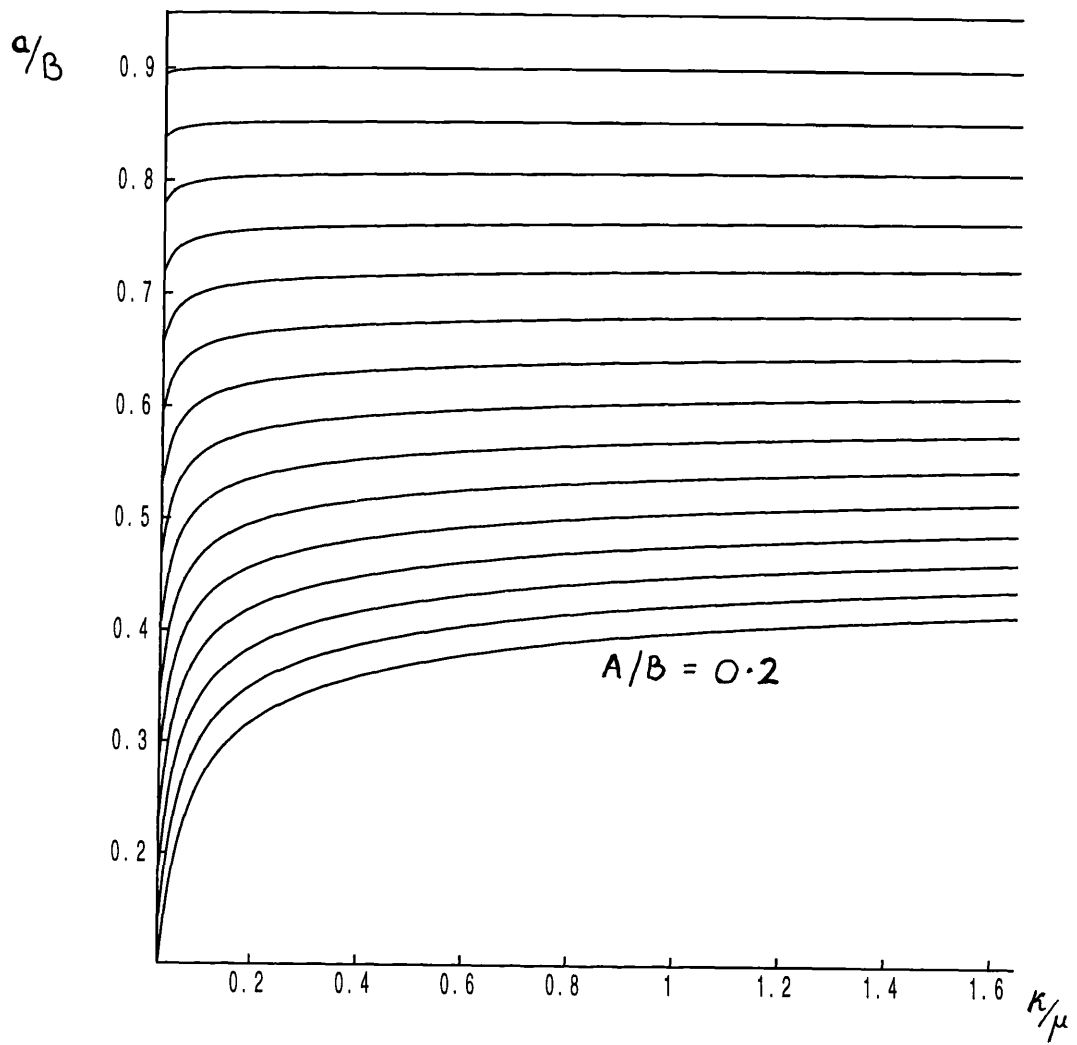


Figure 4.5 Plot of deformed inner radius a/B against κ/μ for a variety of initial thicknesses $A/B = 0.2 (0.05) 0.95$.

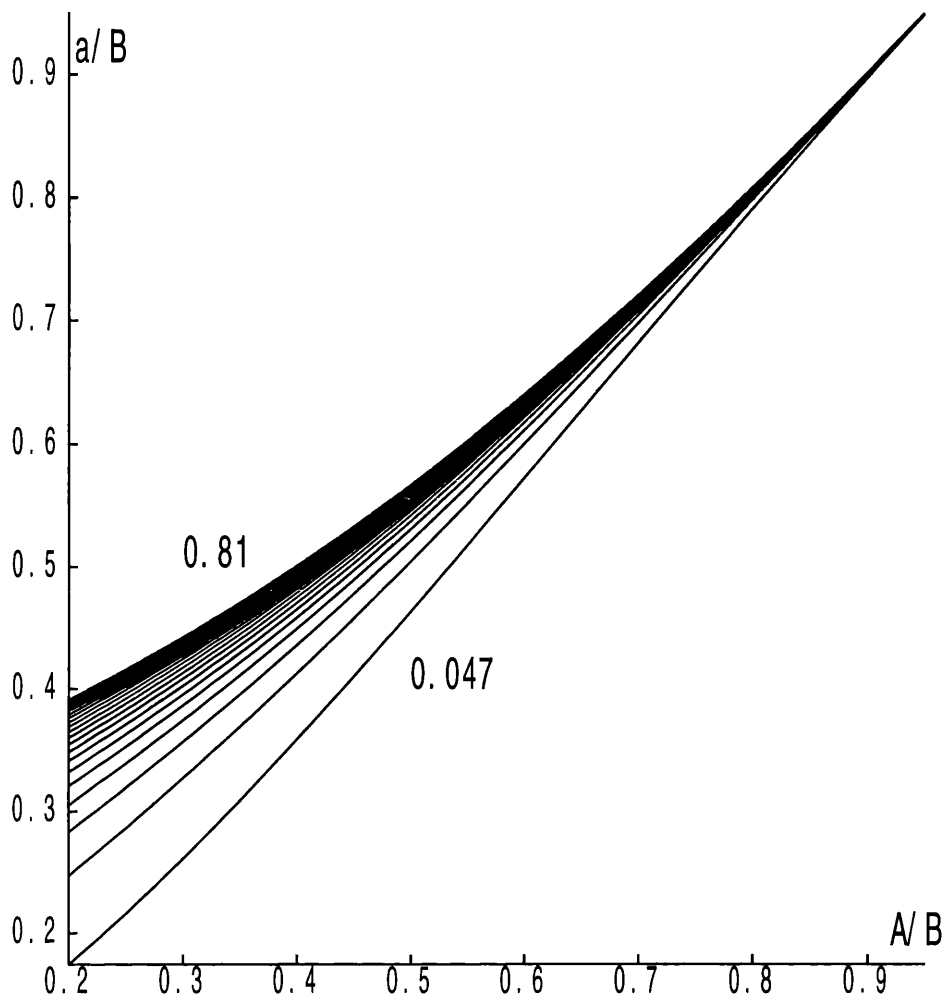


Figure 4.6 Plot of deformed inner radius a/B against initial thickness A/B for highly compressive materials. $\kappa/\mu = 0.047, \dots, 0.81$.

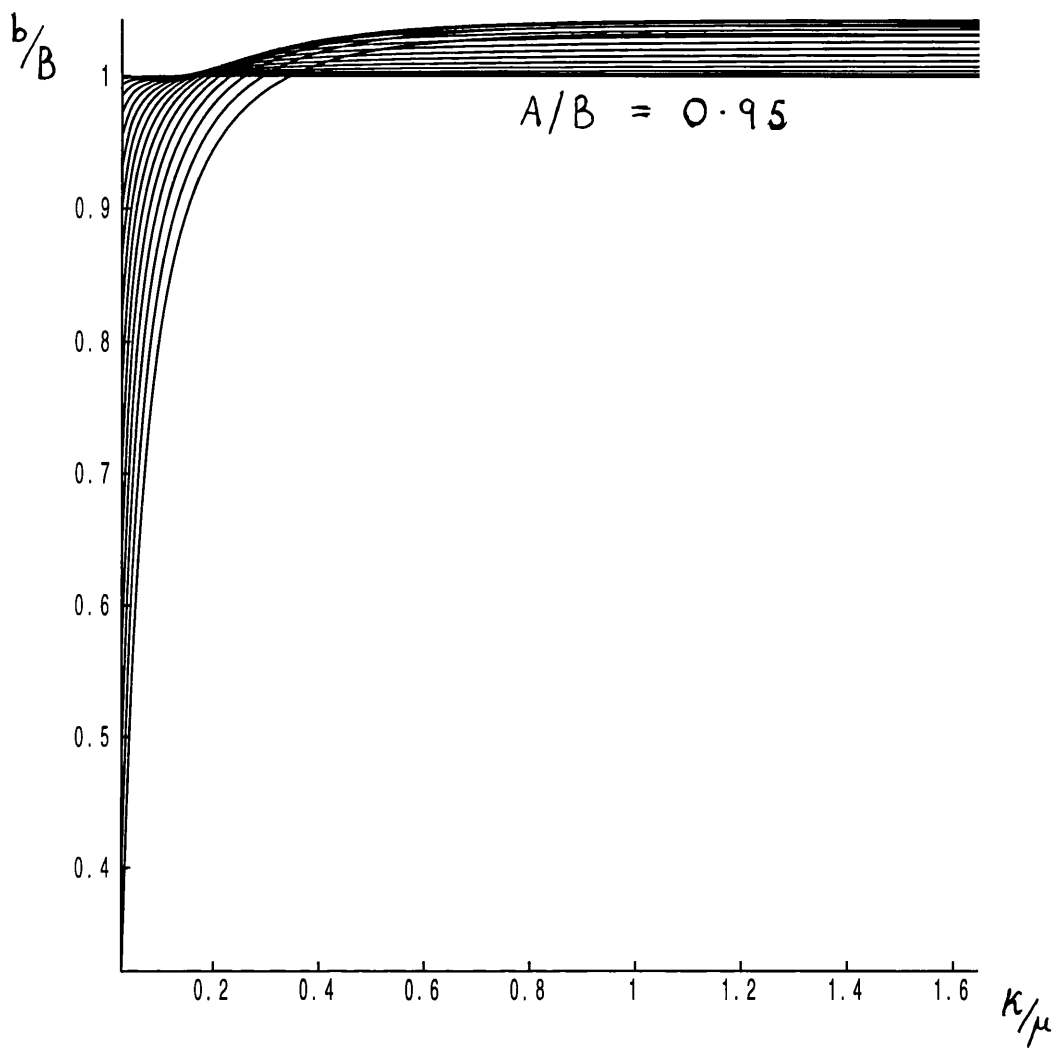


Figure 4.7 Plot of the deformed outer radius b/B against κ/μ for a wide range of initial thicknesses A/B , $A=0.2$ (0.05) 0.95.

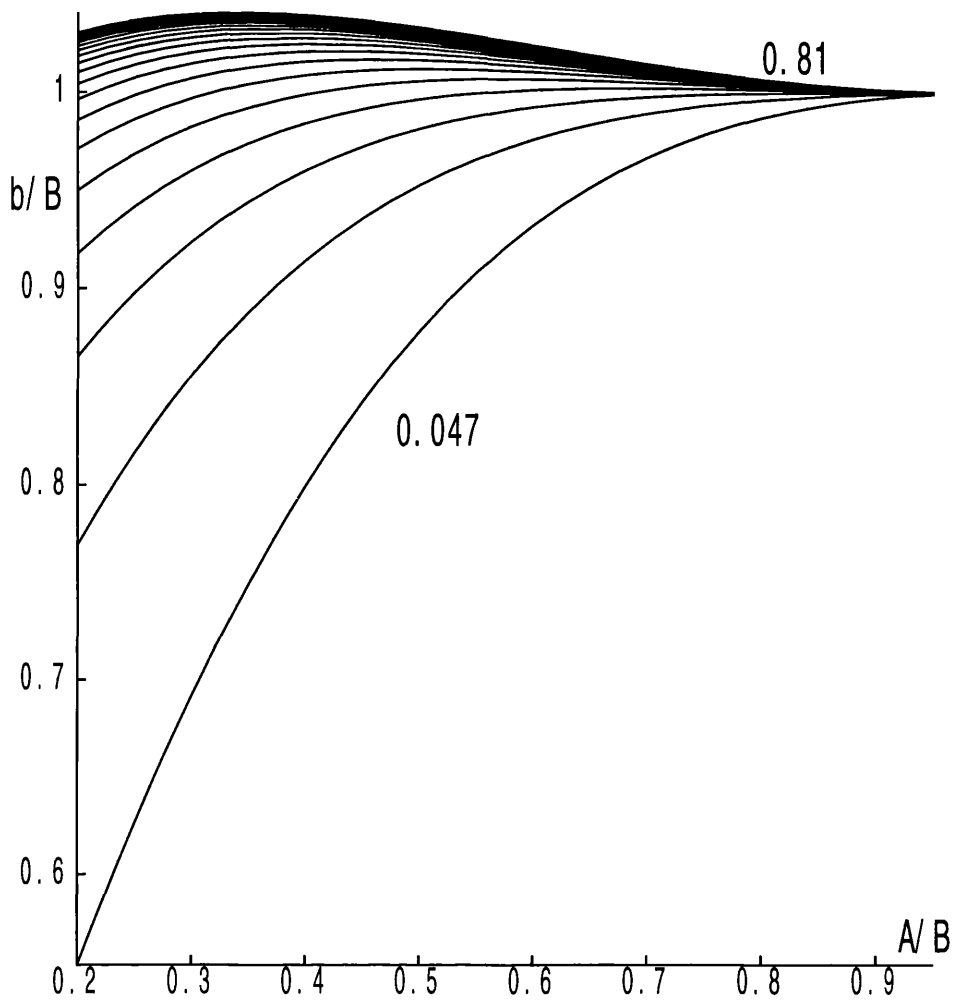


Figure 4.8 Plot of the deformed outer radius b against the initial thickness A/B for κ/μ close to zero.

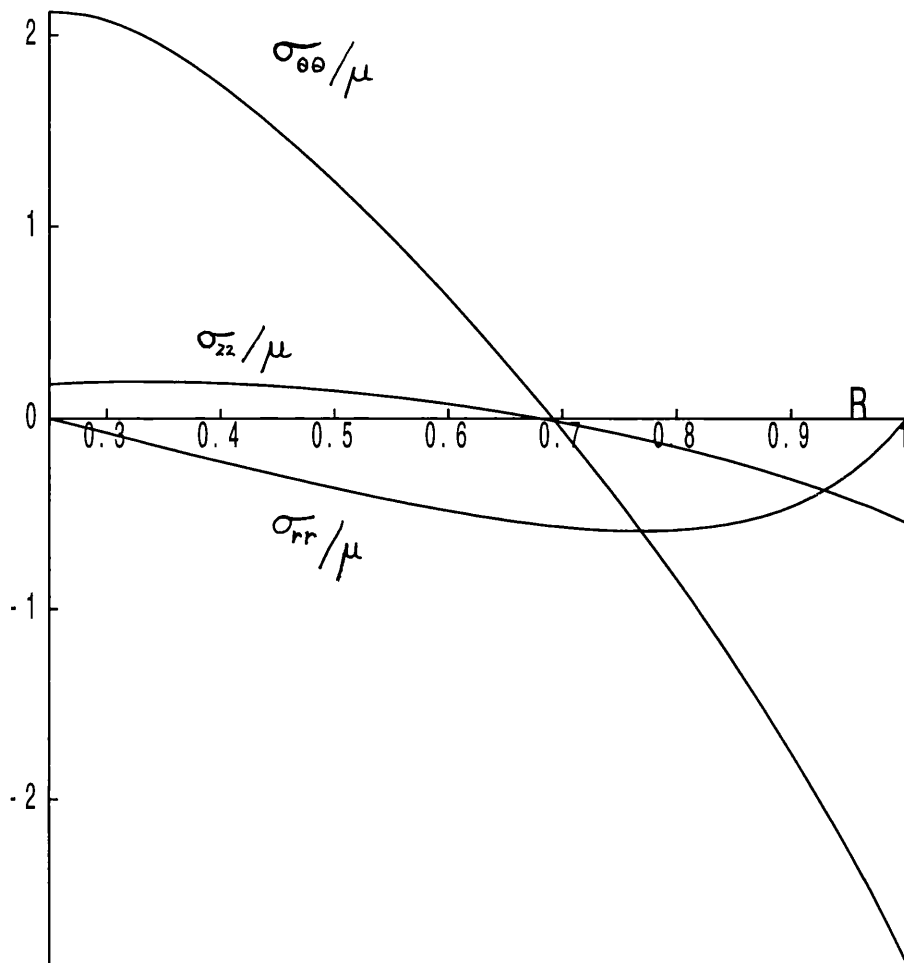


Figure 4.9 Plot of the non-dimensionalised stresses $\sigma_{\theta\theta}/\mu, \sigma_{zz}/\mu, \sigma_{rr}/\mu$, against the undeformed radius R for a tube with $A/B = 0.25, \beta = 0.25$.

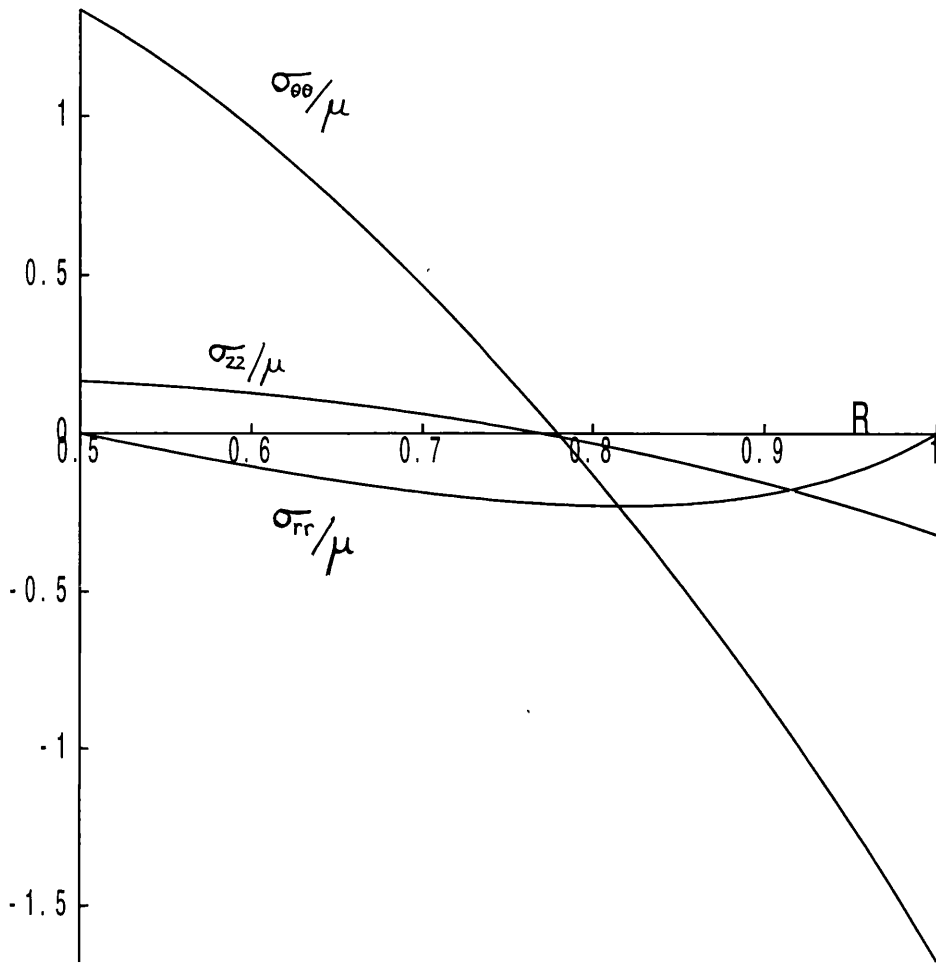


Figure 4.10 Plot of the non-dimensionalised stresses $\sigma_{\theta\theta}/\mu, \sigma_{zz}/\mu, \sigma_{rr}/\mu$, against the undeformed radius R for a tube with $A/B = 0.5, \beta = 0.25$.

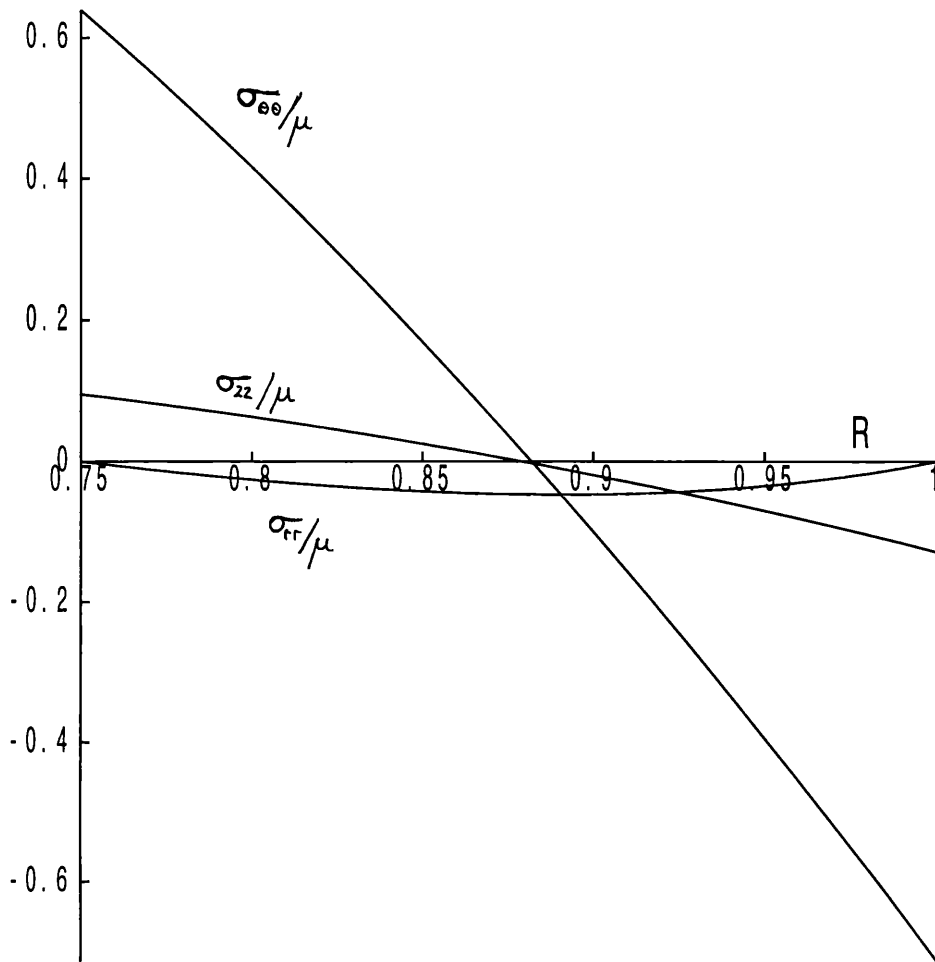


Figure 4.11 Plot of the non-dimensionalised stresses $\sigma_{\theta\theta}/\mu, \sigma_{zz}/\mu, \sigma_{rr}/\mu$, against the undeformed radius R for a tube with $A/B = 0.75, \beta = 0.25$.

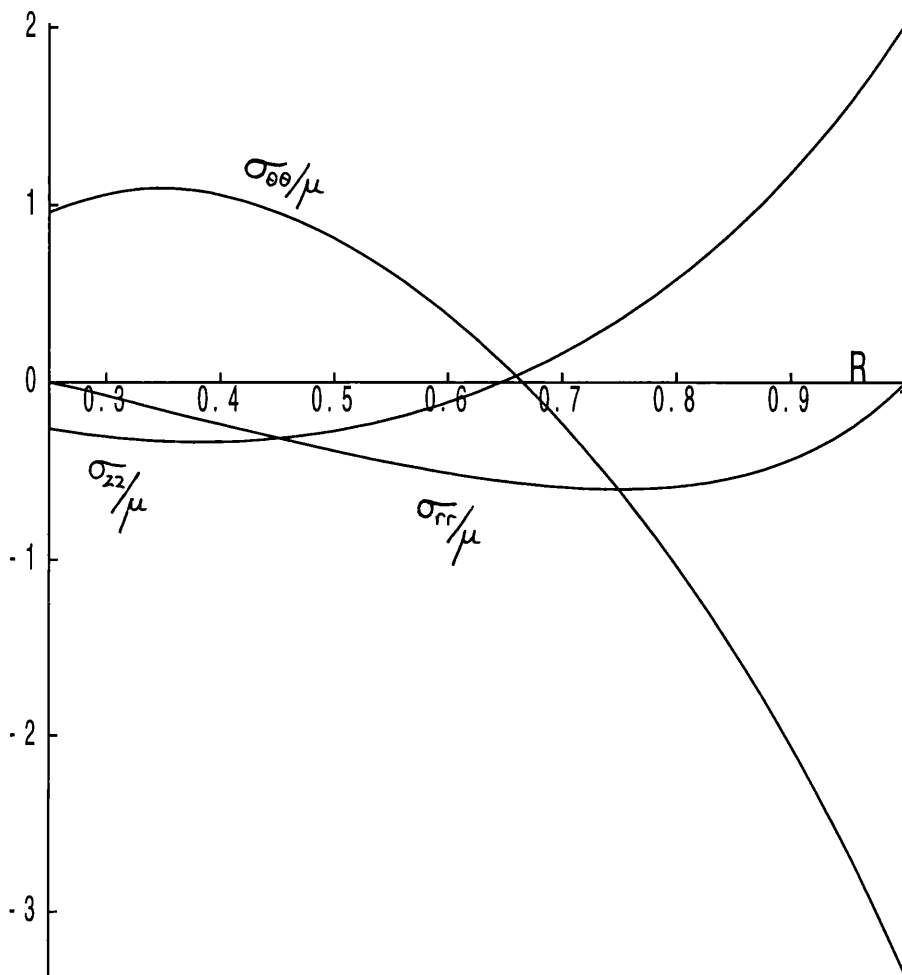


Figure 4.12 Plot of the non-dimensionalised stresses $\sigma_{\theta\theta}/\mu$, σ_{zz}/μ , σ_{rr}/μ , against the undeformed radius R for a tube with $A/B = 0.25$, $\beta = -0.25$.

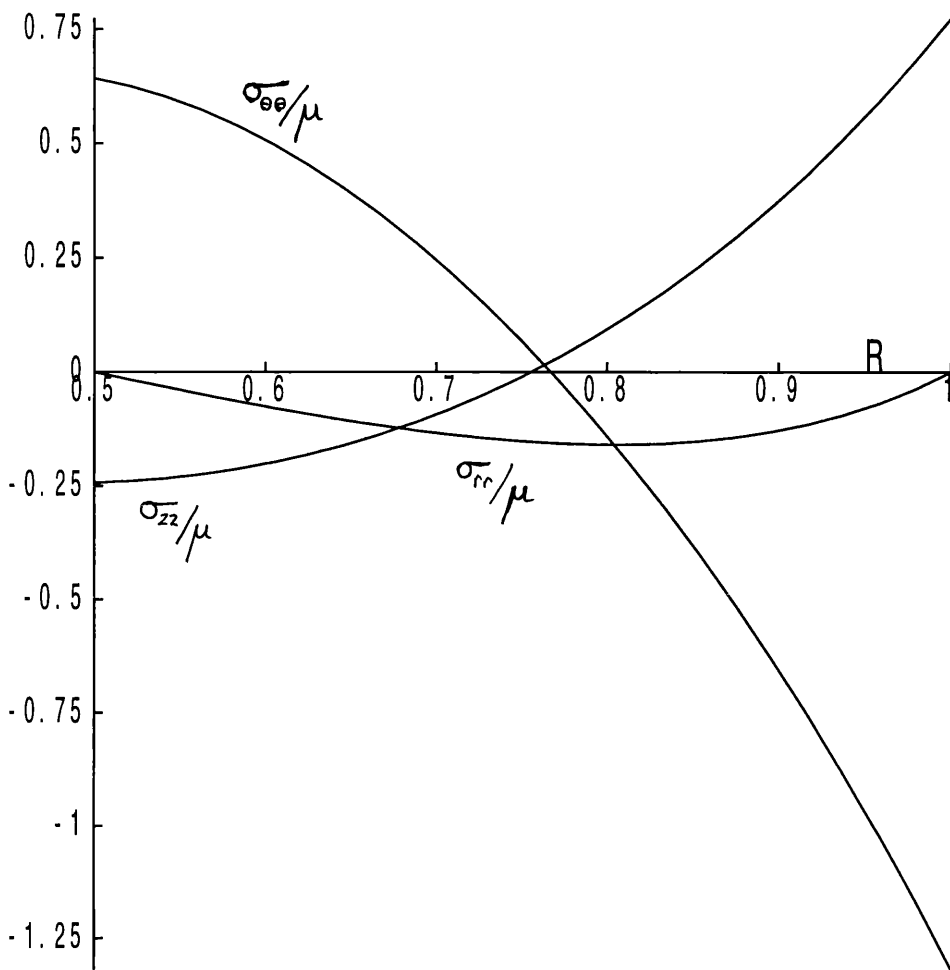


Figure 4.13 Plot of the non-dimensionalised stresses $\sigma_{\theta\theta}/\mu$, σ_{zz}/μ , σ_{rr}/μ , against the undeformed radius R for a tube with $A/B = 0.5$, $\beta = -0.25$.

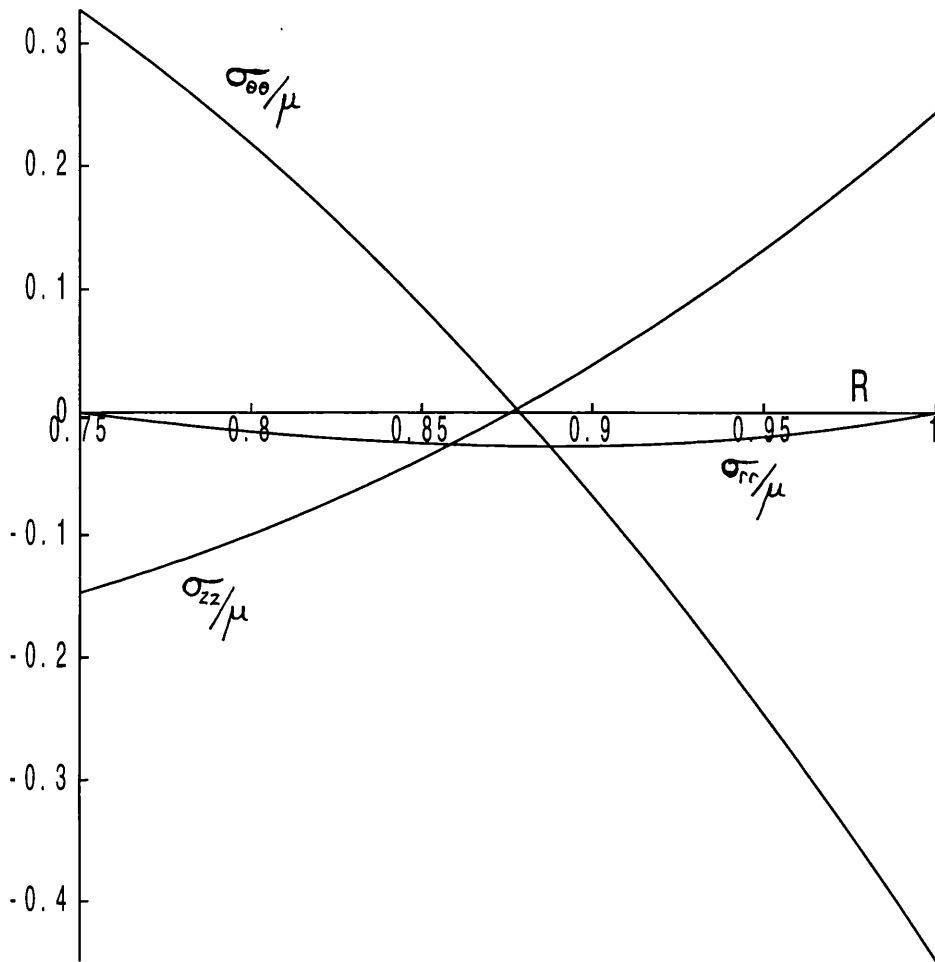


Figure 4.14 Plot of the non-dimensionalised stresses $\sigma_{\theta\theta}/\mu$, σ_{zz}/μ , σ_{rr}/μ , against the undeformed radius R for a tube with $A/B = 0.75$, $\beta = -0.25$.

4.6 Blatz-Ko Materials

Blatz–Ko (1962) proposed the strain-energy

$$W = \frac{\mu}{2}(\lambda_1^{-2} + \lambda_2^{-2} + \lambda_3^{-2} + 2\lambda_1\lambda_2\lambda_3 - 5). \quad (4.6.1)$$

based on experiments on foamed polyurethane rubber and we should hence expect to obtain highly compressive behaviour. Considering the bulk modulus κ defined in (4.2.4) we find

$$\kappa/\mu = \frac{5}{3},$$

where μ is the ground state shear modulus. Thus as expected this strain energy form will model highly compressible materials. To solve the eversion problem for this material we adopt the same method as described in section 4.1. We first note that the eversion of cylindrical tubes composed of Blatz–Ko material has received some formal attention. Carroll and Horgan (1990) provide a closed form parametric solution to the problem. Unfortunately this solution is too complicated to be of any practical use. The solution derived in this paper is identical to the solution found in Chung, Horgan and Abeyarante (1986) after a simple modification.

In Figure 4.15 we plot three curves for the axial stretch λ_z , the deformed outer radius b/B and the deformed inner radius a/B for various initial geometries.

We see that for all undeformed thickness ratios A/B the axial stretch $\lambda_z > 1$ with λ_z monotonic decreasing in A/B . We can also see that as $A \rightarrow B$ then $\lambda_z \rightarrow 1$ and $a \rightarrow b$ as we would expect for a membrane cylinder. From Figure 4.15 we observe that b/B is monotonic increasing and for a thick cylinder with $A/B = 0.25$, say, we find $\lambda_\theta \cong 5$ which represents a large deformation. We find that the deformed radius a/B is also monotonic increasing and hence the deformed radii are qualitatively similar to the exact material with both a/B and b/B monotonic increasing in A/B .

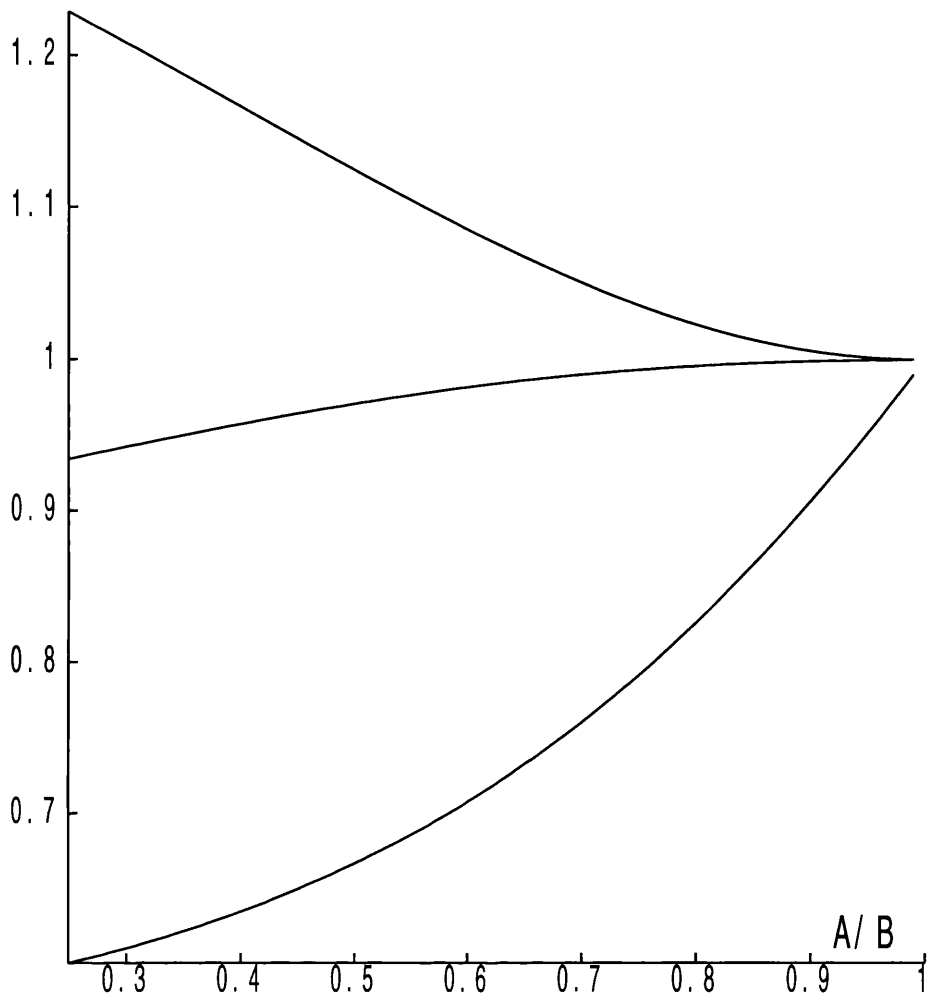


Figure 4.15 Plot of the axial stretch λ_z (upper curve), the deformed outer radius b/B and the deformed inner radius a/B (lower curve) against the initial thickness.

Chapter 5

The Incremental Equations

5.1 Basic Incremental Theory

Suppose that a ‘small’¹ superimposed deformation is made to the body in its current configuration. This new state becomes the current configuration and the everted state is now regarded as the new reference configuration. In terms of the reference configuration we write the equation of motion as

$$\text{Div } \mathbf{S} + \rho_r \mathbf{b} = \rho_r \mathbf{x}_{tt}, \quad (5.1.1)$$

where \mathbf{S} is the nominal stress, ρ_r denotes the material density in the reference configuration, \mathbf{b} is a body or external force ‘vector’ and \mathbf{x}_{tt} is the material acceleration. For equilibrium problems $\mathbf{x}_{tt} \equiv 0$ and so (5.1.1) reduces to

$$\text{Div } \mathbf{S} + \rho_r \mathbf{b} = \mathbf{0}. \quad (5.1.2)$$

In the absence of body forces $\mathbf{b} \equiv \mathbf{0}$ and the equilibrium equation is then

$$\text{Div } \mathbf{S} = \mathbf{0}. \quad (5.1.3)$$

Applying an increment to \mathbf{x} ; $\mathbf{x} \rightarrow \mathbf{x} + \dot{\mathbf{x}}$, which results in an incremental stress $\dot{\mathbf{S}}$, we have

$$\text{Div } \dot{\mathbf{S}} = \mathbf{0}. \quad (5.1.4)$$

¹we do not quantify precisely the meaning of small, but assume it is small compared to the eversion deformation

Now taking the everted solution as the reference configuration

$$\operatorname{div} \dot{\mathbf{S}}_o = \mathbf{0} , \quad (5.1.5)$$

where div is the divergence operator in the everted configuration and $\dot{\mathbf{S}}_o$ is the increment in the nominal stress referred to the everted configuration. Henceforth a superposed dot will represent an increment in the appropriate quantity and the subscript zero will specify evaluation in the current configuration. In component form with respect to an orthonormal system of base vectors (5.1.5) is

$$\dot{S}_{oji,j} + \dot{S}_{oji} \mathbf{e}_k \cdot \mathbf{e}_{j,k} + \dot{S}_{okj} \mathbf{e}_i \cdot \mathbf{e}_{j,k} = 0 , \quad (i = 1, 2, 3) . \quad (5.1.6)$$

For the problem considered here we shall require cylindrical coordinates. The values of $\mathbf{e}_i \cdot \mathbf{e}_{j,k}$, where i, j, k are any combination of $(1, 2, 3)$ which correspond to the (θ, z, r) directions, are easily calculated and can be found in Haughton and Ogden (1979,a) for example. The surface tractions per unit area in the reference configuration are

$$\mathbf{T} = \mathbf{S}^T \mathbf{N} ,$$

and, since no extra loading is imposed on the surface of the body, the incremental boundary conditions are given by

$$\dot{\mathbf{S}}_o^T \mathbf{n} = \mathbf{0} , \quad (5.1.7)$$

where \mathbf{n} is the unit outward normal to the surface of the body when referred to the current state. From (2.1.2) we see that

$$\mathbf{F} = \frac{\partial \mathbf{x}}{\partial \mathbf{X}} , \quad (5.1.8)$$

so the incremental deformation gradient is then

$$\dot{\mathbf{F}} = \frac{\partial \dot{\mathbf{x}}}{\partial \mathbf{X}} . \quad (5.1.9)$$

If we evaluate this in the current configuration we yield

$$\dot{\mathbf{F}}_0 = \frac{\partial \dot{\mathbf{x}}_0}{\partial \mathbf{x}} = \boldsymbol{\eta} . \quad (5.1.10)$$

5.2 Incompressible Incremental Equations

For the incremental constitutive law we first note

$$\mathbf{S} = \frac{\partial W}{\partial \mathbf{F}^T} - p\mathbf{F}^{-1}. \quad (5.2.1)$$

which is the constitutive law for an incompressible material. Here \mathbf{F} is the deformation gradient, $W = W(\lambda_1, \lambda_2, \lambda_3)$ is the strain-energy function of the material and p is a Lagrange multiplier which arises through the incompressibility constraint. It is worth noting that p can be regarded as acting as a hydrostatic stress. We note that in (5.2.1) we have defined

$$\left(\frac{\partial W}{\partial \mathbf{F}}\right)_{ij} = \frac{\partial W}{\partial F_{ij}}. \quad (5.2.2)$$

We note this as many texts, including Ogden (1984), define $\left(\frac{\partial W}{\partial \mathbf{F}}\right)_{ij} = \frac{\partial W}{\partial F_{ji}}$.

Taking the increment of (5.2.1) to the first order,

$$\dot{\mathbf{S}} = \frac{\partial^2 W}{\partial \mathbf{F}^T \partial \mathbf{F}^T} \dot{\mathbf{F}}^T - \dot{p}\mathbf{F}^{-1} - p\dot{\mathbf{F}}^{-1}. \quad (5.2.3)$$

Thus in the current configuration this becomes

$$\dot{\mathbf{S}}_o = \mathbf{B} \boldsymbol{\eta}^T - \dot{p}\mathbf{I} + p \boldsymbol{\eta}, \quad (5.2.4)$$

where \mathbf{B} is the fourth order tensor of instantaneous moduli in the current configuration, \mathbf{I} is the identity and we have written $\boldsymbol{\eta}$ for $\dot{\mathbf{F}}_o$. In component form this is,

$$\dot{S}_{oij} = B_{ijkl}\eta_{lk} + p\eta_{ij} - \dot{p}\delta_{ij}. \quad (5.2.5)$$

The non-zero components of \mathbf{B} , given in Haughton and Ogden (1979,a), are, for an incompressible material,

$$\left. \begin{aligned} B_{ijij} &= \lambda_i^2 \frac{\sigma_i - \sigma_j}{\lambda_i^2 - \lambda_j^2}, & \lambda_i \neq \lambda_j, \\ B_{iijj} &= B_{jjii} = \lambda_i \lambda_j \frac{\partial^2 W}{\partial \lambda_i \partial \lambda_j}, \\ B_{ijij} - B_{ijji} &= B_{ijij} - B_{jii j} = \sigma_i, & i \neq j. \end{aligned} \right\} \quad (5.2.6)$$

where

$$\sigma_i = \frac{\partial W}{\partial \lambda_i}.$$

5.3 Compressible Incremental Equations

From the proposed elastic constitutive law (5.2.1) it is clear that a separate treatment must be considered to obtain an incremental constitutive law for a compressible material. However, as will be revealed in due course, the modifications are only slight. We can in fact propose a set of equations where the Lagrange multiplier terms are omitted.

Thus for an unconstrained material we may write

$$\mathbf{S} = \frac{\partial W}{\partial \mathbf{F}^T}. \quad (5.3.1)$$

Taking the increment of (5.3.1) to the first order,

$$\dot{\mathbf{S}} = \frac{\partial^2 W}{\partial \mathbf{F}^T \partial \mathbf{F}^T} \dot{\mathbf{F}}^T \quad (5.3.2)$$

Thus in the current configuration this becomes

$$\dot{\mathbf{S}}_o = \mathbf{B} \boldsymbol{\eta}^T, \quad (5.3.3)$$

In component form this is,

$$\dot{S}_{oij} = B_{ijkl} \eta_{lk} \quad (5.3.4)$$

The non-zero components of \mathbf{B} , given in Haughton and Ogden (1979,a), are, for a compressible material,

$$\left. \begin{aligned} B_{ijij} &= \lambda_i^2 \frac{\sigma_i - \sigma_j}{\lambda_i^2 - \lambda_j^2}, & \lambda_i &\neq \lambda_j, \\ JB_{iijj} &= JB_{jjii} = \lambda_i \lambda_j \frac{\partial^2 W}{\partial \lambda_i \partial \lambda_j}, \\ B_{ijij} - B_{ijji} &= B_{ijij} - B_{jii j} = \sigma_i, & i &\neq j. \end{aligned} \right\} \quad (5.3.5)$$

If we set $J = 1$, we obtain the non-zero components of \mathbf{B} for an incompressible material as given in (5.2.6).

Chapter 6

Bifurcation Analysis

6.1 Incremental Deformation Gradient

The existence of a cylindrical everted configuration for a cylindrical shell has been established for a variety of incompressible and compressible materials, we now proceed to apply an incremental deformation to examine possible bifurcation modes and hence the existence of a cylindrical configuration.

Three different modes of bifurcation will be considered: Asymmetric (the most general case where the incremental displacements depend on r , θ and z), Prismatic (no z dependence) and Axisymmetric (no θ dependence). Applying an incremental deformation to the body and letting \mathbf{x} be the position vector of a material point in the current configuration, we can write

$$\mathbf{x} = r\mathbf{e}_3 + z\mathbf{e}_2, \quad (6.1.1)$$

and hence

$$\dot{\mathbf{x}}_o = v(r, \theta, z)\mathbf{e}_1 + w(r, \theta, z)\mathbf{e}_2 + u(r, \theta, z)\mathbf{e}_3. \quad (6.1.2)$$

We also write

$$\mathbf{e}_r = (\cos \theta, \sin \theta, 0), \quad \mathbf{e}_\theta = (-\sin \theta, \cos \theta, 0), \quad \mathbf{e}_z = (0, 0, 1), \quad (6.1.3)$$

where the (1,2,3) directions correspond to the (θ, z, r) directions respectively. With respect to the current position vector \mathbf{x} , we have

$$\mathbf{e}_1 = \frac{1}{r} \frac{\partial \mathbf{x}}{\partial \theta} = \mathbf{e}_\theta, \quad \mathbf{e}_2 = \frac{\partial \mathbf{x}}{\partial z} = \mathbf{e}_z, \quad \mathbf{e}_3 = \frac{\partial \mathbf{x}}{\partial r} = \mathbf{e}_r, \quad (6.1.4)$$

hence we write

$$\boldsymbol{\eta} = \text{grad } \dot{\mathbf{x}}_o \equiv \frac{\partial}{\partial x_i}(\dot{\mathbf{x}}) \otimes \mathbf{e}_i, \quad (6.1.5)$$

where $\dot{\mathbf{x}}$ is given in (6.1.2). Substituting (6.1.2) with (6.1.4) into (6.1.5) we yield

$$\begin{aligned} \boldsymbol{\eta} = & \frac{1}{r} \frac{\partial}{\partial \theta} (v \mathbf{e}_1 + w \mathbf{e}_2 + u \mathbf{e}_3) \otimes \mathbf{e}_1 + \frac{\partial}{\partial z} (v \mathbf{e}_1 + w \mathbf{e}_2 + u \mathbf{e}_3) \otimes \mathbf{e}_2 \\ & + \frac{\partial}{\partial r} (v \mathbf{e}_1 + w \mathbf{e}_2 + u \mathbf{e}_3) \otimes \mathbf{e}_3 \end{aligned} \quad (6.1.6).$$

Hence $\boldsymbol{\eta}$ has components

$$\boldsymbol{\eta} = \begin{bmatrix} (u + v_\theta)/r & v_z & v_r \\ w_\theta/r & w_z & w_r \\ (u_\theta - v)/r & u_z & u_r \end{bmatrix}, \quad (6.1.7)$$

in cylindrical coordinates where (θ, z, r) subscripts denote partial derivatives.

At this point it is necessary to decide on whether the material is incompressible or compressible before developing any further analysis. As will be seen in due course the incompressibility constraint allows considerable manipulation of the equilibrium equations.

6.2 Incompressible Materials

For an incompressible material we have

$$tr(\boldsymbol{\eta}) \equiv (u + v_\theta)/r + w_z + u_r = 0 . \quad (6.2.1)$$

We shall produce all subsequent bifurcation analysis for the Asymmetric mode as this has the incremental displacements u, v, w dependent on r, θ, z . For equation (5.1.5) let us consider the radial equilibrium equation which corresponds to $i = 3$,

$$\dot{S}_{0j3,j} + \dot{S}_{0j3}\mathbf{e}_k \cdot \mathbf{e}_{j,k} + \dot{S}_{0kj}\mathbf{e}_3 \cdot \mathbf{e}_{j,k} = 0 , \quad (6.2.2)$$

where the summation convention is used and $,j$ denotes differentiation in the j -th direction. For non-zero components of $\mathbf{e}_k \cdot \mathbf{e}_{j,k}$, from (6.1.4) we yield

$$\mathbf{e}_{1,1} = -\frac{\mathbf{e}_3}{r}, \quad \mathbf{e}_{3,1} = \frac{\mathbf{e}_1}{r} ,$$

and hence

$$\mathbf{e}_3 \cdot \mathbf{e}_{1,1} = -\frac{1}{r}, \quad \mathbf{e}_1 \cdot \mathbf{e}_{3,1} = \frac{1}{r} .$$

Thus using these in (6.2.2) we have

$$\dot{S}_{0j3,j} + \frac{\dot{S}_{033}}{r} - \frac{\dot{S}_{011}}{r} = 0 , \quad (6.2.3)$$

which is now our incremental equation of motion in the r -direction. A similar method produces the corresponding equations for the θ, z directions. In the z direction we have

$$\dot{S}_{0j2,j} + \frac{\dot{S}_{032}}{r} = 0 ,$$

and in the θ direction

$$\dot{S}_{0j1,j} + \frac{\dot{S}_{031}}{r} + \frac{\dot{S}_{013}}{r} = 0 .$$

From (6.2.3) and using (5.2.4) we write

$$\dot{S}_{0j3,j} = \{B_{j3qp}\eta_{pq} + p\eta_{j3} - \dot{p}\delta_{j3}\}_{,j} .$$

On substitution of $j = 1, 2, 3$, using (5.2.6) for the non-zero B_{ijkl} and (6.1.7), we obtain

$$\begin{aligned}
\dot{S}_{013,1} &= (B_{1313}(u_{\theta\theta} - v_{\theta})/r + (B_{1331} + p)v_{r\theta})/r \\
\dot{S}_{023,2} &= B_{2323}u_{zz} + (B_{2332} + p)w_{rz} \\
\dot{S}_{033,3} &= B_{3311}(v_{\theta r} + u_r)/r - B_{3311}(v_{\theta} + u)/r^2 + B'_{3311}(v_{\theta} + u)/r \\
&+ B'_{3322}w_z + B_{3322}w_{zr} + (B'_{3333} + p')u_r + (B_{3333} + p)u_{rr} - \dot{p}_r
\end{aligned} \tag{6.2.4}$$

From (5.2.5) and using (6.1.7) we may also write

$$\dot{S}_{033} = B_{3311}(v_{\theta} + u)/r + B_{3322}w_z + (B_{3333} + p)u_r - \dot{p}. \tag{6.2.5}$$

Substitution of (6.2.4), (6.2.5) into (6.2.3) yields

$$\begin{aligned}
\dot{p}_r &= B_{1313}u_{\theta\theta}/r^2 + (rB'_{1133} - B_{1111} - B_{1313})v_{\theta}/r^2 \\
&+ (B_{1331} + B_{1133})v_{r\theta}/r + B_{3333}u_{rr} + B_{2323}u_{zz} \\
&+ (B_{3333} + rB'_{3333} + rp')u_r/r + (rB'_{1133} - B_{1111})u/r^2 \\
&+ (B_{2332} + p)w_{rz} + B'_{3322}w_z + B_{3322}w_{zr} + pu_{rr} \\
&+ B_{3322}w_z/r + p(u_r - v_{\theta}/r - u/r + v_{r\theta})/r - B_{1122}w_z/r,
\end{aligned} \tag{6.2.6}$$

If, for example, we were considering the Prismatic or Axisymmetric cases the equations would simplify, in (6.2.4) we would lose (6.2.4)₁ or (6.2.4)₂ due to the loss of the z or θ -dependence respectively. Appealing to the incompressibility condition (6.2.1) we differentiate with respect to r to obtain

$$r^2u_{rr} + ru_r - u + rv_{r\theta} - v_{\theta} + r^2w_{rz} = 0, \tag{6.2.7}$$

rewriting (6.2.1) yields

$$\frac{w_z}{r} = -\frac{u_r}{r} - \frac{(u + v_{\theta})}{r^2}.$$

Re-expressing (6.2.7) for w_{rz} and using the above equation we see that the coefficient of the p term becomes identically zero. In doing so we eliminate explicit dependence on w . Thus (6.2.6) can be simplified to

$$\begin{aligned}
\dot{p}_r &= (rB'_{1133} - rB'_{2233} - B_{1111} + B_{1122} - B_{1313} + B_{3223})v_{\theta}/r^2 \\
&+ (B_{1331} + B_{1133} - B_{3223} - B_{2233})v_{r\theta}/r + B_{1313}u_{\theta\theta}/r^2 + B_{2323}u_{zz} \\
&+ (B_{3333} - B_{2233} - B_{3223})u_{rr} \\
&+ (rB'_{3333} + rp' - rB'_{2233} + B_{3333} - 2B_{2233} + B_{1122} - B_{3223})u_r/r \\
&+ (rB'_{1133} - rB'_{2233} - B_{1111} + B_{1122} + B_{3223})u/r^2,
\end{aligned} \tag{6.2.8}$$

A similar treatment for \dot{p}_θ and \dot{p}_z produces

$$\begin{aligned}
\dot{p}_\theta = & (rB'_{3131} + B_{3131} + B_{1111} - B_{1122} - B_{2112})u_\theta/r - (rB'_{3131} + B_{3131})v/r \\
& + (B_{1111} - B_{1122} - B_{2112})v_{\theta\theta}/r + B_{2121}rv_{zz} + B_{3131}rv_{rr} \\
& + (B_{1133} - B_{1122} - B_{2112} + B_{3113})u_{r\theta} + (rB'_{3131} + B_{3131})v_r ,
\end{aligned} \tag{6.2.9}$$

$$\begin{aligned}
\dot{p}_z = & B_{1212}w_{\theta\theta}/r^2 + (rB'_{3223} + rp' + B_{3223} - B_{1221})u_z/r \\
& + B_{3232}w_{rr} + (B_{2222} - B_{1221} - B_{1122})w_{zz} + (rB'_{3232} + B_{3232})w_r/r \\
& + (B_{2233} + B_{3223} - B_{1221} - B_{1122})u_{rz} ,
\end{aligned} \tag{6.2.10}$$

where (\prime) denotes differentiation with respect to r . Use of the incompressibility condition (6.2.1) and the connexions (5.2.6) has allowed us to couple equations (6.2.8)-(6.2.10) for u and decouple (6.2.8), (6.2.9) for w . To solve these equations we use a standard separation of variables method and thus set

$$\begin{aligned}
u &= f(r) \cos m\theta \cos \alpha z , \\
v &= g(r) \sin m\theta \cos \alpha z , \\
w &= h(r) \cos m\theta \sin \alpha z , \\
\dot{p} &= k(r) \cos m\theta \cos \alpha z .
\end{aligned} \tag{6.2.11}$$

Since we require the incremental displacements to be single valued we shall assume that the mode number m is an integer $m \geq 0$. We can interpret the parameter α and associated end conditions in several different ways. Taking equations (6.2.11) as they appear above we might insist that the incremental end displacement w should be zero on the ends. This leads to

$$\alpha = n\pi/\ell, \quad n = 1, 2, 3, \dots \tag{6.2.12}$$

In this case we also have $\dot{s}_{o32} = B_{3232}(w_r + u_z) = 0$, $z = -\ell, 0$. To be definite we shall regard n as being fixed at the value unity so that the parameter α is inversely proportional to the length of the tube. It is easily verified that we obtain the same

incremental equations to solve if (6.2.11) is replaced by

$$\begin{aligned}
u &= f(r) \sin m\theta \sin \alpha z , \\
v &= g(r) \cos m\theta \sin \alpha z , \\
w &= h(r) \sin m\theta \cos \alpha z , \\
\dot{p} &= k(r) \sin m\theta \sin \alpha z .
\end{aligned} \tag{6.2.13}$$

We still have (6.2.12) provided that we interpret the end conditions appropriately.

The expressions (6.2.11) are then substituted into (6.2.8)–(6.2.10) and eliminating $h(r)$ via the incompressibility condition we obtain coupled equations for $f(r)$, $g(r)$, $k(r)$,

$$\begin{aligned}
mk &= (rB'_{3131} + B_{3131} + B_{1111} - B_{1122} - B_{2112})mf/r + (rB'_{3131} + B_{3131})g/r \\
&\quad + (B_{1111} - B_{1122} - B_{2112})m^2g/r + r\alpha^2 B_{2121}g - rB_{3131}g'' \\
&\quad + (B_{1133} - B_{1122} - B_{2112} + B_{3113})mf' - (rB'_{3131} + B_{3131})g' ,
\end{aligned} \tag{6.2.14}$$

$$\begin{aligned}
\alpha^2 k &= -m^2\{f' + (mg + f)/r\}B_{1212}/r^2 + (rB'_{3232} + rp' + B_{3223} - B_{1221})\alpha^2 f/r \\
&\quad + B_{3232}\{f''' + (f'' + mg'')/r - 2(f' + mg')/r^2 + 2(f + mg)/r^3\} \\
&\quad - (B_{2222} - B_{1221} - B_{1122})\alpha^2(f + mg)/r \\
&\quad - (B_{2222} - B_{2233} - B_{3223})\alpha^2 f' \\
&\quad + (rB'_{3232} + B_{3232})\{f'' + (f' + mg')/r - (f + mg)/r^2\}/r ,
\end{aligned} \tag{6.2.15}$$

$$\begin{aligned}
k' &= (r(B'_{1133} - B'_{2233}) - B_{1111} + B_{1122} - B_{1313} + B_{3223})mg/r^2 \\
&\quad + (B_{1331} + B_{1133} - B_{3223} - B_{2233})mg'/r + (B_{3333} - B_{2233} - B_{3223})f'' \\
&\quad + (r(B'_{3333} + p' - B'_{2233}) + B_{3333} - 2B_{2233} + B_{1122} - B_{3223})f'/r \\
&\quad + (r(B'_{1133} - B'_{2233}) - B_{1111} + B_{1122} + B_{3223})f/r^2 \\
&\quad - m^2 B_{1313}f/r^2 - \alpha^2 B_{2323}f .
\end{aligned} \tag{6.2.16}$$

The corresponding boundary conditions (5.1.7) on the curved surfaces are then

$$\left. \begin{aligned}
rg' - g - mf &= 0 , \\
r^2 f'' + rf' + (\alpha^2 r^2 + m^2 - 1)f &= 0 , \\
(B_{1133} - B_{2233})(f + mg) + (B_{3333} - B_{2233} + \sigma_3)rf' - rk &= 0 ,
\end{aligned} \right\} r = a, b. \tag{6.2.17}$$

We choose

$$\mathbf{y} = (f, f', f'', g, g', k)^T, \quad (6.2.18)$$

equations (6.2.14)-(6.2.16) can then be written

$$\mathbf{y}' = \mathbf{A}\mathbf{y}$$

where the components of the matrix \mathbf{A} have the form

$$\mathbf{A} = \begin{bmatrix} 0 & 1 & 0 & 0 & 0 & 0 \\ 0 & 0 & 1 & 0 & 0 & 0 \\ A_{31} & A_{32} & A_{33} & A_{34} & A_{35} & A_{36} \\ 0 & 0 & 0 & 0 & 1 & 0 \\ A_{51} & A_{52} & 0 & A_{54} & A_{55} & A_{56} \\ A_{61} & A_{62} & A_{63} & A_{64} & A_{65} & 0 \end{bmatrix}, \quad (6.2.19)$$

the non-zero components are obtained from (6.2.14)-(6.2.16). The boundary conditions (6.2.17) become $\mathbf{C}\mathbf{y} = \mathbf{0}, r = a, b$ where

$$\mathbf{C} = \begin{bmatrix} -m & 0 & 0 & -1 & r & 0 \\ C_{21} & r & r^2 & 0 & 0 & 0 \\ 0 & C_{32} & 0 & 0 & 0 & -1 \end{bmatrix}. \quad (6.2.20)$$

The above equations have been solved for the three materials (3.2.3)-(3.2.5) using a wide range of parameters m and α . In each case we have used two different numerical methods that are detailed in chapter 9. We have found that a straightforward method involving the evaluation of a 3×3 determinant is not adequate for this problem and a more sophisticated compound matrix method is required. In both cases the general scheme of the solution process is as follows; given a strain-energy function and an initial thickness ratio A/B we can solve the eversion problem defined by (3.1.15) and (3.1.17) to obtain a and λ , (b is then given by (3.1.8)). In order to present our results graphically we can regard this solution to the eversion problem as a point in the $b/B-A/B$ plane (say). We now choose a combination of parameters m and α and turn attention to the bifurcation problem. This will be tackled in chapter 7 once we have completed our bifurcation analysis by studying the compressible case.

6.3 Compressible Materials

Here we will develop the bifurcation theory for cylinders of compressible material. Loss of the constraint $tr(\boldsymbol{\eta}) = 0$ leaves us with a more complicated system of equations where all analysis will be produced for the most general case, the Asymmetric mode. The incremental equation of motion in the radial direction is

$$\dot{S}_{0j3,j} + \frac{\dot{S}_{033}}{r} - \frac{\dot{S}_{011}}{r} = 0 . \quad (6.3.1)$$

We can apply the following method to produce similar equations for the θ , z directions. From (6.3.1) and using (5.3.4) we obtain

$$\dot{S}_{0j3,j} = \{B_{j3pq}\eta_{qp}\}_{,j} . \quad (6.3.2)$$

On substituting $j = 1, 2, 3$ and finding the non-zero B_{ijkl} from (5.3.5) we have

$$\begin{aligned} \dot{S}_{013,1} &= (B_{1313}(u_{\theta\theta} - v_{\theta})/r + B_{1331}v_{r\theta})/r \\ \dot{S}_{023,2} &= B_{2323}u_{zz} + B_{2332}w_{rz} \\ \dot{S}_{033,3} &= B_{3311}(v_{\theta r} + u_r)/r - B_{3311}(v_{\theta} + u)/r^2 \\ &\quad + B'_{3311}(v_{\theta} + u)/r + B'_{3322}w_z \\ &\quad + B_{3322}w_{zr} + B'_{3333}u_r + B_{3333}u_{rr} \end{aligned} \quad (6.3.3)$$

From (6.3.1) and using (5.3.4) we can also see

$$\dot{S}_{033} = B_{3311}(v_{\theta} + u)/r + B_{3322}w_z + B_{3333}u_r . \quad (6.3.4)$$

Substituting (6.3.3), (6.3.4) and (6.1.7) into (6.3.1) and rearranging we produce

$$\begin{aligned} &B_{2323}u_{zz} + (B_{2332} + B_{2233})w_{zr} + (B_{1331} + B_{1133})\frac{v_{r\theta}}{r} \\ &+ (rB'_{1133} - B_{1313} - B_{1111})\frac{v_{\theta}}{r^2} + B_{3333}u_{rr} \\ &+ (rB'_{3333} + B_{3333})\frac{u_r}{r} + (rB'_{1133} - B_{1111})\frac{u}{r^2} \\ &+ (rB'_{2233} - B_{1122} + B_{2233})\frac{w_z}{r} + B_{1313}\frac{u_{\theta\theta}}{r^2} = 0 \end{aligned} , \quad (6.3.5)$$

where (') denotes differentiation with respect to r . Duplicating the above analysis in the z direction produces

$$\begin{aligned}
& (rB'_{3223} + B_{1122} + B_{3223})\frac{u_z}{r} + (rB'_{3232} + B_{3232})\frac{w_r}{r} \\
& + (B_{2233} + B_{3223})u_{rz} + (B_{1122} + B_{1221})\frac{v_{z\theta}}{r} \quad , \quad (6.3.6) \\
& + B_{1212}\frac{w_{\theta\theta}}{r^2} + B_{2222}w_{zz} + B_{3232}w_{rr} = 0
\end{aligned}$$

and in the θ direction

$$\begin{aligned}
& (B_{1122} + B_{3131}v_{rr} + B_{1111}\frac{v_{\theta\theta}}{r^2} + B_{2121}v_{zz} + B_{2112})\frac{w_{\theta z}}{r} \\
& + (rB'_{3131} + B_{3131})\frac{v_r}{r} + (B_{1111} + rB'_{3113} + B_{1313})\frac{u_{\theta}}{r^2} \quad . \quad (6.3.7) \\
& - (rB'_{3113} + B_{1313})\frac{v}{r^2} + (B_{1133} + B_{3113})\frac{u_{r\theta}}{r} = 0
\end{aligned}$$

Here we have not achieved any simplification of the system (6.3.5)–(6.3.7) such as coupling or decoupling the equations for one of the incremental displacement variables as we did in the previous section. We therefore propose to solve the system of 3 equations in 3 variables u , v , w by setting

$$\begin{aligned}
u &= f(r) \cos m\theta \cos \alpha z \quad , \\
v &= g(r) \sin m\theta \cos \alpha z \quad , \quad (6.3.8) \\
w &= h(r) \cos m\theta \sin \alpha z \quad .
\end{aligned}$$

where we assume the incremental displacement variables are single valued with the mode number m an integer greater than zero. We again interpret α by insisting that we have zero incremental end displacement w which gives

$$\alpha = n\pi/\ell, \quad n = 1, 2, 3, \dots \quad (6.3.9)$$

Here we also have

$$\dot{S}_{\circ 31} = B_{3131}(w_r + u_z) = 0 \quad , \quad z = -\ell, 0 \quad . \quad (6.3.10)$$

In (6.3.9) we shall regard n as being fixed at unity so that α is inversely proportional to the length of the tube. As before we can replace (6.3.8) with (6.2.13) with suitable restrictions. Substituting (6.3.8) into (6.3.5)–(6.3.7) produces respectively

$$\begin{aligned}
& (rB'_{3333} + B_{3333})f'/r + (rB'_{1133} - B_{1313} - B_{1111})mg/r^2 \\
& + (B_{1331} + B_{1133})mg'/r - (rB'_{2233} - B_{1122} + B_{2233})\alpha h/r \quad , \quad (6.3.11) \\
& + (rB'_{1133} - B_{1111} - m^2B_{1313} - \alpha^2r^2B_{2323})f/r^2 \\
& - (B_{2332} + B_{2233})\alpha h' + B_{3333}f'' = 0
\end{aligned}$$

$$\begin{aligned}
& (rB_{3223} + B_{1122} + B_{3223})\alpha f/r + (B_{2233} + B_{3223})\alpha f' \\
& + (B_{1122} + B_{1221})\alpha mg/r - (m^2B_{1212} - \alpha^2r^2B_{2222})h/r^2 \quad , \quad (6.3.12) \\
& + (rB'_{3232} + B_{3232})h'/r + B_{3232}h'' = 0
\end{aligned}$$

$$\begin{aligned}
& (B_{1111} + rB'_{3113} + B_{1313})mf/r^2 + (B_{1133} + B_{3113})mf'/r \\
& - (rB'_{3131} + B_{3131})g'/r - B_{3131}g'' - (B_{1122} + B_{2112})m\alpha h/r \quad . \quad (6.3.13) \\
& + (m^2B_{1111} + rB'_{3113} + B_{1313} + \alpha^2r^2B_{2121})g/r^2 = 0
\end{aligned}$$

The corresponding boundary conditions (5.1.7) on the curved surfaces become

$$\left. \begin{aligned}
rg' - g - mf &= 0 \quad , \\
\alpha f - h' &= 0 \quad , \\
B_{1133}\left(1 - \frac{m^2}{r}\right)f + B_{3333}f' \\
+mB_{1133}g' - \alpha B_{2233}h &= 0 \quad .
\end{aligned} \right\} \quad r = a, b. \quad (6.3.14)$$

If we write

$$\mathbf{y} = (f, f', g, g', h, h'), \quad (6.3.15)$$

we can express (6.3.11)–(6.3.13) as

$$\mathbf{y}' = \mathbf{A}\mathbf{y}. \quad (6.3.16)$$

where

$$\mathbf{A} = \begin{bmatrix} 0 & 1 & 0 & 0 & 0 & 0 \\ A_{21} & A_{22} & A_{23} & A_{24} & A_{25} & A_{26} \\ 0 & 0 & 0 & 1 & 0 & 0 \\ A_{41} & A_{42} & A_{43} & A_{44} & A_{45} & 0 \\ 0 & 0 & 0 & 0 & 0 & 1 \\ A_{61} & A_{62} & A_{63} & 0 & A_{65} & A_{66} \end{bmatrix}. \quad (6.3.17)$$

where A_{ij} are easily obtained from (6.3.11)–(6.3.13). The corresponding boundary equations are then

$$\mathbf{C}\mathbf{y} = \mathbf{0}, \quad r = a, b, \quad (6.3.18)$$

where \mathbf{y} is given in (6.3.15)

$$\mathbf{C} = \begin{bmatrix} -m & 0 & -1 & r & 0 & 0 \\ \alpha & 0 & 0 & 0 & 0 & -1 \\ C_{31} & C_{32} & 0 & C_{34} & C_{35} & 0 \end{bmatrix}. \quad (6.3.19)$$

The C_{ij} are available from (6.3.14).

The above equations are now solved for a compressible Varga form, a Blatz-Ko material and an exact solution material which are detailed in chapter 4. However, before solving these equations we must change the independent variable from r to R . As discussed before we do not have the incompressibility condition to attain $r = r(R)$ analytically and therefore upon solving the equations numerically we shall have to employ an interpolating method to give $r = r(R)$ at any point. As we change the independent variable to R we will also need $R = R(r)$ at any point which can be found by using inverse interpolation.

6.3.1 Varga Materials

For the material (4.4.1) we have introduced a further parameter β into the equations. As discussed in chapter 4 we can choose β to determine the compressibility of the material and hence compare the results to the incompressible Varga material and other compressible forms. We will therefore have a three parameter system in β , m and α to consider. Taking various combinations of these parameters will allow us to study the effects of compressibility, length to radius ratio and choice of mode number on the bifurcation mode produced. Bearing in mind that we have three variables to consider here, we will interpret the data differently from the incompressible case. By choosing the undeformed thickness A/B as our bifurcation variable we remove the necessity of requiring three dimensional plots for our data. We will retain this method when discussing all compressible bifurcations.

6.3.2 Blatz-Ko

Using the strain-energy form (4.6.1) we have a two parameter system in m and α for a highly compressive foam rubber. The experiments of Truesdell (1977) suggest

the existence of many unstable bifurcation modes and hence we shall compare our results with the experimental data and look for stable tubes being produced.

6.3.3 Exact Solution

The material, defined in (4.2.3) is highly compressible like the Blatz–Ko material. However here we are able to investigate the bifurcation of an elastic cylinder which solves the theoretical problem exactly. Here we also study the two parameter system in m and α .

Chapter 7

Incompressible Bifurcation Results

7.1 Numerical Results

The first significant result that we have discovered for bifurcations of everted cylinders is the relative independence of any bifurcation modes $m \geq 2$ on the length of the cylinder (modes $m = 0$ and $m = 1$ behave rather differently and so they are considered separately). To illustrate this we plot in Figures 7.1, 7.2 and 7.3 the critical values of the parameter b/B against $\log(L/B)$ for a variety of mode numbers m . These figures correspond to the three-term Ogden, the Neo-Hookean and the Varga materials respectively. We note here that b/B is **not** a principal stretch, it has been chosen to clarify the results detailed in the figures as it is not possible to see any detail if principal stretches are plotted. For each material we find similarly shaped curves for other thickness ratios A/B . This indicates that a cylinder can be regarded as having infinite length if, approximately, $L/B > 5$. For cylinders with a length ratio much smaller than this we would expect end effects to play an important part and so there is only a small range of values of L/B for which the cylinder is not effectively infinitely long. Also note from Figures 7.1–7.3 how the higher order mode numbers are less dependent on the length ratio of the cylinder. This is significant because, as we show below, the higher order mode

numbers are likely to be the most important.

For the three materials detailed in Figures 7.1–7.3 we find that there is virtually no material dependence on the values of b/B produced for the given mode numbers. We can also see that the type of material doesn't appear to affect the values of L/B at which we may consider the cylinder to be effectively infinitely long.

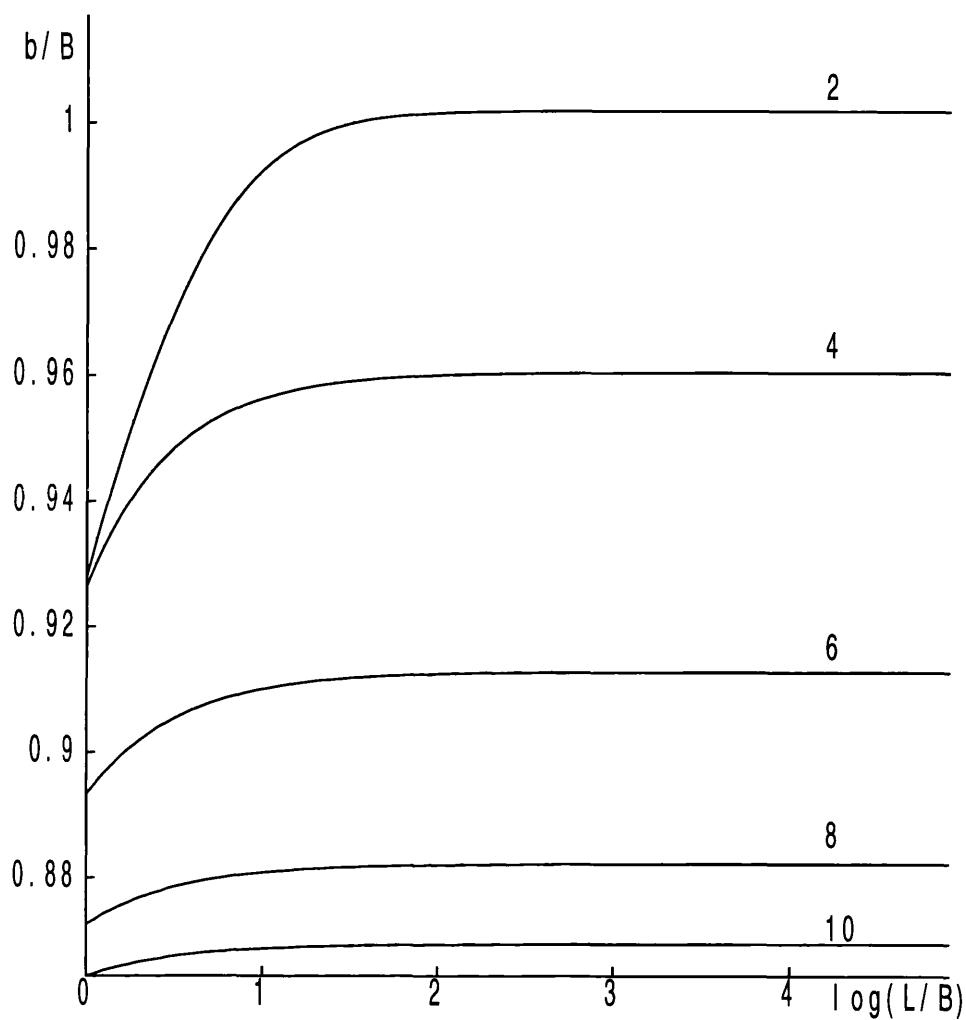


Figure 7.1 Plot of the critical values of b/B vs. $\log(L/B)$ for a cylinder with thickness ratio $A/B = 0.75$. Mode numbers $m = 2, 4, 6, 8, 10$ are shown for the three-term material defined in (3.2.5).

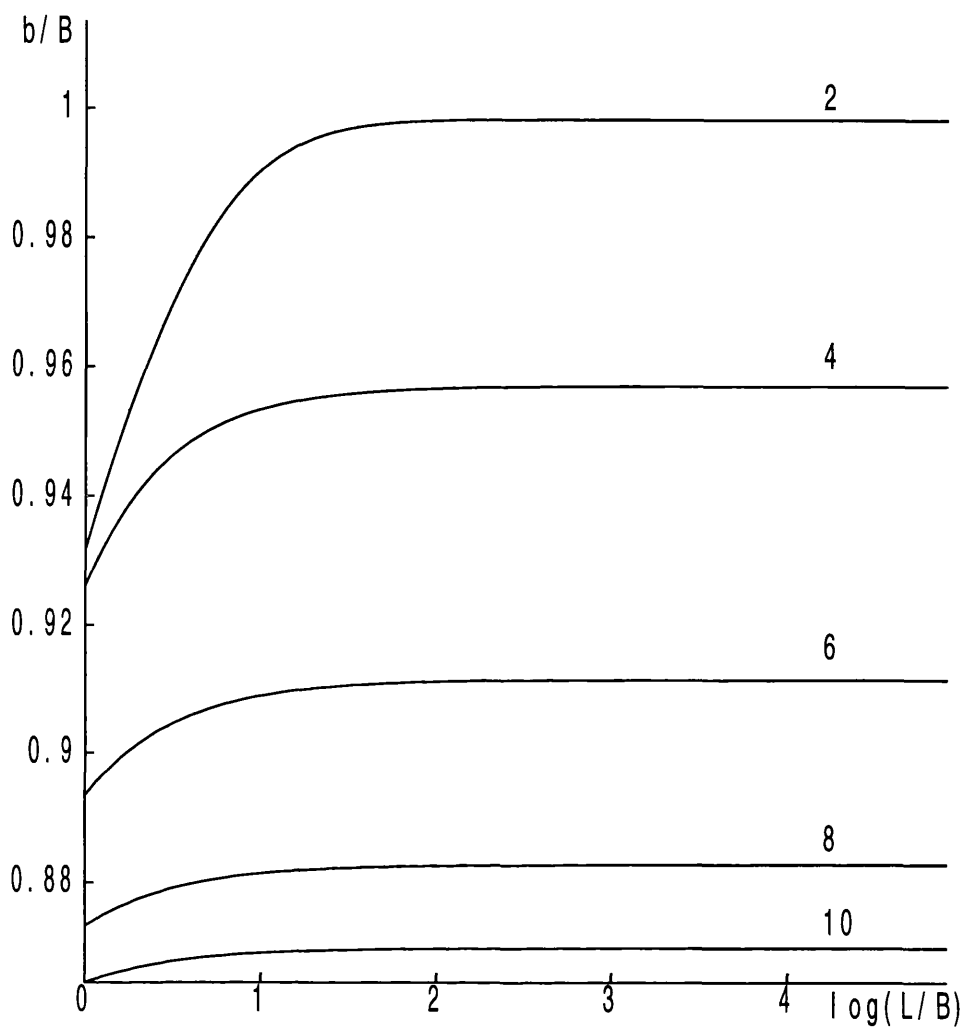


Figure 7.2 Plot of the critical values of b/B vs. $\log(L/B)$ for a cylinder with thickness ratio $A/B = 0.75$. Mode numbers $m = 2, 4, 6, 8, 10$ are shown for the Neo-Hookean material defined in (3.2.4).

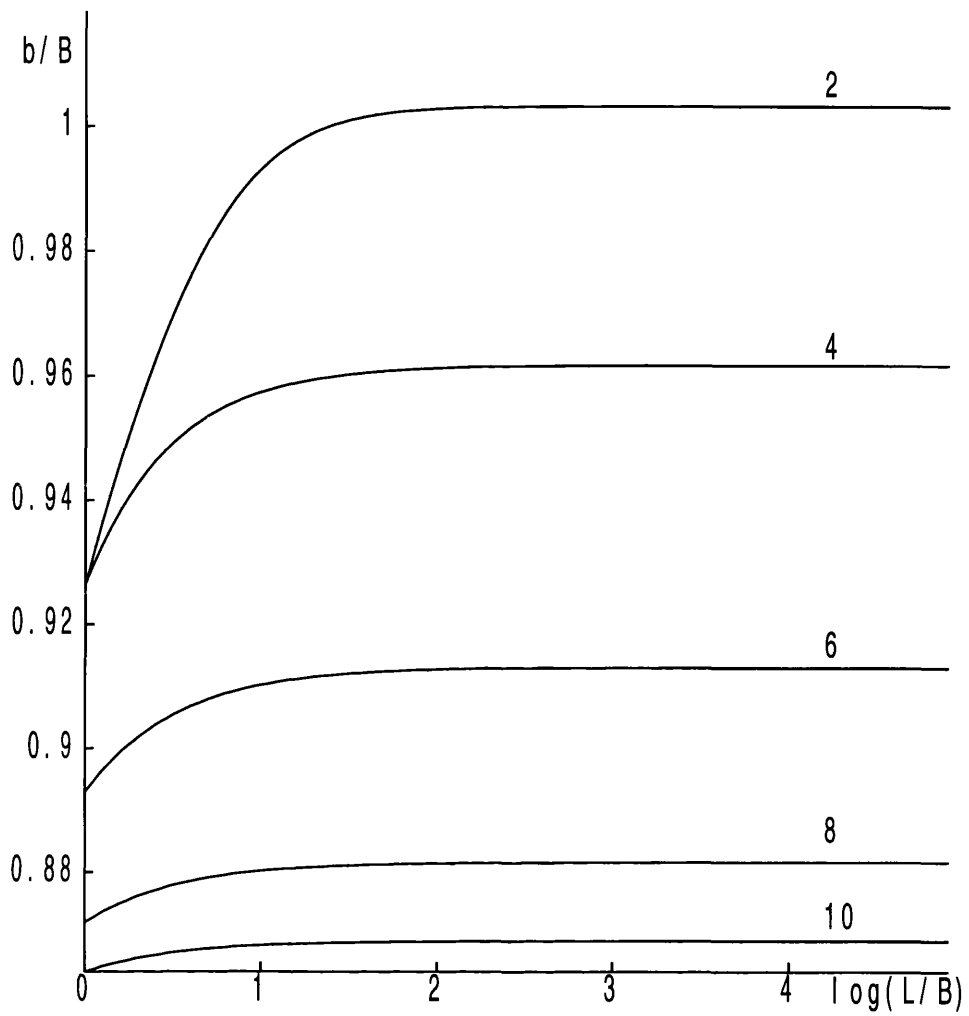


Figure 7.3 Plot of the critical values of b/B vs. $\log(L/B)$ for a cylinder with thickness ratio $A/B = 0.75$. Mode numbers $m = 2, 4, 6, 8, 10$ are shown for the Varga material defined in (3.2.3).

In Figure 7.4 we plot the critical values of b/B against undeformed thickness A/B for a more extensive range of values of the mode number m . Here we retain the value of λ defined by the eversion problem but we regard the value of b/B (say) as the unknown quantity to solve for. In physical terms we could interpret this as follows. First we evert the cylinder, then, keeping the deformed length of the cylinder fixed, we expand or compress the cylinder radially until we reach a bifurcation point. We have chosen the three-term material (3.2.5) and a value of $L/B = 20$, which, as illustrated in Figure 7.1, would produce the same results for all cylinders $5 < L/B < \infty$. Only those bifurcation points in the vicinity of the eversion curve have been recorded.

Very similar results are obtained for both the Varga and Neo-Hookean materials. To interpret the results given in Figure 7.4 consider a moderately thick cylinder with $A/B = 0.75$, say. This would be inverted to give a value of b/B , slightly greater than unity, as indicated by the upper eversion curve in Figure 7.4. If we were to then compress the tube (maintaining the value of λ_z) so that the value of b/B decreased until we reached the curve for mode $m = 2$ we would then expect the tube to buckle in a similar way to compressed cylinders that have not been everted. (See, for example, Haughton and Ogden (1979b, table 1). In particular, we can see from Figure 7.4 that if the cylinder is sufficiently thick it will undergo a spontaneous bifurcation upon eversion and we would not expect the perfectly cylindrical shape to be stable. However, we shall not attempt a formal stability analysis here. Clearly, we would like to establish a limiting value for the intersection of the bifurcation curves with the eversion curve. The indication from Figure 7.4 is that the infinite mode ($m \rightarrow \infty$) may be important. However, if we return to the incremental equations (6.2.14)–(6.2.16) it is readily seen that only the trivial solution exists in the limit and so the infinite mode is not attainable. To investigate this point further we shall present some results in tabular form. Finally, we note that all of the curves in Figure 7.4 pass through the point (1,1) since the value $A/B = 1$ represents the ideal limit of a membrane cylinder. If such a membrane is everted then its properties are unchanged and any mode of bifurcation can occur instantaneously if it is subjected to a compression.

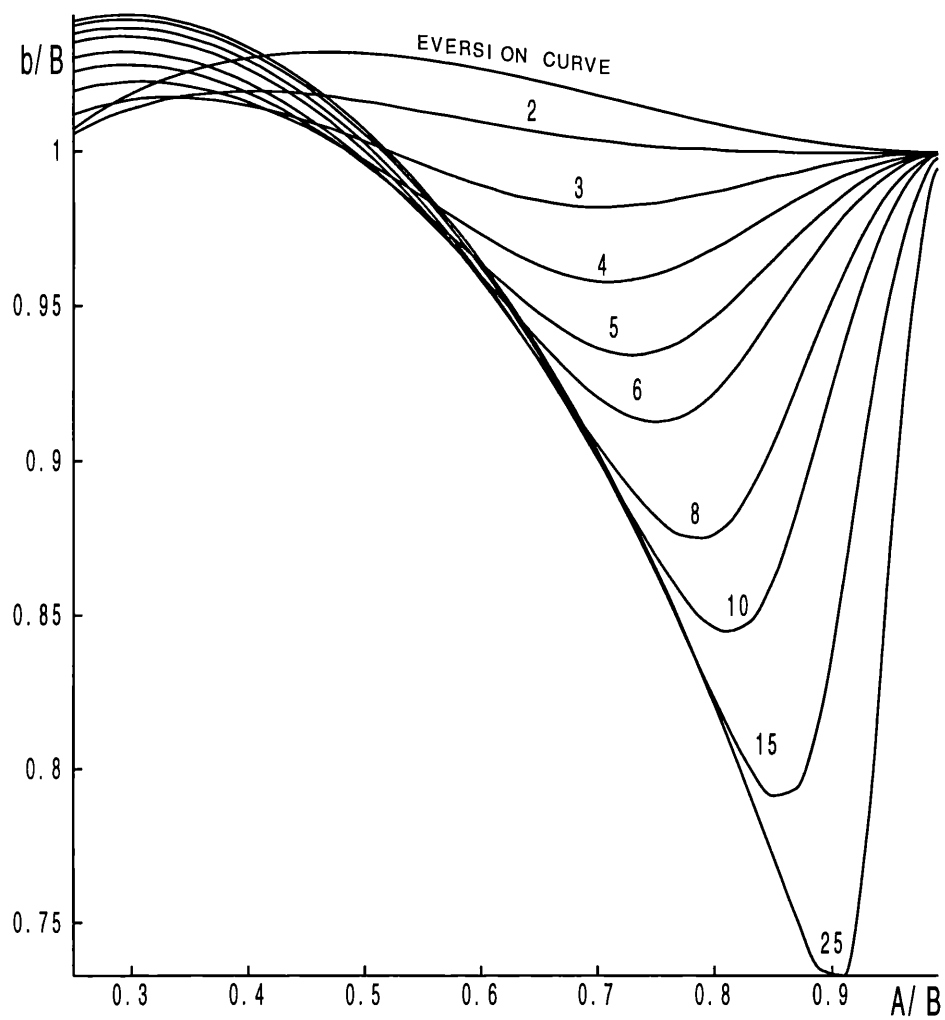


Figure 7.4 Plot of critical values of b/B vs. thickness A/B for the three-term material (3.2.5). Also included is the curve of b/B for the eversion of the tube.

7.2 Comparison of Numerical Methods

We take this opportunity to illustrate the different results produced by the two numerical methods detailed in chapter 9. In Table 1a we list the critical values of initial dimensions A/B for a cylinder of length $L/B=20$ (but recall from Figures 7.1–7.3 that this is essentially an infinitely long cylinder). The three-term strain-energy function (3.2.5) has been used and we have recorded results for various mode numbers m . These critical values correspond to the points of intersection of the bifurcation curves with the eversion curve shown in Figure 7.4, for example. In each case the method used has given the results “correct” to five decimal places.

Of particular interest is the different results predicted by the two methods for mode numbers in excess of 20. The determinantal method displays the classic signs of a numerical instability, which is most clearly demonstrated in the values predicted for A/B , while the compound matrix method predicts a local maximum for A/B of about 0.41629 which occurs for mode numbers around $m = 60$. It is natural to conclude that all cylinders of this material whose initial thickness exceeds this critical value will be unstable when everted. In practice the cylindrical shape will not be obtained.

The numerical instability illustrated above also occurs for other materials but for very different ranges of mode number. The two methods only agree for mode numbers less than 10 for the Neo-Hookean strain-energy, but agree for all modes up to 150 in the case of a Varga material.

In table 1b we illustrate the critical values of A/B for the Neo-Hookean material (3.2.4). In particular we note that there is a local maximum of $A/B = 0.42315$ which occurs for mode number $m = 14$.

In table 1c we give the critical values of A/B for the Varga material (3.2.3). In this case it can be seen that a maximum for A/B is not attained for mode numbers up to 200,000. Even if the critical value of A/B is monotonic increasing with mode number m it is likely to have an upper bound which appears to be $A/B = 0.43054$. It is interesting to note that the three materials (3.2.3)–(3.2.5) all give maximum critical values of $A/B \simeq 0.42$ – 0.43 although for very different

mode numbers m . As is indicated by Figure 7.4 the mode numbers $m = 2, 3, \dots$ all give qualitatively similar results.

Table 1a. Critical values of A/B three-term strain-energy (3.2.5).

m	Determinantal Method			Compound Matrices		
	A/B	λ	b/B	A/B	λ	b/B
5	0.34738	1.105672	1.02568	0.34738	1.105672	1.02568
10	0.39679	1.086108	1.03000	0.39679	1.086110	1.03000
15	0.40838	1.081978	1.03065	0.40838	1.081978	1.03065
20	0.41250	1.080546	1.03084	0.41250	1.080546	1.03084
25	0.41425	1.079941	1.03092	0.41433	1.079914	1.03093
30	0.41431	1.079922	1.03093	0.41526	1.079598	1.03097
35	0.41344	1.080220	1.03089	0.41575	1.079429	1.03099
40	0.29928	1.128521	1.01856	0.41602	1.079336	1.03100
45	0.29685	1.129806	1.01810	0.41617	1.079286	1.03101
50	0.42407	1.076626	1.03132	0.41625	1.079259	1.03101
55	0.44712	1.069239	1.03192	0.41628	1.079248	1.03101
60	0.43972	1.071550	1.03177	0.41629	1.079246	1.03101
65	0.25709	1.153095	1.00915	0.41628	1.079248	1.03101
70	0.42118	1.077593	1.03121	0.41626	1.079254	1.03101
75	0.38953	1.088780	1.02953	0.41623	1.079265	1.03101

Table 1b. Critical values for the Neo-Hookean material (3.2.4) using compound matrices.

m	A/B	λ	b/B
2	0.24308	1.241213	0.96717
4	0.34660	1.163506	0.99538
6	0.39107	1.137040	1.00344
8	0.41098	1.126270	1.00635
10	0.41941	1.121895	1.00746
12	0.42251	1.120313	1.00785
13	0.42303	1.120046	1.00792
14	0.42315	1.119985	1.00793
15	0.42301	1.120059	1.00791
16	0.42267	1.120229	1.00787
18	0.42168	1.120735	1.00775
20	0.42047	1.121352	1.00760
25	0.41728	1.122991	1.00719
30	0.41435	1.124506	1.00680
35	0.41184	1.125816	1.00647

Table 1c. Critical values for the Varga material (3.2.3) using the compound matrix method, $L/B = 20$.

m	A/B	λ	b/B	m	A/B	λ	b/B
25	0.41009	1.063359	1.04184	3000	0.43038	1.058267	1.04154
50	0.42025	1.060776	1.04172	4000	0.43042	1.058257	1.04154
75	0.42393	1.059857	1.04166	5000	0.43045	1.058251	1.04154
100	0.42552	1.059463	1.04164	10000	0.43049	1.058240	1.04154
150	0.42725	1.059035	1.04160	15000	0.43051	1.058236	1.04154
200	0.42807	1.058834	1.04159	20000	0.43052	1.058234	1.04154
300	0.42891	1.058627	1.04157	30000	0.43052	1.058232	1.04154
400	0.42932	1.058527	1.04156	40000	0.43053	1.058230	1.04154
500	0.42957	1.058466	1.04156	50000	0.43053	1.058230	1.04154
750	0.42987	1.058391	1.04155	100000	0.43054	1.058228	1.04154
1000	0.43004	1.058350	1.04155	150000	0.43054	1.058228	1.04154
1500	0.43021	1.058309	1.04154	200000	0.43054	1.058228	1.04154
2000	0.43029	1.058288	1.04154				

7.3 Analysis of Limiting Cases

As mentioned earlier the cases of modes $m = 0, m = 1$ are rather different and we now turn our attention to these special cases. In Figure 7.5 we plot critical values of b/B along with the eversion curve for the three-term material (3.2.5) for the case mode $m = 1$, a number of different length ratio's L/B are shown. In this case there are multiple solutions to the incremental equations close to the eversion curve. In Figure 7.6 we show an enlarged detail of Figure 7.5. Figures 7.5–7.6 seem to suggest that the mode $m = 1$ curves approach the eversion curve as $L/B \rightarrow \infty$. However, this limiting case $L/B \rightarrow \infty$ ($\alpha \rightarrow 0$) is amenable to further analysis. In the limit $\alpha \rightarrow 0$, with $m = 1$, the equilibrium equations (6.2.14) and (6.2.16) become

$$\begin{aligned} k = & -(rB'_{3131} + B_{3131} + B_{1111} - B_{1221})f/r - (rB'_{3131} + B_{3131})g/r \\ & -(B_{1111} - B_{1221})g/r + rB_{3131}g'' - (B_{1331} - B_{1221})f' \\ & +(rB'_{3131} + B_{3131})g' , \end{aligned} \quad (7.3.1)$$

and

$$\begin{aligned} k' = & (B_{3223} - B_{1111} - B_{1313})g/r^2 + (B_{1331} - B_{2332})g'/r \\ & (B_{3333} - B_{2332})f'' + (rB'_{3333} + rp' + B_{3333} - B_{2332})f'/r \\ & +(B_{2332} - B_{1111})f/r^2 - B_{1313}f/r^2 , \end{aligned} \quad (7.3.2)$$

respectively and equation (6.2.15) is identically satisfied. If we use the incompressibility constraint (6.2.1) and (6.2.11) we can eliminate $g(r)$ from the above to produce

$$\begin{aligned} k = & (rB'_{3131} + B_{3131} + B_{1133} + B_{1331} - B_{1111})f' \\ & (rB'_{3131} + 4B_{3131})rf'' + B_{3131}r^2f''' , \end{aligned} \quad (7.3.3)$$

and

$$\begin{aligned} k' = & (rB'_{3131} - rB'_{1331} + rB'_{3333} - rB'_{1133} + B_{3131} - 2B_{1133} - 2B_{1331} \\ & + B_{3333} + B_{1111})f'/r + (B_{3333} - B_{1331} - B_{1133})f'' , \end{aligned} \quad (7.3.4)$$

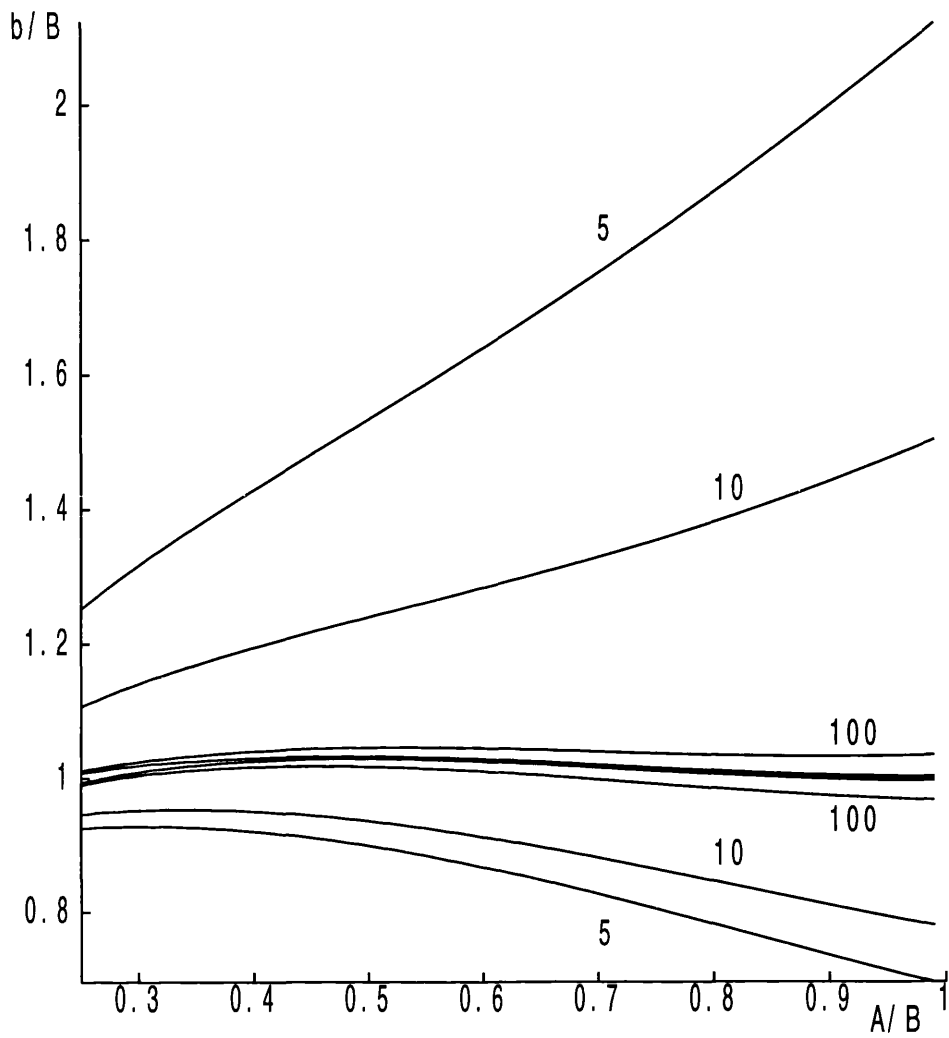


Figure 7.5 A plot of critical values of b/B along with the eversion curve for the three-term material (3.2.5) against undeformed thickness A/B for the case mode $m = 1$ and length ratio's $L/B = 5, 10, 100, 1000$ (unlabelled).

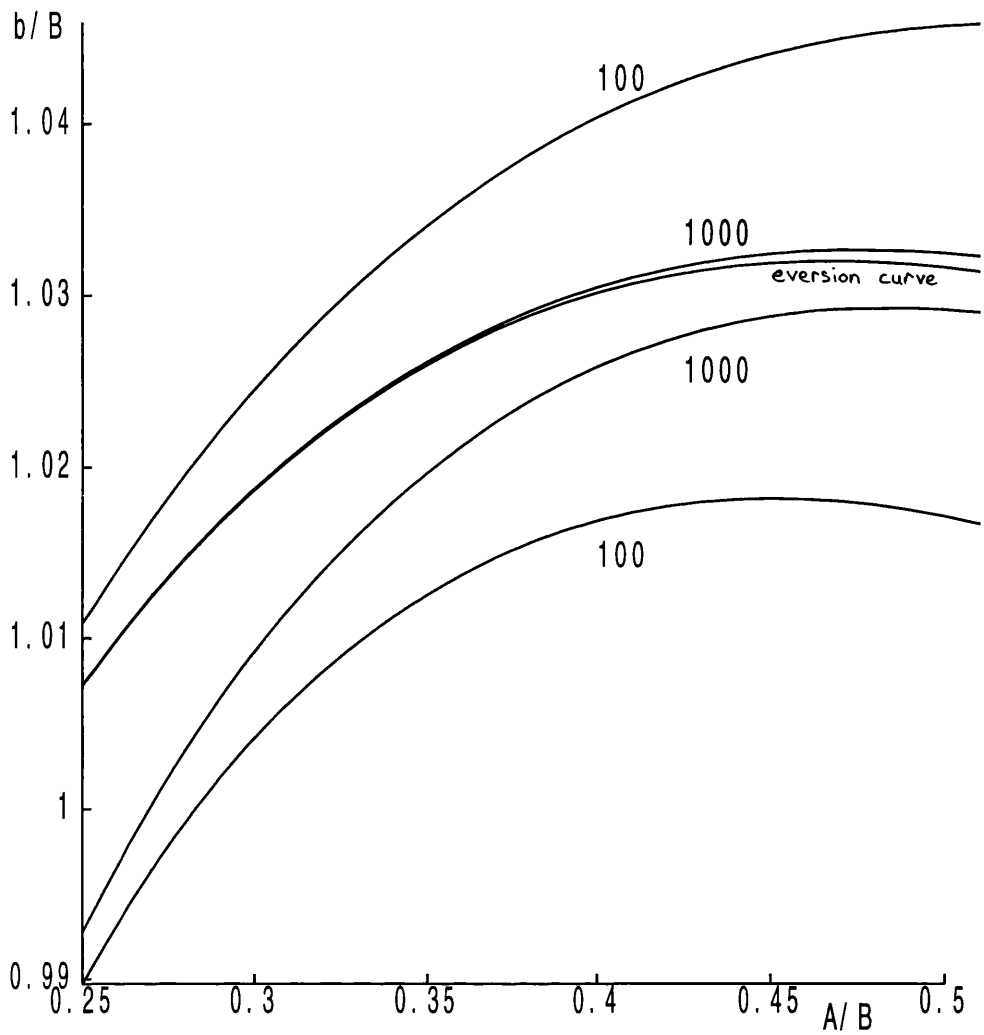


Figure 7.6 A plot of critical values of b/B along with the eversion curve for the three-term material (3.2.5) against undeformed thickness A/B for the case mode $m = 1$ and length ratio's $L/B = 100, 1000$.

Differentiating (7.3.3) with respect to r and subtracting the resultant equation from (7.3.4), to eliminate $k(r)$, gives rise to

$$\frac{d}{dr} \{ r^3 B_{3131} f''' + r^2 (r B'_{3131} + 3 B_{3131}) f'' + r (r B'_{3131} - B_{3131} + G(r)) f' \} = 0, \quad (7.3.5)$$

where we have written

$$G(r) = 2B_{1331} + 2B_{1133} - B_{1111} - B_{3333}.$$

The boundary conditions (6.2.17) reduce to two equations,

$$\left. \begin{aligned} r f'' + f' &= 0, \\ r^2 B_{3131} f''' + r (r B'_{3131} + 4 B_{3131}) f'' + (r B'_{3131} - B_{3131} + G) f' &= 0, \end{aligned} \right\} r = a, b. \quad (7.3.6)$$

Using the boundary conditions to set the first constant of integration to be zero, we can formally integrate (7.3.5) three times to get

$$f'(r) = \frac{C_1 \lambda_1}{r^3} \int \frac{r^3}{\lambda_1^2 B_{3131}} dr + \frac{C_2 \lambda_1}{r^3}, \quad (7.3.7)$$

where C_1 and C_2 are constants. In this case the existence of bifurcation requires a non-trivial $f'(r)$. Consulting (7.3.7) we see that this forces there to be a non-trivial (C_1, C_2) . With this in mind we substitute (7.3.7) into (7.3.6) to obtain

$$C_1 \left\{ \int \frac{r^3}{\lambda_1^2 B_{3131}} dr + \frac{r}{\lambda B_{3131}} \left(\frac{r^2}{\lambda} \right)' \right\} + C_2 = 0, \quad r = a, b, \quad (7.3.8)$$

which, after some algebra, gives a bifurcation criterion which can be written

$$\int_a^b \frac{r^3}{\lambda_1^2 B_{3131}} dr + \left[\frac{r^4 \lambda_3}{\lambda_1^2 B_{3131} (\lambda_1 - \lambda_3)} \right]_a^b = 0, \quad (7.3.9)$$

or alternatively

$$\int_a^b \frac{r^3 (\lambda_1 + \lambda_3)^2 \hat{W}_{11}}{(\lambda_1 \lambda_3 \hat{W}_1)^2} dr = 0, \quad (7.3.10)$$

where we have introduced the notation

$$\hat{W}(\lambda_1, \lambda_2) = W(\lambda_1, \lambda_2, (\lambda_1 \lambda_2)^{-1}),$$

with $\hat{W}_1 = \partial\hat{W}/\partial\lambda_1$ and $\hat{W}_{11} = \partial^2\hat{W}/\partial\lambda_1^2$. We have also made use of (5.2.6) and (3.1.5) with (3.1.7). Clearly, a sufficient condition to exclude mode 1 bifurcations in the limiting case of an infinitely long tube is $\hat{W}_{11} > 0$. This condition is satisfied for the three materials considered here (3.2.3)–(3.2.5) and is satisfied by all commonly used incompressible strain–energy functions. We have conducted further extensive numerical investigations into the behaviour of the mode $m = 1$ bifurcations. It seems that as $L/B \rightarrow \infty$ the pairs of mode $m = 1$ bifurcation curves bracketing the eversion curve, as shown in Fig.’s 7.5 and 7.6, approach the eversion curve. However, as noted above, the bifurcation criterion in the limit as $\alpha \rightarrow 0$ is determined by the existence of a non–trivial solution for $f'(r)$. In the case of a cylinder of finite length ($\alpha \neq 0$), on which our numerical method is based, the bifurcation criterion is governed by the existence of a non–trivial $f(r)$. If the numerical method used to produce Figures 7.5 and 7.6 is used to consider the limiting case as ($\alpha \rightarrow 0$) then the fact that non–trivial $f(r)$ exists for any value of the deformation manifests itself by the introduction of spurious $m = 1$ bifurcation points. The numerical method then breaks down before we can definitely say that as $\alpha \rightarrow 0$ the two bifurcation curves meet, cross the eversion curve and cease to exist, which seems to be the most likely outcome. Also, since the bifurcation curves are very close to the eversion curve, it may well be that imperfections in actual cylinders of sufficient length will allow mode $m = 1$ bifurcation modes to be exhibited for almost any value of A/B .

Finally we consider the case of symmetric bifurcations ($m = 0$) where there is no θ dependence in the incremental equations (6.2.14)–(6.2.16). In this special case the system of equations (6.2.14)–(6.2.16) simplifies considerably, but, unfortunately, the simplified system still requires a numerical solution. In this particular case we find that the results for everted cylinders closely match those for an inflated, uneverted, cylinder. For an axial stretch λ around unity the cylinder requires a considerable radial expansion to reach a mode $m = 0$ bifurcation point. It is clear that the axisymmetric mode does not play a significant role for everted cylinders.

7.4 Conclusions

We recall that Truesdell (1977) describes the eversion of a tube composed of *foam rubber*. This tube has a thickness ratio of $A/B = 5/6$ and a length ratio of $L/B = 4$. From Figure 7.4 a value of $A/B = 5/6$ would place an everted cylinder clear of any bifurcation modes. We also see from Figure 7.5 that a length ratio $L/B = 4$ would modify the critical value of b/B only very slightly and the results given in tables 1a, b and c confirm that the critical thickness is around 0.4 to 0.43, depending on the actual material model, but almost certainly less than 0.5. Also, we observe from Figure 7.5 that an initial length to radius ratio $L/B = 4$ will put the eversion curve well away from any possible mode $m = 1$ bifurcation points. Consequently we would expect that the cylindrical shape would be attained when the tube was everted. However, the tube undergoes a spontaneous bifurcation into a non-cylindrical shape when it is everted. There seem to be several possible explanations for this apparent discrepancy between the theory and experimental results. It may be that imperfections in the cylinder have a significant effect so that the actual eversion curve is moved closer to the possible bifurcation points, or perhaps the approximate nature of the end conditions applied to the simple eversion problem introduces significant errors. We investigate the second possibility within the context of compressible materials in the following chapter. Alternatively, the geometry of the tube may not be significant, but the mathematical model of the material may be inadequate. Clearly, none of the incompressible materials considered here is likely to accurately model the behaviour of a *foam rubber*. While Truesdell (1977) suggests that the compressibility of the material should be irrelevant, it will have some effect, at least on the basic eversion solution.

In the next chapter we will investigate how the compressibility of the material affects the bifurcation modes produced. We will also present a new material which satisfies the basic eversion problem exactly and hence eliminates any errors due to the approximate end conditions.

Chapter 8

Compressible Bifurcation Results

Before we present any results on the bifurcation of compressible materials we must first discuss the significance of not being able to attain $r = r(R)$, as we stated in section 6.3. In chapter 7 the results were interpreted in terms of b/B and we looked for the intersection of the bifurcation modes with the eversion curve. Here we will approach the problem by using the initial thickness A/B as the only variable and seek to find limiting values of A/B beyond which we will be certain of bifurcation modes being produced. We followed this idea in chapter 7 when we compared the different numerical methods.

8.1 Varga materials

The compressible Varga form is given in (4.4.1). We begin by studying the effects of varying the length of the cylinder on the critical thickness A/B . In Figure 8.1 we plot the critical values of A/B against the compressibility κ/μ for various length to radius ratios L/B . We fix the mode number m to be 2. Immediately it can be seen that as we increase L/B the critical thickness A/B increases and the bifurcation curves appear to converge to some limiting curve of critical thickness. We note that although the curves converge to a limit we do not encounter any points of intersection between distinct curves. Considering the case $L/B \rightarrow \infty$ analytically, which, in the incremental deformation (6.3.8), is equivalent to $\alpha \rightarrow 0$, we obtain the following simplification of the system (6.3.11)–(6.3.13) with corresponding boundary conditions (6.3.14).

$$\begin{aligned} & (rB'_{3333} + B_{3333})f'/r + (rB'_{1133} - B_{1313} - B_{1111})mg/r^2 \\ & + (rB'_{1133} - B_{1111} - m^2B_{1313})f/r^2 + B_{3333}f'' \\ & + (B_{1331} + B_{1133})mg'/r = 0, \end{aligned} \quad (8.1.1)$$

$$m^2B_{1212}h/r^2 - (rB'_{3232} + B_{3232})h'/r - B_{3232}h'' = 0, \quad (8.1.2)$$

$$\begin{aligned} & -(rB'_{3131} + B_{3131})g'/r - B_{3131}g'' + (m^2B_{1111} + rB'_{3113} + B_{1313})g/r^2 \\ & (B_{1111} + rB'_{3113} + B_{1313})mf/r^2 + (B_{1133} + B_{3113})mf'/r = 0. \end{aligned} \quad (8.1.3)$$

$$\left. \begin{aligned} rg' - g - mf &= 0 \\ h' &= 0 \\ B_{1133}(1 - \frac{m^2}{r})f + B_{3333}f' + mB_{1133}g' &= 0 \end{aligned} \right\} r = a, b. \quad (8.1.4)$$

In the simplified system (8.1.1)–(8.1.3) are decoupled for $h(r)$. We have isolated (8.1.2) for h , but are unable to solve it analytically due to the unknown form of $r(R)$ required in the instantaneous moduli. Without use of an incompressibility condition we are unable to eliminate g from (8.1.1) and (8.1.3) and follow the analysis we produced for the incompressible case.

Turning our attention to Figure 8.1 we observe that as κ/μ increases, and hence the material tends towards the incompressible limit, the bunching effect is more evident. For small values of κ/μ , and hence more compressible materials, we observe that the critical thickness A/B obtained has a greater dependence on the initial length to radius ratio L/B of the undeformed tube. We can therefore say that the more compressible a material the greater the length to radius ratio L/B must be before we may consider it as being effectively infinitely long. This graph seems to suggest that for a particular value of L/B the critical thickness A/B obtained is directly proportional to κ/μ and hence to the compressibility of the material.

We can readily see that for $\kappa/\mu > 10$ the critical thickness A/B is relatively constant for shorter cylinders. This corresponds to the results on incompressible materials where we find that for $L/B > 5$ the cylinder behaves as if it were infinitely long. For short highly compressible tubes we may expect that both the compressibility and the end effects will affect the value of the critical thickness A/B obtained as a higher proportion of the deformed tube will be non-cylindrical.

Using the above results as our motivation we now examine the effects that the compressibility of the material has on the critical thickness A/B obtained upon bifurcation. We achieve this by varying the parameter β which is connected to κ/μ by (4.4.4). As before we plot κ/μ to add physical meaning to any results obtained. In Figure 8.2 we plot the critical thickness A/B against the compressibility factor κ/μ for a wide variety of mode numbers. The most noticeable feature of the graphs is that for $\kappa/\mu > 5$ the critical thickness A/B appears to be virtually constant for any given mode number. We can also see that as we increase the mode number m the critical thickness A/B increases and the curves converge to some asymptotic value. This suggests that the higher mode numbers, and in particular the infinite mode ($m \rightarrow \infty$), will be the most important as they produce the thinnest bifurcated shells. If we consider the infinite mode analytically, as we

did in the incompressible case, we attain the following system

$$\begin{aligned}
 B_{1313}f/r^2 &= 0 , \\
 B_{1212}h/r^2 &= 0 , \\
 B_{1111}g/r^2 &= 0 .
 \end{aligned}
 \tag{8.1.5}$$

Here we have divided equations (6.3.11)–(6.3.13) by m^2 and considered the limit $m \rightarrow \infty$. From (8.1.5) we once again find that only the trivial solution exists for the system. We can therefore conclude that the infinite mode is not attainable.

Once again we find our bifurcation curves in Figure 8.2 bunching together without the existence of any points of intersection between the curves. It is only for $\kappa/\mu < 5/2$, which corresponds to $\beta < 1$, where we see any real change in the critical thickness. Here we find that the critical thickness A/B decreases as the material becomes highly compressive. Figure 8.2 demonstrates that the main area of interest in our bifurcation curves is for $\kappa/\mu < 2/3$, which corresponds to $\beta < 0$, and to highly compressible material forms. We now study this area in more detail.

In Figure 8.3 we plot the critical thickness A/B against the mode number m . Here we vary the compressibility factor κ/μ and consider three compressible Varga forms which correspond to both $\beta < 0$ and $\beta > 0$. From Figure 8.3 we easily conclude that the critical thickness A/B is approximately constant for $m > 25$ so we plot, in Figure 8.4, the same curves for a limited range of mode numbers.

On inspection of Figure 8.4 we can clearly see that as we increase m the curves diverge from one another. It can also be seen that the more compressible materials have the smaller critical values of A/B and hence these materials will support the eversion of thicker cylinders before they undergo spontaneous bifurcation. As shown in Figure 8.3, if we increase the mode number m we find that all curves level out to produce asymptotic behaviour. The data for the mode number m is in fact a discrete set of points and have been joined up for ease of presentation.

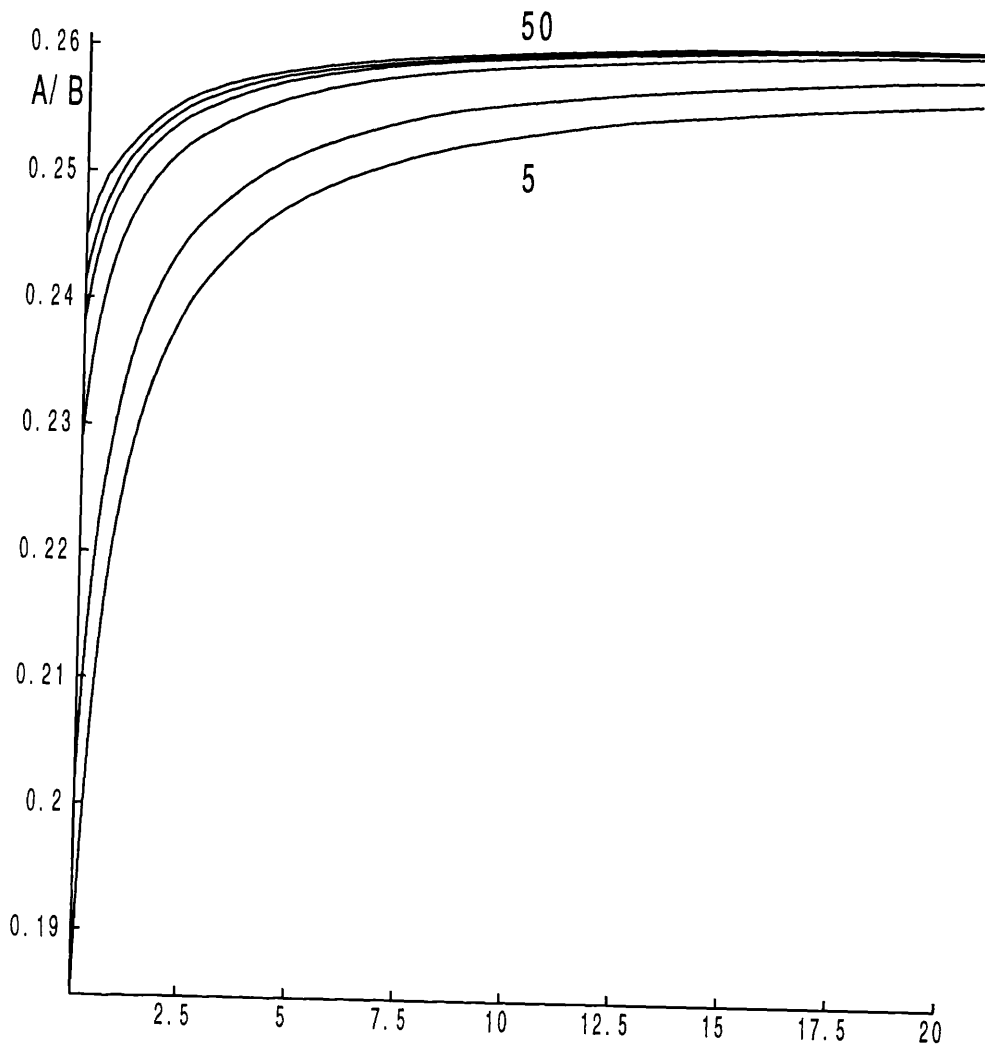


Figure 8.1 Plot of the critical values of A/B vs. κ/μ for the compressible Varga material for mode 2. $L/B = 5, 6, 10, 15, 20, 50$.

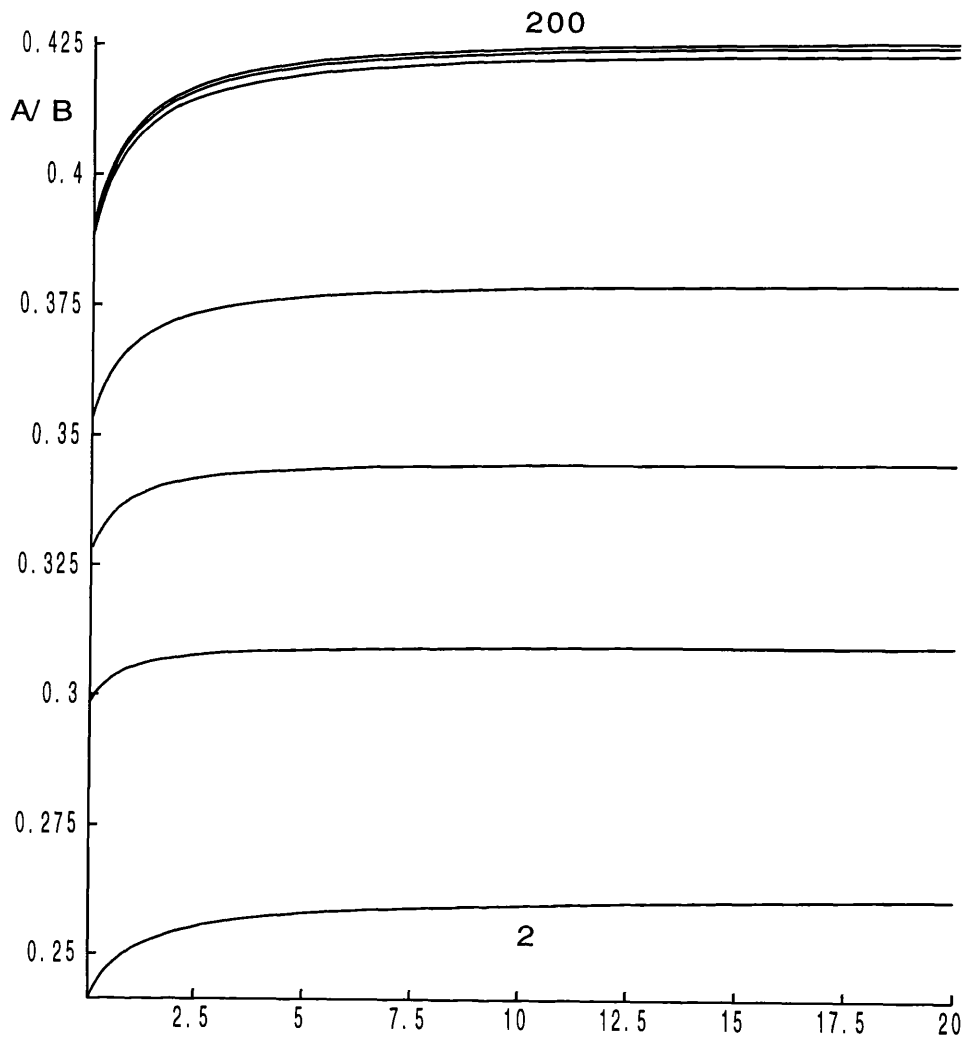


Figure 8.2 Plot of the critical values of A/B vs. κ/μ for the compressible Varga material. Mode numbers $m = 2, 4, 8, 10, 100, 150, 200$, $L/B = 20$.

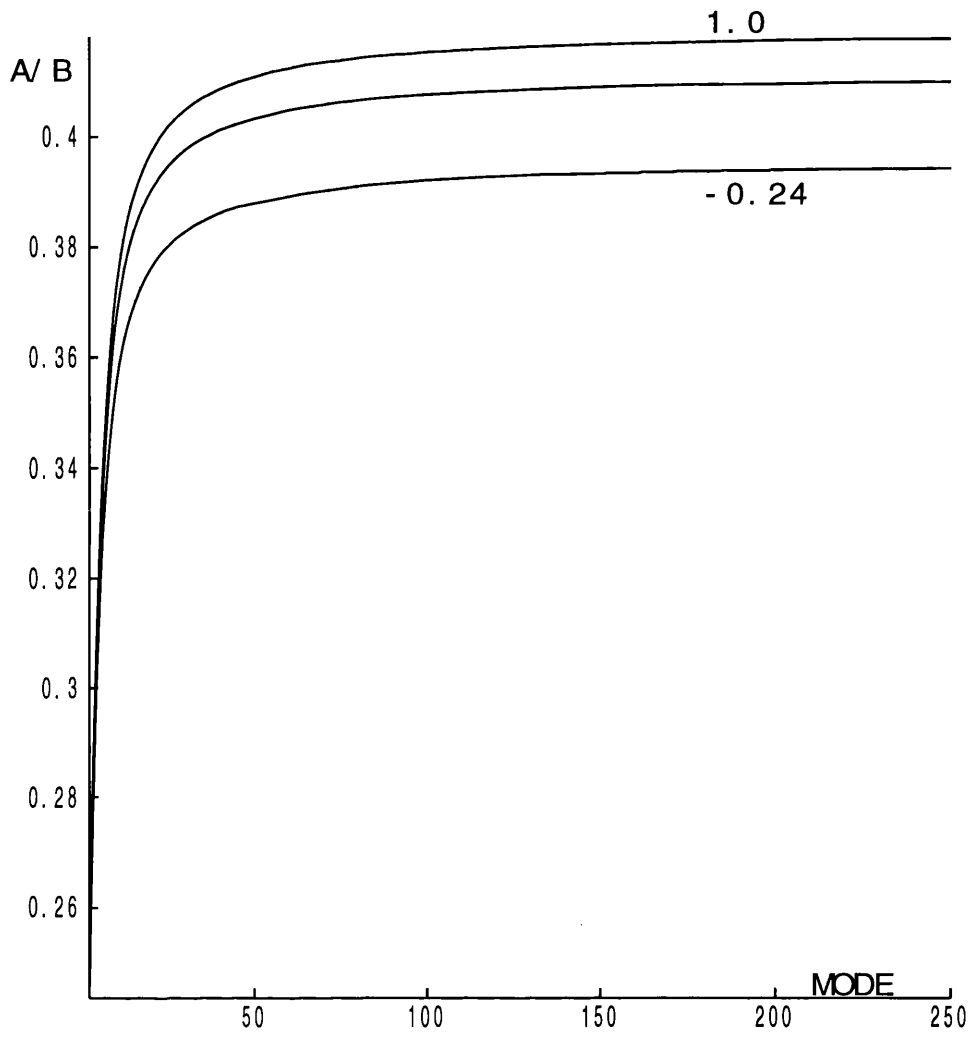


Figure 8.3 Plot of the critical values of A/B vs. m for the compressible Varga material for $L/B = 20$, $\beta = -0.24, 0.24, 1.0$.

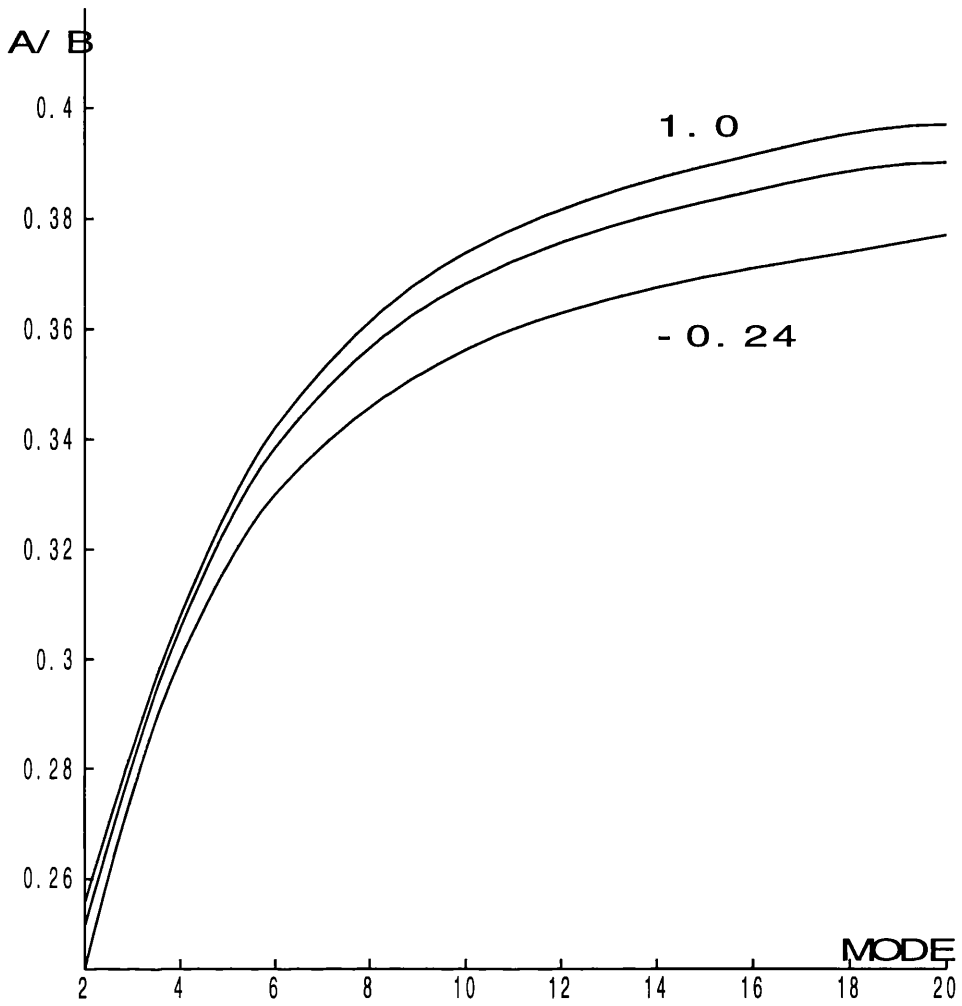


Figure 8.4 Plot of the critical values of A/B vs. m for the compressible Varga material in more detail . $L/B = 20$, $\beta = -0.24, 0.24, 1.0$.

8.2 Blatz–Ko materials

The Blatz–Ko strain–energy form is defined in (4.6.1). This material has $\kappa/\mu = 5/3$ and is therefore highly compressible. We may therefore expect to be able to draw comparisons between the bifurcation of Blatz–Ko materials and highly compressible Varga materials, which are shown in Figures 8.1–8.4.

In Figure 8.5 we plot the cylinder thickness A/B against the length to radius ratio L/B of the cylinder for a range of mode numbers. We can clearly see from the Figure that the length only effects the lower mode numbers significantly. For $m \geq 6$ we find that for $L/B > 5$ the cylinder behaves as an infinite one. Indeed for $m \geq 9$ we observe that the critical radius produced with a short cylinder with $L/B = 2$ is indistinguishable from the critical radius produced by an infinitely long cylinder. For the lower mode numbers ($m \leq 5$) we see that as we decrease the length of the tube the critical radius at which the tube bifurcates decreases dramatically. However this is not important as for very short highly compressive tubes we would expect the end effects to play a significant role. We also observe that as m increases the critical radius A also increases and thus we would expect the higher order ($m \rightarrow \infty$) mode numbers to be the most important. We are therefore able to consider all tubes to be effectively infinitely long.

Another point of interest is the non–monotonic increasing relationship between the mode number m and the critical thickness A/B . However A/B is monotonic increasing in L/B for a particular mode number m . We observe that the lower mode numbers ($m = 2, 3$) intersect several of the higher order mode number curves. This behaviour was not evident in the bifurcation of the highly compressible Varga forms where we found no intersection of curves. Although we may expect similar behaviour due to the comparable compressibilities of the materials it must be stressed that both materials are governed by different strain–energy functions and that it is these functions that determine the bifurcation criteria. This point is illustrated in chapter 7 when we investigated $L/B \rightarrow \infty$ analytically. Here we established that the bifurcation condition was dependent on the strain energy derivatives.

In Figure 8.6 we focus our attention on the relationship between the critical radius A and the mode number m . Here we consider a tube with $L/B = 20$ which we regard as infinite. The first thing we note is the existence of multiple bifurcation points for any given mode number. It should however be noted that this is a discrete set of points and that the lines are just to give a representation of the data. We hence place no importance on the anomalous line. From the graph it is clear that as we increase m more bifurcation points are produced and the value of the critical radius increases. We would expect the uppermost curve to be the most important since all tubes thicker than this will be unstable. The minimum turning point on the upper curve is explained by consulting the previous figure where we see that for small mode numbers the bifurcation curves cross each other.

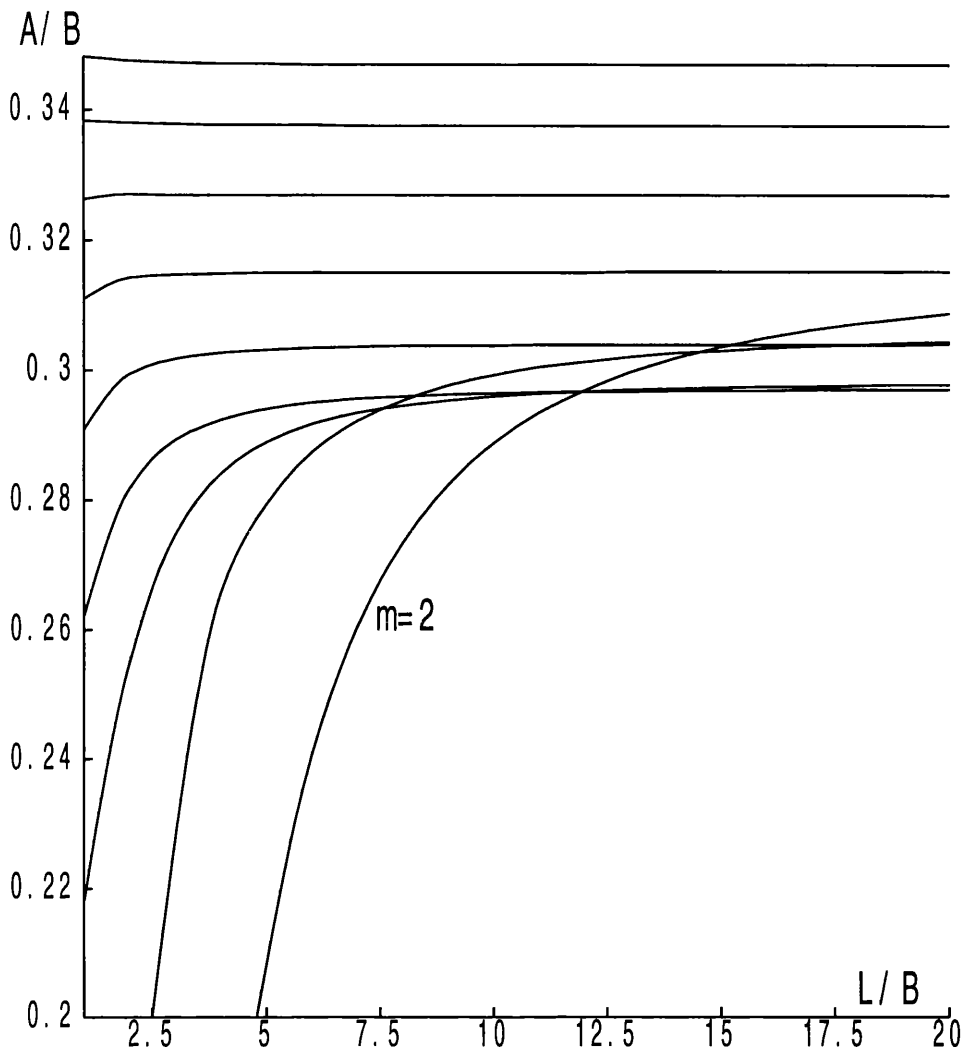


Figure 8.5 Plot of the critical values of A/B vs. L/B for the Blatz-Ko material.
 Mode numbers $m = 2, 3, 4, 5, 6, 7, 8, 9, 10$.

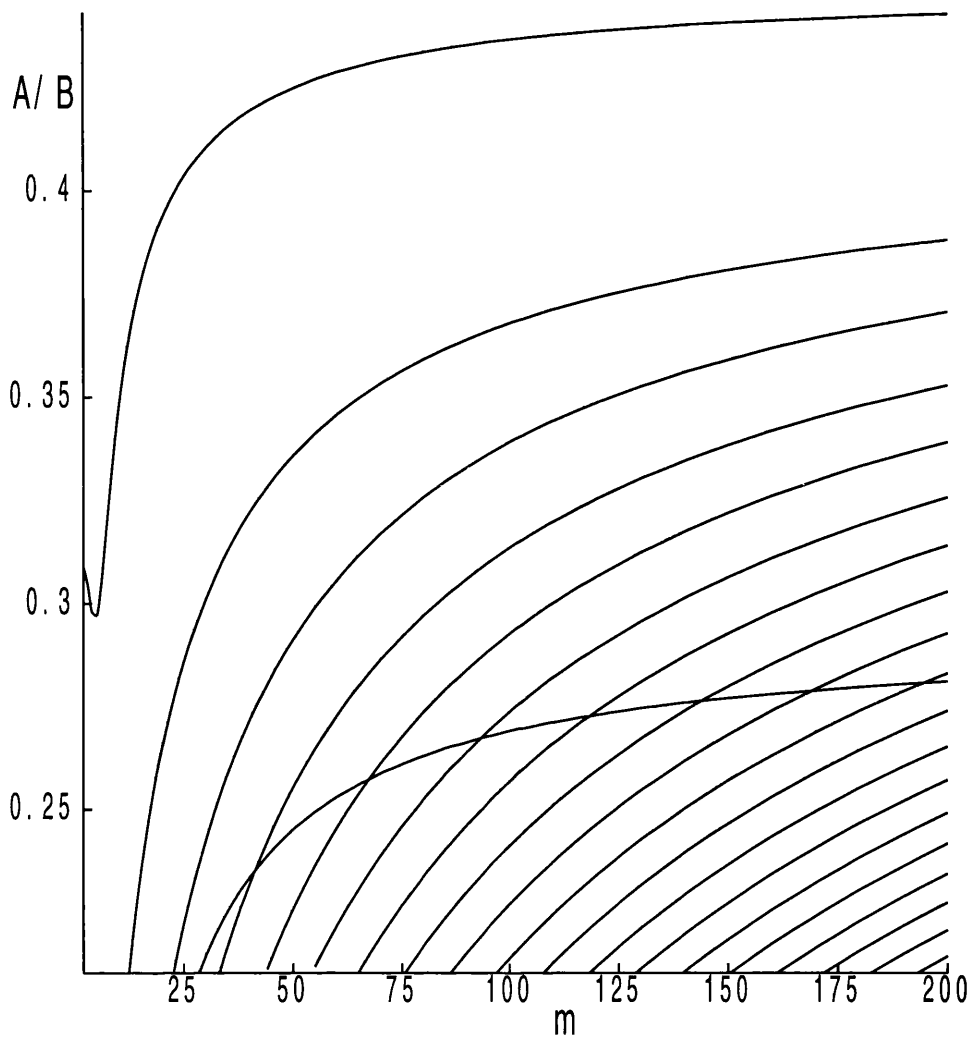


Figure 8.6 Plot of the critical values of A/B vs. the mode number m for the Blatz-Ko material.

8.3 Exact Solution

The “exact” material is defined in (4.2.3) and has $\kappa/\mu = 2/3$ which is highly compressible. As before we will compare the bifurcation results to those obtained for other highly compressible forms. We will not expect any correlation of the results due to similar compressibilities but we will be able to compare and contrast these results with both the Varga and Blatz–Ko forms, which produced qualitatively different results.

Here we first consider the effect of the length to radius ratio on the bifurcation modes produced. In Figure 8.7 we plot the critical thickness A/B against the length to radius ratio L/B for a selection of mode numbers m .

The uppermost curve corresponds to $m = 200$. We can see that the critical value of A/B is then monotonic decreasing with the mode number m until $m = 5$. For low mode numbers ($m < 4$) we see that the picture is not clear. Considering $m = 2$ we see that as the cylinder becomes longer the critical initial thickness at which the tube bifurcates appears to be monotonic increasing. In the case of $m = 3$ we see that for $L/B > 10$ the cylinder can be regarded as infinite. These small mode numbers produce results which are similar to the Blatz-Ko material, which is another highly compressive foam rubber. As we increase m ($m > 5$) we see that for $L/B > 5$ the cylinder behaves as an infinite one. This result ties in with the results for incompressible materials. Again we would expect end effects to play an important role in cylinders with $L/B < 5$. We also observe that as the mode number m is increased the critical thickness A/B is monotonic increasing with no maximum occurring for $m < 200$. This is not too surprising as the incompressible Varga doesn’t attain a local maximum until $m = 200,000$. Unfortunately we are not able to consider $m > 200$ for the “exact” material as the numerical method breaks down, producing target values outwith the computers range.

In Figure 8.8 we show how the critical thickness behaves as a function of the mode number m . Here we plot only the uppermost values of A/B for any given mode number. We consider a length to radius ratio of $L/B = 50$, which is

effectively infinite. This is comparable to the uppermost curve in Figure 8.6 for the Blatz–Ko material. The sharp spike corresponds to the mode two bifurcation curve crossing the mode three bifurcation curve in Figure 8.7. This is also consistent with the low mode numbers for the Blatz-Ko material. We can also see that A/B is monotonic increasing in m and appears to be bounded above.

If we consider $m \rightarrow \infty$, then we can use (8.1.1)–(8.1.3) to investigate the limit analytically. Remembering that $L/B = 50$ we are considering a cylinder which is effectively infinitely long. It can be seen from these equations that the only attainable solution is the trivial solution. Investigating $m \rightarrow \infty$ numerically poses new problems. Both numerical methods are unable to compute the determinant values for large values of m . From Figure 8.8 we can say that the maximum critical thickness of $A/B < 0.55$. If we consider the maximum critical values for the compressible Varga and the Blatz–Ko materials we can compare these values to see if any pattern emerges. On inspection of Figure 8.2 we see that as $m \rightarrow \infty$ the maximum critical value is approximately 0.425 for the compressible Varga. From the uppermost curve in Figure 8.6 we find that the maximum critical thickness for the Blatz–Ko material is approximately 0.43.

We can now discuss the possible range of of cylinders which will bifurcate upon eversion for each material. Since the exact solution material has the greatest value of critical thickness it will undergo a spontaneous bifurcation for the thinnest shells. We also find that the compressible Varga material has the thickest initial geometry before it experiences any bifurcation modes. If we consider the compressibilities of the three material classes we do not obtain any correlation between the compressibility of the material and the cylinder thickness necessary to produce bifurcation. As discussed before, we are interested in the uppermost bifurcation curves because they produce the greatest values of the critical thickness A/B . The compressible Varga has a very wide range of possible compressibilities and supports the eversion of the thickest shells before we reach a bifurcation point. This holds for any value of κ/μ and hence any compressibility. We expect that any cylinder thicker than these values will undergo bifurcation upon eversion. We find that the exact solution material will produce bifurcation modes for the

thinnest cylinders. It may be significant that this material solves the theoretical problem exactly and doesn't require any loads to satisfy the end conditions.

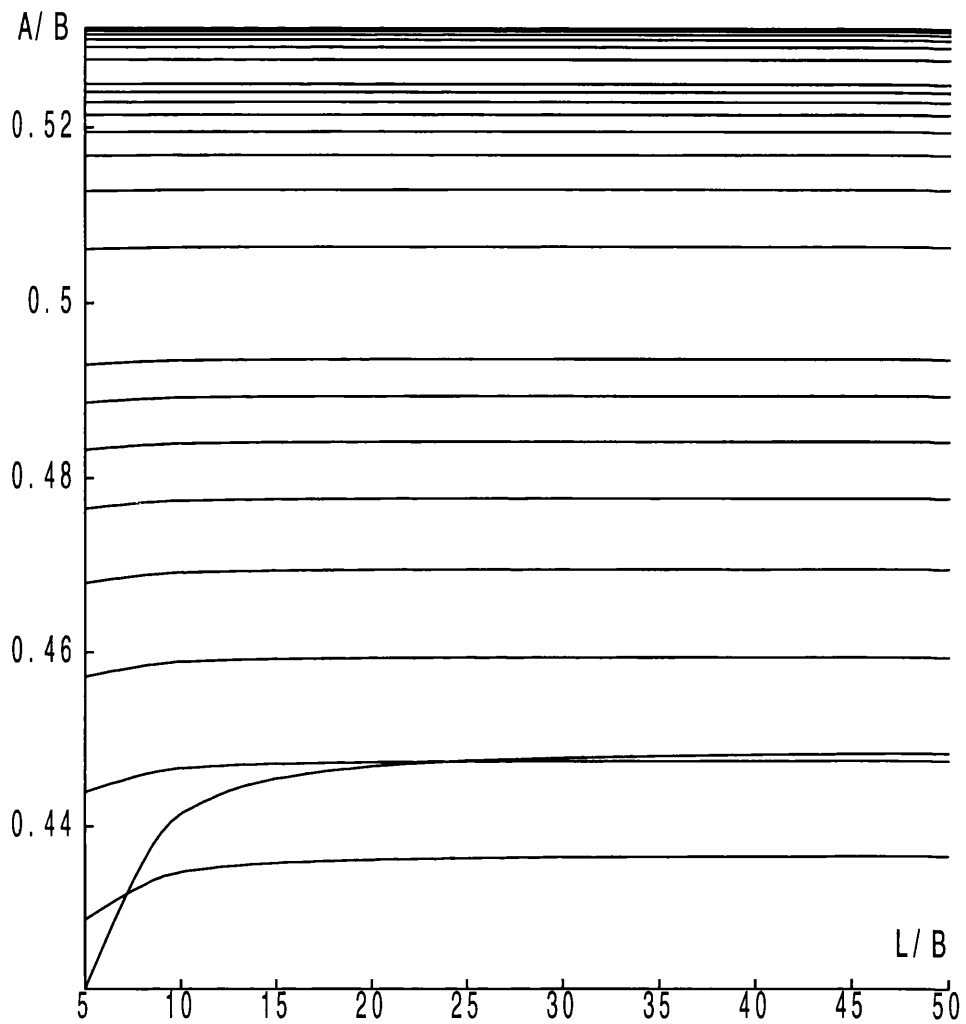


Figure 8.7 Plot of the critical values of A/B vs. L/B for the Exact Solution material. Mode numbers $m = 2, 3, 4, 5, 6, 7, 8, 9, 10, 15, \dots, 200$.

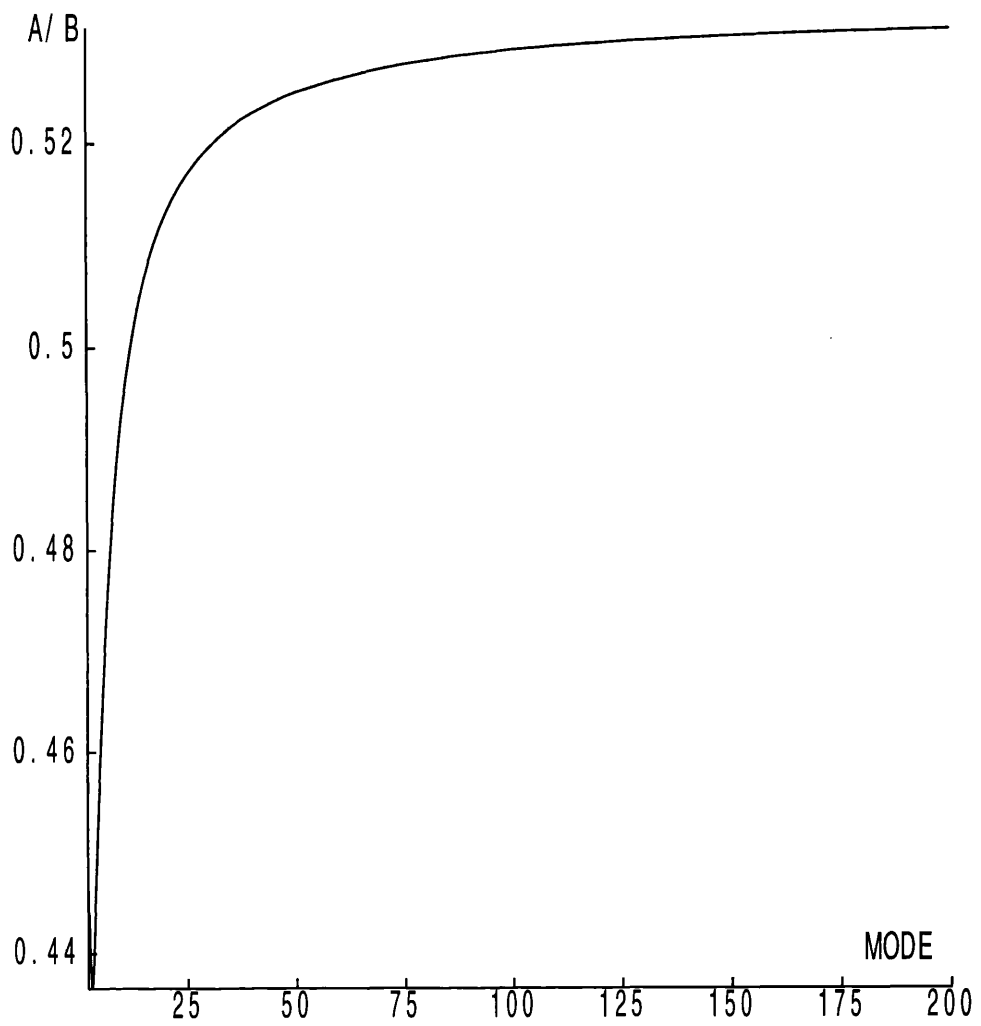


Figure 8.8 Plot of the critical values of A/B vs. m for the Blatz-Ko material.
 $L/B = 50$.

8.4 Conclusions

In this chapter we have demonstrated the existence of bifurcation modes for a variety of compressible materials. We have found that although the compressibility of the material affects the critical thickness at which a cylinder bifurcates, we do find that bifurcation is possible for the three classes of material considered here. We find that for even very compressible materials the critical radius for the existence of bifurcation remains low. We also find that except for very short cylinders all cylinders can be regarded as infinitely long. We find that all cylinders with $L/B \geq 5$ are effectively infinitely long. This suggests that only reasonably thick cylinders ($A/B < 0.5$) will lose the cylindrical shape upon eversion. This is in contrast to the experimental result reported by Truesdell (1977) where a foam rubber cylinder with initial thickness $A/B = 5/6$ underwent a spontaneous bifurcation when it was everted.

To explain this discrepancy we investigate the differences between the theoretical analysis and the experimental result. Firstly, we have observed that the theoretical eversion problem used approximate end conditions to simplify the resulting analysis. Although we expect that this should produce some error, the work carried out in section 4.2 suggests that it shouldn't be significant. For the exact solution material (4.2.3) we were able to construct a strain-energy function that solved the point-wise boundary conditions. This material is highly compressible, even more so than the Blatz-Ko material, and we should hence expect it to provide a reasonable model for the material used by Truesdell (1977). However, when we study the bifurcation problem for this material we find that there is no correlation of the results with those reported by Truesdell (1977), although it is worth noting that the critical radius ratio for this material is higher than that of materials of comparable compressibility that satisfy the approximate end conditions.

If, for comparison, we consider thick-walled (incompressible) elastic cylinders subject to an external pressure we know that a very modest change in the outer radius causes the cylinder to collapse. This is illustrated in Haughton and Ogden

(1979,b), table 1. It is therefore probable that we must decrease the everted outer radius of the cylinder to induce a bifurcation for thinner-walled cylinders. This point is also shown in section 7.1, Figure 7.4. We have conducted our own limited experiment on a thick-walled foam rubber paint roller ($A/B = 0.27$) detailed in photograph 1. On everting this tube we noticed several dominant features. It can be seen clearly from the photo that the belled ends are prominent but were confined to the ends of the cylinder, at least 95% of the everted cylinder is a right circular cylinder. Secondly the everted outer radius was much smaller than the theory predicted and the everted inner radius was zero, something that we have shown can not happen for the exact solution material of section 4.2. This would seem to suggest that the required reduction in the outer deformed radius would be achieved if we had a more accurate constitutive model. We have considered a wide range of strain-energy functions, with a wide range of compressibilities, in this thesis, but these do not offer a solution. We recall that a highly compressible foam rubber is modelled by an equivalent homogeneous material, see Blatz-Ko (1962) for example. However, on closer inspection the behaviour of a foam rubber can be characterised as follows. The compression of such a material requires the bending of the matrix walls surrounding the voids in the overall material. This requires very little effort and so gives rise to a highly compressible material. However, to produce a uniaxial extension of such a material we must first rotate and then subject the matrix material to a uniaxial extension which would require a far greater effort. We can then stipulate that a foam rubber material exhibits different behaviour in extension and compression. This may not be important for many deformations and the homogeneous model will provide the desired results. However, for the eversion of a cylindrical shell, the everted outer surface is in a state of azimuthal tension while the everted inner surface is in a state of compression. If the material is actually stiffer in tension than the homogeneous model suggests then the outer everted radius would be smaller than predicted by the homogeneous model, precisely the effect that we are looking for.

Materials that behave differently in tension and compression have been con-

sidered by Green and Mkrtychian (1976a). Such materials can be thought of as a combination of two homogeneous models, one for the material in a state of pure dilatation, one for pure compression, and two transversely isotropic materials, one when two principal stretches are greater than unity, one when two principal stretches are less than unity, with appropriate matching conditions. An explicit model of such a linear elastic material has been given by Green and Mkrtychian (1976b), but there are no models for finite elastic materials.

Chapter 9

Numerical Methods

In this chapter we describe the numerical methods that have been used to solve the incremental equations (6.2.14)–(6.2.16) with boundary conditions (6.2.17). In particular, with regard to the compound matrix method, we give both a general description of the method and details of how it is applied to the particular problems considered in this thesis.

Firstly, consider the general homogeneous problem of $2n$ first order ordinary differential equations written in vector form

$$\frac{dy}{dx} = \mathbf{A}(x, \gamma)y, \quad a \leq x \leq b, \quad (9.1)$$

where \mathbf{A} is a $2n \times 2n$ matrix depending on the independent variable x and a parameter γ . The boundary conditions are evenly distributed between the two ends of the range and can be written

$$\mathbf{B}(x, \gamma)y = \mathbf{0}, \quad x = a, \quad (9.2)$$

and

$$\mathbf{C}(x, \gamma)y = \mathbf{0}, \quad x = b, \quad (9.3)$$

where both \mathbf{B} and \mathbf{C} are $n \times 2n$ matrices. The aim is to determine values of the parameter (eigenvalue) γ so that non-trivial solutions exist. This seems to be typical of the problems encountered in both fluids and solid mechanics, but other cases with an odd number of equations and or an uneven distribution of boundary

conditions can be treated in a similar way. (In some respects an even distribution of boundary conditions over the two ends constitutes the worst possible case as it involves most work).

We can always choose n linearly independent vectors $\mathbf{y}^{(i)}$, $i = 1, 2, \dots, n$ that satisfy all n boundary conditions at $x = a$, say. The general solution to (9.1) can then be written

$$\mathbf{y} = \sum_{i=1}^n k_i \mathbf{y}^{(i)}, \quad (9.4)$$

for some constants k_1, k_2, \dots, k_n .

We define \mathbf{M} to be the $2n \times n$ matrix whose i^{th} column is $\mathbf{y}^{(i)}$. We then have

$$\mathbf{y} = \mathbf{M}\mathbf{k}, \quad (9.5)$$

where \mathbf{k} is the n -vector $(k_1, k_2, \dots, k_n)^T$. For future use we note from (9.1) that

$$\frac{d\mathbf{M}}{dx} = \mathbf{A}\mathbf{M}. \quad (9.6)$$

Equations (9.1) can be numerically integrated using each of $\mathbf{y}^{(i)}(a)$, ($i = 1, 2, \dots, n$) in turn as initial conditions to produce solutions $\mathbf{y}^{(i)}(b)$. The remaining boundary conditions (9.3) then become

$$\mathbf{C}(b, \gamma) \sum_{i=1}^n k_i \mathbf{y}^{(i)}(b) = \mathbf{C}\mathbf{M}\mathbf{k} = \mathbf{0}, \quad x = b. \quad (9.7)$$

The condition for the existence of non-trivial solutions is

$$\det(\mathbf{C}\mathbf{M}) = 0. \quad (9.8)$$

If the above $n \times n$ determinant is evaluated directly then we have essentially the method described by Haughton and Ogden (1979b) which has been used successfully for many problems of this type in elasticity. However, this method has proved to be inadequate for many problems in fluid mechanics, in particular the Orr-Sommerfeld problem, and also for the elastic bifurcation problem considered in this thesis.

The compound matrix method avoids the necessity of evaluating a determinant directly which is the source of numerical instabilities even for very small values of n . The Laplace expansion of $\det(\mathbf{C}\mathbf{M})$ gives

$$\det(\mathbf{CM}) = \sum_{i=1}^{\binom{2n}{n}} \psi_i \phi_i, \quad (9.9)$$

where ψ_i and ϕ_i are $n \times n$ minors of \mathbf{C} and \mathbf{M} respectively. The summation takes place over all possible $n \times n$ minors of \mathbf{M} taking rows of \mathbf{M} in ascending order. Given a ϕ_i , ψ_i takes the corresponding columns of \mathbf{C} . The compound matrix method takes the set $\{\phi_i, i = 1, \dots, \binom{2n}{n}\}$ as a new set of dependent variables. The differential equations satisfied by the $\binom{2n}{n}$ -vector $\boldsymbol{\phi}$ are determined directly. The derivative of each minor gives $n \times n$ determinants the j^{th} determinant has its j^{th} row differentiated and all other rows are unaltered. The differentiated row can be expressed as a linear combination of the rows of \mathbf{M} by using (9.6) and hence as a linear combination of elements of $\boldsymbol{\phi}$. The coefficients that are required in this linear combination come from the original coefficient matrix \mathbf{A} . The $\binom{2n}{n}$ differential equations are augmented with initial conditions chosen to be consistent with the original boundary conditions at $x = a$. Since \mathbf{M} has rank n at least one of the compound matrix variables must be non-zero at $x = a$. Having integrated the $\binom{2n}{n}$ equations *once only* we have the value of $\boldsymbol{\phi}$ at $x = b$. The condition (9.9) can be expressed as some (often trivial) linear combination of the components of $\boldsymbol{\phi}$ at $x = b$ with coefficients obtained from the matrix \mathbf{C} . The parameter γ is then chosen to ensure that this “target” condition is satisfied. Essentially we have replaced the evaluation of an $n \times n$ determinant and the solution of $2n$ 1st order ordinary differential equations n times with a single solution of $\binom{2n}{n}$ 1st order ordinary differential equations. The timing of the two methods is comparable but, as we shall see the second method returns a much higher degree of accuracy.

We now show how the compound matrix method is applied to the incremental equations (6.2.14)-(6.2.16) with boundary conditions (6.2.17). First we choose

$$\mathbf{y} = (f, f', f'', g, g', k)^T, \quad (9.10)$$

. Equations (6.2.14)-(6.2.16) can then be written

$$\mathbf{y}' = \mathbf{A}\mathbf{y}$$

where the components of the matrix \mathbf{A} have the form

$$\mathbf{A} = \begin{bmatrix} 0 & 1 & 0 & 0 & 0 & 0 \\ 0 & 0 & 1 & 0 & 0 & 0 \\ A_{31} & A_{32} & A_{33} & A_{34} & A_{35} & A_{36} \\ 0 & 0 & 0 & 0 & 1 & 0 \\ A_{51} & A_{52} & 0 & A_{54} & A_{55} & A_{56} \\ A_{61} & A_{62} & A_{63} & A_{64} & A_{65} & 0 \end{bmatrix}, \quad (9.11)$$

the non-zero components are obtained from (6.2.14)-(6.2.16). The boundary conditions (6.2.17) become $\mathbf{C}\mathbf{y} = \mathbf{0}$, $r = a, b$ where

$$\mathbf{C} = \begin{bmatrix} -m & 0 & 0 & -1 & r & 0 \\ C_{21} & r & r^2 & 0 & 0 & 0 \\ 0 & C_{32} & 0 & 0 & 0 & -1 \end{bmatrix}. \quad (9.12)$$

Since this problem involves six equations with three boundary conditions at each end of the interval we shall require $\binom{6}{3} = 20$ compound variables and we shall consequently have to solve a system of 20 equations. The compound variables ϕ_i can be defined and a shorthand notation introduced as follows;

$$\phi_1 = \begin{vmatrix} y_1^{(1)} & y_1^{(2)} & y_1^{(3)} \\ y_2^{(1)} & y_2^{(2)} & y_2^{(3)} \\ y_3^{(1)} & y_3^{(2)} & y_3^{(3)} \end{vmatrix} = (1, 2, 3), \quad (9.13)$$

$$\phi_2 = \begin{vmatrix} y_1^{(1)} & y_1^{(2)} & y_1^{(3)} \\ y_2^{(1)} & y_2^{(2)} & y_2^{(3)} \\ y_4^{(1)} & y_4^{(2)} & y_4^{(3)} \end{vmatrix} = (1, 2, 4),$$

and similarly,

$$\begin{aligned} \phi_3 &= (1, 2, 5), & \phi_4 &= (1, 2, 6), & \phi_5 &= (1, 3, 4), & \phi_6 &= (1, 3, 5), & \phi_7 &= (1, 3, 6), \\ \phi_8 &= (1, 4, 5), & \phi_9 &= (1, 4, 6), & \phi_{10} &= (1, 5, 6), & \phi_{11} &= (2, 3, 4), & \phi_{12} &= (2, 3, 5), \\ \phi_{13} &= (2, 3, 6), & \phi_{14} &= (2, 4, 5), & \phi_{15} &= (2, 4, 6), & \phi_{16} &= (2, 5, 6), & \phi_{17} &= (3, 4, 5), \\ \phi_{18} &= (3, 4, 6), & \phi_{19} &= (3, 5, 6), & \phi_{20} &= (4, 5, 6), \end{aligned}$$

where we just have to take a permutation of the integers from 1-6 in groups of three.

The generation of the differential equations satisfied by ϕ is a straightforward but lengthy process. Lindsay and Rooney (1992) have produced a utility that

generates standard fortran code for the required equations given the matrix \mathbf{A} .

To illustrate the process,

$$\begin{aligned} \phi'_1 &= \begin{vmatrix} y_1^{(1)} & y_1^{(2)} & y_1^{(3)} \\ y_2^{(1)} & y_2^{(2)} & y_2^{(3)} \\ y_3^{(1)} & y_3^{(2)} & y_3^{(3)} \end{vmatrix} + \begin{vmatrix} y_1^{(1)} & y_1^{(2)} & y_1^{(3)} \\ y_2^{(1)} & y_2^{(2)} & y_2^{(3)} \\ y_3^{(1)} & y_3^{(2)} & y_3^{(3)} \end{vmatrix} + \begin{vmatrix} y_1^{(1)} & y_1^{(2)} & y_1^{(3)} \\ y_2^{(1)} & y_2^{(2)} & y_2^{(3)} \\ y_3^{(1)} & y_3^{(2)} & y_3^{(3)} \end{vmatrix} \\ &= \begin{vmatrix} y_2^{(1)} & y_2^{(2)} & y_2^{(3)} \\ y_2^{(1)} & y_2^{(2)} & y_2^{(3)} \\ y_3^{(1)} & y_3^{(2)} & y_3^{(3)} \end{vmatrix} + \begin{vmatrix} y_1^{(1)} & y_1^{(2)} & y_1^{(3)} \\ y_3^{(1)} & y_3^{(2)} & y_3^{(3)} \\ y_3^{(1)} & y_3^{(2)} & y_3^{(3)} \end{vmatrix} + \begin{vmatrix} y_1^{(1)} & y_1^{(2)} & y_1^{(3)} \\ y_2^{(1)} & y_2^{(2)} & y_2^{(3)} \\ \sum_{i=1}^6 A_{3i}y_i^{(1)} & \sum_{i=1}^6 A_{3i}y_i^{(2)} & \sum_{i=1}^6 A_{3i}y_i^{(3)} \end{vmatrix}, \end{aligned}$$

having used (9.10) and (9.11). Hence

$$\phi'_1 = \sum_{i=3}^6 A_{3i}\phi_{i-2}.$$

The other equations are obtained in a similar way. The initial conditions are obtained directly from (6.2.17). Choosing y_1 , y_3 , and y_5 as free variables (other choices are possible but not every combination is consistent with (6.2.17)), we express all of the initial conditions in terms of $\phi_6 = (1, 3, 5)$. For example,

$$\phi_1(a) = \begin{vmatrix} y_1^{(1)}(a) & y_1^{(2)}(a) & y_1^{(3)}(a) \\ y_2^{(1)}(a) & y_2^{(2)}(a) & y_2^{(3)}(a) \\ y_3^{(1)}(a) & y_3^{(2)}(a) & y_3^{(3)}(a) \end{vmatrix}.$$

Using (9.12) this becomes

$$\phi_1(a) = \begin{vmatrix} y_1^{(1)} & y_1^{(2)} & y_1^{(3)} \\ -(C_{21}y_1^{(1)}/a + ay_3^{(1)}) & -(C_{21}y_1^{(2)}/a + ay_3^{(2)}) & -(C_{21}y_1^{(3)}/a + ay_3^{(3)}) \\ y_3^{(1)} & y_3^{(2)} & y_3^{(3)} \end{vmatrix} = 0.$$

Similarly,

$$\phi_2(a) = \begin{vmatrix} y_1^{(1)}(a) & y_1^{(2)}(a) & y_1^{(3)}(a) \\ y_2^{(1)}(a) & y_2^{(2)}(a) & y_2^{(3)}(a) \\ y_4^{(1)}(a) & y_4^{(2)}(a) & y_4^{(3)}(a) \end{vmatrix},$$

which can be written

$$\phi_2(a) = \begin{vmatrix} y_1^{(1)} & y_1^{(2)} & y_1^{(3)} \\ -(C_{21}y_1^{(1)}/a + ay_3^{(1)}) & -(C_{21}y_1^{(2)}/a + ay_3^{(2)}) & -(C_{21}y_1^{(3)}/a + ay_3^{(3)}) \\ -my_1^{(1)} + ay_5^{(1)} & -my_1^{(2)} + ay_5^{(2)} & -my_1^{(3)} + ay_5^{(3)} \end{vmatrix} = -a^2\phi_6(a),$$

having again used (9.12). The completed initial vector $\phi(a)$ is

$$\begin{aligned} \phi(a) = \phi_6(a)[0, -a^2, -a, 0, a, 1, 0, 0, a^2C_{32}, aC_{32}, -C_{21}, -C_{21}/a, \\ 0, -ma, 0, 0, m, -C_{32}C_{21}, -C_{32}C_{21}/a, -maC_{32}] \end{aligned} \quad (9.14)$$

where $\phi_6(a) \neq 0$ is arbitrary.

Finally, the target condition is obtained by using the boundary conditions (9.12) at $r = b$. Using similar shorthand notation to that introduced in (9.13) we require

$$(my_1 + y_4 - ry_5, C_{21}y_1 + ry_2 + r^2y_3, C_{32}y_2 - y_6) = \mathbf{0}, \quad r = b.$$

Expanding this determinant leaves us with the target condition

$$\begin{aligned} -mr^2C_{32}\phi_1 + C_{32}C_{21}(\phi_2 - r\phi_3) - mr(\phi_4 + r\phi_7) \\ + C_{21}(\phi_9 - r\phi_{10}) - r^2C_{32}(\phi_{11} - r\phi_{12}) \\ + r(\phi_{15} - r\phi_{16}) + r^2(\phi_{18} - r\phi_{19}) \end{aligned} \quad (9.15)$$

$$= 0, r = b.$$

The compound matrix method then consists of solving the system of 20 1st order equations

$$\phi' = \hat{A}\phi, \quad (9.16)$$

(say) where \hat{A} is a known 20×20 matrix subject to initial conditions (9.14). The bifurcation parameter within the system is then adjusted until the target condition (9.15) is satisfied.

The accuracy of the method depends only on the accuracy obtained in the solution of (9.16).

References

- Adeleke, S. A. (1983), On the problem of eversion for incompressible elastic materials. *J. Elasticity* **13**, 63–69.
- Blatz, P.J. and Ko, W.L. (1962), Applications of finite elasticity theory to deformation of rubbery materials. *Trans. Soc. Rheology*, **6**, 223–251.
- Carroll, M.M. (1988), Finite strain solutions in compressible elasticity. *J. Elasticity* **20**, 65–92.
- Carroll, M.M. and Horgan, C.O. (1990), Finite strain solutions for a compressible elastic solid. *Quarterly of Appl. Math.* **48**, 767–780.
- Chadwick, P. (1972), The existence and uniqueness of solutions of two problems in the Mooney-Rivlin theory for rubber. *J. Elasticity*, **2**, 123–128.
- Chadwick, P. and Haddon, E.W. (1972), Inflation-extension and eversion of a tube of incompressible isotropic elastic material. *J. Inst. Maths. Applic.* **10**, 258–278.
- Chung, D.T. , Horgan, C.O. and Abeyarante, R. (1986), The finite deformations of internally pressurized hollow cylinders and spheres for a class of compressible elastic materials. *Internat. J. Solids Struct*, **22**, 1557–1570.
- Gilbert, F. and Backus, G. (1966), Propagation Matrices In Elastic Wave and Vibration Problems, *Geophysics* **XXXI**, 326–332.
- Green, A.E. and Mkrtychian, J.Z. (1977a), Elastic solids with different moduli in tension and compression, *J. Elasticity* **7**, 369–386.

- Green, A.E. and Mkrтчichian, J.Z. (1977b)**, Torsion and extension of a tube with different moduli in tension and compression. *J. Inst. Maths Applics* **20**, 221–226.
- Haughton, D.M. (1987)**, Inflation of thick-walled compressible elastic spherical shells. *IMA J. Appl. Math.* **39**, 259–272.
- Haughton, D. M. and Ogden, R. W. (1979,a)**, Bifurcation of inflated circular cylinders of elastic material under axial loading–I. Membrane theory for thin-walled tubes. *J. Mech. Phys. Solids.* **27**, 179–212.
- Haughton, D. M. and Ogden, R. W. (1979,b)**, Bifurcation of inflated circular cylinders of elastic material under axial loading–II. Exact theory for thick-walled tubes. *J. Mech. Phys. Solids.* **27**, 489–512.
- Haughton, D.M. and Orr A. (1995)**, On the eversion of incompressible elastic cylinders, *Int. J. Non-Linear Mechanics.* **30**, No 2, 81–95.
- Lakin, W.D. ,Ng, B.S. and Reid, W.H. (1978)**, Approximations to the Eigenvalue Relation for the Orr–Sommerfeld Problem, *Phil. Trans. R. Soc. Lond. A* **289**, 347–371.
- Lindsay, K.A. (1992)**, The application of compound matrices to convection problems in multi-layered continua. *Math. Models and Methods in Applied Sciences* **2**, 121–141. Paper 92/03.
- Lindsay, K.A. and Rooney, C. E. (1992)**, A note on Compound matrices, *Journal of Computational Physics* **133**, 472–477.
- Ng, B.S. and Reid, W.H. (1979)**, An Initial Value Method for Eigenvalue Problems Using Compound Matrices, *J. Computational Physics* **30** , 125–136.
- Medri, G. (1982)**, A nonlinear elastic model for isotropic materials with different behaviour in tension and compression, *J. of Eng. Materials and Tech.* **104**, 26–28.

- Ogden, R. W. (1972a), Large deformation isotropic elasticity: on the correlation of theory and experiment for incompressible rubberlike solids. *Proc. Roy. Soc. Lond. A* **326**, 565–584.
- Ogden, R. W. (1972b), Large deformation isotropic elasticity: on the correlation of theory and experiment for compressible rubberlike solids. *Proc. Roy. Soc. Lond. A* **328**, 567–583.
- Ogden, R.W. (1984), Non-Linear Elastic Deformations. *Ellis Howard*.
- Rivlin, R.S. (1949), Large elastic deformations of isotropic materials. VI Further results in the theory of torsion, shear and flexure. *Phil. Trans. Roy. Soc. Lond. A* **242**, 173–195.
- Sawyers K.N. and Rivlin R.S. (1974), Bifurcation Conditions for a Thick Elastic Plastic under Thrust, *Int. J. Solids Structures*, **10**, 483–501.
- Truesdell, C. and Noll, W. (1965), The non-linear field theories of mechanics. *Handbuch der physik III/3*. Ed. Flugge, S. Springer-Verlag, Berlin.
- Truesdell, C. (1978), Some challenges offered to analysis by rational thermodynamics. *Contemporary developments in continuum mechanics and partial differential equations*. De La Penha, G.M. and Medeiros, L.A. (eds.).
- Varga, O.H. (1966), Stress-strain behaviour of elastic materials. Interscience Publishers, New York.
- Wang, C.C. and Truesdell, C. (1973), Introduction to Rational Elasticity, Nordhoff, Gronigen.

